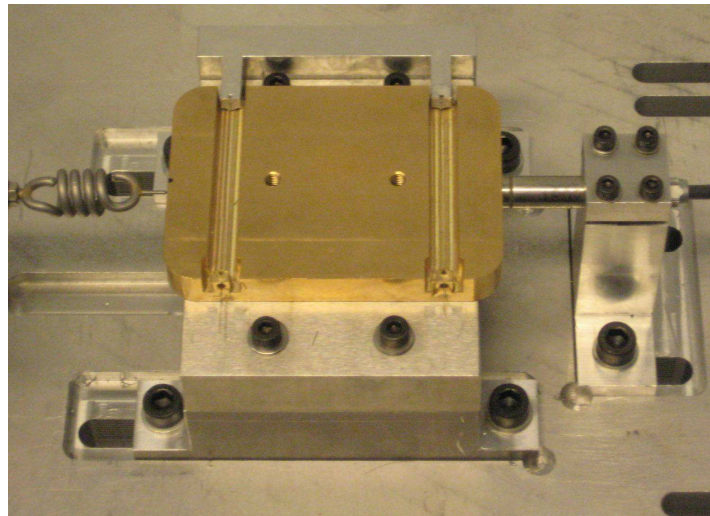


**M.Sc Thesis**

**A new model for the pre-sliding regime of friction**



**Mark J. Appels**  
**March 12, 2010**

Title: A new model for the pre-sliding regime of dry friction

Author: Mark J. Appels

Date: March 12, 2010

Student number: 1132695

Exam Number:

Institute: Delft University of Technology  
Faculty of Mechanical Engineering  
Department of Biomechanical Engineering

Board of examiners: Prof. Dr. F.C.T. van der Helm, BMechE, TUDelft  
Dr. Ir. J. Herder, BMechE, TUDelft  
Dr. Ir. R.A.J. van Ostayen, Mechatronic System Design, TUDelft  
Mr. N. Tolou, BMechE, TUDelft

## Preface

This thesis contains the research that I have performed on the pre-sliding regime of friction. The subject originated from my internship at Anglepoise Ltd. in Portsmouth U.K. At Anglepoise I researched the influence of friction on the maintenance of static balance in statically balanced desk lights. The result of the research was that, in these statically balanced desk lights, rough friction estimation by a simple and inaccurate friction model was enough to improve the functioning of the products. However, I started to wonder how, in situations requiring highly accurate friction estimation, a sophisticated pre-sliding model could be helpful. For clear understanding of this type of friction it was vital to focus upon the physical nature of friction. Currently, friction is assumed to be caused on microscopically level due to the interaction between molecules of contacting surfaces. As a result, instead of a new tool for the design of statically balanced mechanisms, this research turned into the proposal of a new friction model for the pre-sliding regime of dry friction and a measuring setup capable of measuring displacements less than a nanometer.

I would like to thank everybody who helped me to realize this result and helped me to get through the difficult moments where I did not see the use and end of this research. A special thanks to Just Herder who gave guidance throughout the process of graduation, to Jet Human, for the mental support and the enjoyable ours while studying and to Pieter Plumers for his expertise on the operation of the machines in the workplace. Furthermore I would like everybody at Anglepoise who inspired me to start this research.

Mark Appels,  
March 2010

# Table of contents

Paper.....	5
Appendix A – Measurement setup .....	21
A.1 Calculations.....	21
A.2 Material properties.....	24
A.3 Drawings.....	29
A.4 Photo's.....	40
Appendix B – Measurement equipment.....	43
B.1 Capacitive position sensors.....	43
B.2 Piezo Stack Actuator.....	45
B.3 A/D Converter.....	49
B.4 Software.....	51
B.5 Wiring scheme.....	51
Appendix C - Data analysis .....	52
C.1 Experiments 2.....	52
C.2 Experiments 3.....	55
C.3 Simulation 1 .....	57
C.4 Simulation 2 .....	63
C.5 Comparison to other models .....	70
C.6 Calibration sensors.....	74
Appendix D - Contacts.....	78
D.1 Manufacturers measurement equipment.....	78
D.2 Suppliers measurement equipment .....	78
D.3 Manufacturer and material supplier of measurement setup.....	79

# A NEW MODEL FOR THE PRE-SLIDING REGIME OF DRY FRICTION

**Mark J. Appels, Just L. Herder**  
Delft University of Technology  
Faculty of Mechanical Engineering  
Department of Biomechanical Engineering  
Mekelweg 2, 2628CD, Delft  
The Netherlands

## ABSTRACT

In this paper a new friction model for the pre-sliding regime of dry friction is proposed. Current highly accurate friction models that incorporate analysis of the pre-sliding friction regime are all dynamic models. In these models the pre-sliding regime seems to be underdeveloped. The main focus of the models lies upon the analysis of the sliding regime and therefore they are velocity dependent. In the pre-sliding regime frictional behaviour appears to be a function of displacement rather than velocity. Therefore, the proposed model is a static, position dependent model specifically formulated for the pre-sliding regime of friction. Furthermore, the model is formulated in such a way that it corresponds to the physical nature of friction currently assumed to be caused by adhesion. Therefore, the model is a modified Bristle model where clusters of molecular bonds formed due to adhesion are represented as pliable bristles with a maximum deflection and certain stiffness.

For parameter estimation and validation of the model, experiments have been performed by means of a measurement setup. In the experiments, values have been obtained for the system's initial stiffness and the maximum deflection of the bristles. The experiments show that the order of magnitude of the parameters found, correspond to the expected values. The validation experiments point out that the expected relation between the pre-sliding displacement and relaxation displacement could be confirmed. Furthermore, an expected proportional relation between the systems initial stiffness and normal load on the surface could not be invalidated. The effectiveness of the model was tested in simulations of the experimental data and by comparison to simulations made by other models. The results showed that the new model is more accurate and faster in modelling the pre-sliding regime of friction than the LuGre and Dahl model.

## I. INTRODUCTION

Friction is a phenomenon present in every mechanical system consisting of links and joints. Friction causes wear, positioning errors and dissipates energy. The constant innovations in technology cause a constant demand for high accuracy friction analysis. Examples can be found in consumer products like blu-ray players and computer hard disks where lenses require high accuracy positioning while being robust. In addition, there are many industries that use high accurate positioning in order to develop more sophisticated and efficient products. Examples are wafersteppers used in the production of computer chips, electron microscopes and robotics. In all the examples mentioned, friction causes tracking errors and therefore friction analysis should be incorporated in the control of these systems.

Currently, friction is assumed to be the result of the constant breaking and forming of microscopically small molecular bonds between the asperities (i.e. adhesion) of contacting surfaces [1]. The asperities are the microscopically summits that arise above the surface giving it its roughness (Fig. 2). The dynamic models currently used for friction analysis are capable of accurate friction estimation in dynamic situations and capture many dynamic frictional phenomena. However, the analysis of static influences seems to be underdeveloped in these models [2].

Friction can be separated in two regimes [3]; the sliding regime and pre-sliding regime. The sliding regime is considered when a relative motion between two contacting surfaces exists. It is commonly referred to as kinetic friction. The pre-sliding regime is considered prior to this relative motion. In this regime actuation forces are compensated by the friction forces generated at the interface of the contacting surfaces. This results in equilibrium of forces and is commonly referred to as static

friction. The pre-sliding regime is characterized by stiction, nonlinear behaviour, certain randomness, hysteresis and elastic/plastic pre-sliding displacements [2, 4, 5]. In addition, the behaviour in the pre-sliding regime appears to be a function of position rather than velocity [6].

Although many of the currently used highly accurate friction models incorporate modelling of the pre-sliding regime, still some imperfections remain. The simplest models have a discontinuous transition from the pre-sliding to the sliding regime. This is unrealistic and causes problems in numerical analysis. Furthermore, models that are continuous, like Dahl's model [7], the LuGre model [8] and the Leuven model [9] make use of a differential state equation involving time. The presence of the differential state equation requires large computational efforts and therefore numerical analysis is a time consuming process. Finally, the models do not cover all the frictional phenomena present in the pre-sliding regime.

Since every dynamic system also deals with static situations, it seems logical to assume that higher accuracy in friction analysis can be achieved by focussing on the pre-sliding regime. For example, the acceleration and deceleration behaviour of a robotic arm will influence the final position of the movement. Both the acceleration from stationary equilibrium and the deceleration back to stationary equilibrium incorporate the pre-sliding regime. In addition, when the direction of motion of a system reverses, the velocity of the system will go to zero before changing sign and therefore it passes the pre-sliding regime. In the case of maintenance of configuration (e.g. statically balanced devices), the system must be kept within the boundaries of the pre-sliding regime. The latter, also while being robust under influence of external disturbances.

The objective of this study is to formulate a new friction model for modelling the pre-sliding regime of dry friction in metal to metal contacts. The formulated model is a static model that captures stiction, hysteresis, pre-sliding displacement and randomness of friction in the pre-sliding regime. It includes a continuous transition from the pre-sliding regime to the sliding regime in order to facilitate future incorporation in dynamic models. Furthermore, it is aimed to stay close to the physical nature of friction, currently assumed to be caused by adhesion. A second objective is to validate the model and its theoretical background by means of experiments.

In this research, only the pre-sliding regime of a dry metal to metal contact is considered. This clears the way for modelling the elastic behaviour of the asperities at the junctions between contacting surfaces without being influenced by macro effects due to material properties. In addition, only dry metal contacts are considered. In static conditions without hydrostatic lubrication, lubricant is pushed away from the interface between surfaces resulting in a dry contact between the surfaces.

In Section 2 the model's theoretical background is expounded after which in section 3 the new model will be presented. Section 4 contains the measurement setup and method used for parameter estimation and validation of the

theoretical background. The experimental results will be presented at the end of this section. In Section 5 the model's simulation results will be presented followed by the discussion in Section 6 and a conclusion in Section 7.

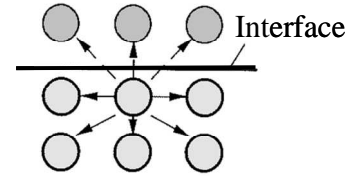


Figure 1: Schematic representation of atomic interaction at an interface as a cause of adhesion [1].



Figure 2: Transfer of material due to adhesion [1]. In the picture, the contact between the asperities (i.e. summits) is formed by many molecular bonds.

## II. THEORETICAL BACKGROUND

The purpose of this section is to give insight in the physical nature of friction in the pre-sliding regime. Hence, a theory for explanation of the frictional phenomena that occur in this regime is expounded. This theory is at the base of the new pre-sliding friction model that is proposed in the next section.

Friction is caused by three phenomena; ploughing due to surface roughness, adhesion and material transfer due to adhesion [10]. Ploughing occurs when the asperities of two contacting surfaces hook into each other rather than sliding across each other. However, when the sliding surfaces have run in properly, ploughing disappears because over time the surfaces smoothen [1]. After running in, the remaining frictional forces are caused by adhesion and material transfer due to adhesion. Adhesion is the bonding between the molecules due to intermolecular forces (Fig. 1) [11]. The forces causing the molecular bonding can be considered to behave like elastic forces [7, 12, 13]. When sliding, in metallic contacts, softer material can be transferred to harder material due to adhesion (Fig. 2) [1, 13]. In other words, when a molecular bond is broken some molecules of the softer material can stick to the molecules of the harder material. Therefore, in [13] the authors stated that the physical properties of the friction force can be considered to be a mix of elastic shear and plastic deformation of the molecules of metals according to the following equation [13].

$$F_f = S + P \quad (1)$$

Where:

- $F_f$ : The friction force ( $N$ )  
 $S$ : The force required to elastically shear the molecular bonds ( $N$ )  
 $P$ : The force required to displace the softer material from the path of the sliding body ( $N$ )

We assume that the pre-sliding regime is divided in two regions; the purely elastic region and the plastic-elastic region. When an actuating force is exerted on a body, the body will displace over a very short distance prior to sliding. This displacement is called the pre-sliding displacement. During this pre-sliding displacement, in the purely elastic region, the molecular bonds are being stretched by shearing. Due to the shearing, the molecular bonds generate a counteracting frictional force ( $S$ ). The stretching of the bonds can be considered to be an elastic pre-sliding displacement since it is no actual plastic displacement (i.e. when molecular bonds break). Once the external force is removed, the bonds will return to their original configuration. In the plastic-elastic region some molecular bonds are stretched by shear but in addition some of the bonds have broken because they are overstretched. During the breaking of the molecular bonds, some material can be transferred due to adhesion. The frictional force that remains after the bond is broken is generated by the displacement of the softer material from the sliding body's pathway ( $P$ ). The elastic properties of the molecular bonds are position dependent rather than velocity dependent. This is explained by imagining the molecular bonds as springs. The spring force generated by elongation of the spring is simply dependent on the elongation of the spring. Therefore, the pre-sliding regime is considered to be position dependent rather than velocity dependent as is in the sliding regime.

Furthermore, the pre-sliding regime is characterized by hysteresis and certain randomness. We speak of hysteresis in the pre-sliding regime when a combination of elastic and plastic deformation has occurred (i.e. the system is in the plastic-elastic region). When an actuation force is exerted on a sliding body, every molecular bond is being stretched while absorbing the actuation force as an elastic displacement (i.e. spring force). However, the stretching of the molecular bonds can only continue up to a maximum displacement. When the maximum displacement is reached, the bond will break. However, the molecular bonds are not equally strong and therefore they will break after different pre-sliding displacements. Contaminations in the surface, like corrosion and imperfections in the molecular structure of the surface, weaken the strength of the bond. In addition, molecular deformations caused by the normal load acting on the interface of the surfaces also weaken or strengthen the molecular bonds. The above means that each molecular bond can absorb a different amount of the actuation force by elastic deformation (shear). Once a bond is disconnected, its elastic property is lost since it now generates a constant friction force ( $P$ ). This means that, when the actuation force is removed from the sliding body and the body is still in the pre-sliding

regime, this bond will not help to pull back the sliding body to its initial equilibrium position. However, the bonds that are still connected and still possess their elastic properties will pull back the body to a new stationary equilibrium position. This new equilibrium is closer to the point where the actuation force got removed than the initial equilibrium position since fewer molecules are pulling back the body. The latter will result in hysteresis. After being pulled back to a new stationary equilibrium, new molecular bonds will be formed due to the normal load acting on the interface of the surfaces.

The randomness of friction in the pre-sliding regime can be explained by the randomness of the location of the asperities of the contacting surfaces. Since the asperities on both surfaces can be located anywhere across the nominal contact area, the molecular bonding can take place anywhere as well. In addition, the micro-scale conditions (e.g. pressure, molecular structure) can also differ across the nominal contact area. Therefore, the amount of pre-tension that exist in a molecular bond prior to an actual friction force is being generated can be considered to be a random variable.

The above theory does not conflict with theories behind other models. However, it has never been described as such in articles concerning these models.

### III. THE NEW MODEL

In the new model, clusters of molecular bonds that are formed due to adhesion at the asperities of contacting surfaces are represented by pliable bristles with certain stiffness. This approach is similar to the bristle model as proposed by Haessig and Friedland [12]. The proposed model consists of two parts; the initialization prior to modelling the pre-sliding frictional behaviour and the modelling according to realization. In this section the proposed new model is presented. At the end of this section the relation of this new model to the bristle model will be discussed

#### Initialization

Prior to modeling the frictional behaviour of the pre-sliding regime, the model has to be initialized. First, the number of bristles to be used by the model has to be determined. Secondly, the bristles have to be placed randomly in order to introduce nonlinearity and randomness in the model. The physical cause of the initialization process is not investigated in this paper. It is rather a necessity in order to create the right circumstances for modelling the pre-sliding frictional behaviour. Hence, in the realization process the frictional behaviour can be modelled according to the assumed physical nature of friction as expounded in the previous section.

In the new model one bristle represents many molecular bonds. Furthermore, the number of bristles to be used by the model is dependent on the load of the interface between the two surfaces. The latter is traced back to the proportional relation between the real contact area and the load of the interface [1, 13]. Therefore, the number of bristles is determined according to the following equation (2):

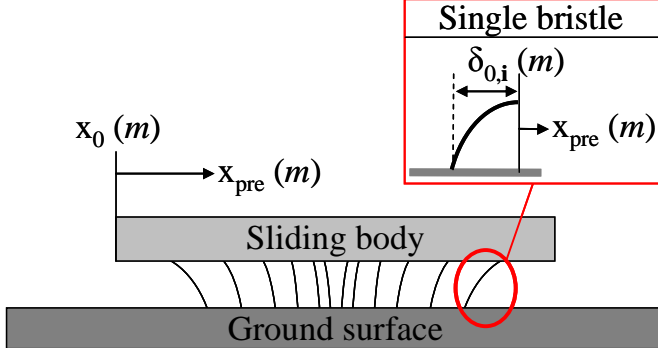


Figure 3: Schematic representation of molecular bonds by a pliable bristle with pre-tensioning at equilibrium position ( $\delta_{0,i}$ ). Where;  $x_0$ : The initial position of the sliding body and  $x_{pre}$ : The pre-sliding displacement of the sliding body.

$$N = c \cdot \mu_c \cdot F_n \quad (2)$$

Where:

- $N$ : The number of bristles to be used (-)
- $c$ : A scaling factor ( $1/N$ )
- $\mu_c$ : The Coulomb friction coefficient (-)
- $F_n$ : The normal force acting on the surface interface (N)

In equation (2) the scale factor  $c$  is added in order to influence the number of bristles to be used by the model. A very small value of  $c$  leads to a linear model by using a minimum of one bristle. A large value of  $c$  leads to a very nonlinear model for the frictional behaviour by using many bristles. The use of the Coulomb friction coefficient causes the number of bristles used by the model to be proportional to the Coulomb friction force. Due to this, the initial stiffness of the system becomes related to the normal load on the interface as well.

In order to introduce nonlinearity and randomness in the model, the bristles are pre-tensioned (i.e. deflected). This corresponds to the proposed initial deformation of the molecular bonds at the asperities due to the normal load. The placement of the bristles and thereby the introduction of pre-tension in the bristles is done by means of a normal distribution function according to:

$$\delta_{ini} = norm(\mu_1, \sigma_1, N) \quad (3)$$

Where:

- $\delta_{ini}$ : The initial deflection of the bristles (m)
- $\mu_1$ : The mean value of the distribution function (m)
- $\sigma_1$ : The standard deviation from the mean (m)

In formula (3),  $\delta_{ini}$  is a vector containing the initial deflection of  $N$  bristles. The number of bristles used in the model is limited. Therefore, while initializing, the distribution function introduces an internal stress ( $F_{int}$ ) between the two surfaces according to:

$$F_{int} = \sigma_b \cdot \sum_{i=1}^N \delta_{ini,i} \quad (4)$$

Where:

- $F_{int}$ : The internal stress (N)
- $\sigma_b$ : The bristle stiffness (N/m)

Since there is no actuation force acting on the sliding body the internal stress between the surfaces should equal zero (i.e. equilibrium of forces). Therefore, before starting modelling the pre-sliding frictional behaviour, the bristles have to settle. This means that an equilibrium configuration ( $\delta_0$ ) where the sum of all the forces generated by the bristles ( $F_{int}$ ) equals zero has to be found. This is called the preliminary settling of the body. The settling displacement ( $\Delta\delta$ ) is calculated according to:

$$\Delta\delta = \frac{F_{int}}{\sigma_{ini}} \quad (5)$$

$$\delta_0 = \delta_{ini} + \Delta\delta \quad (6)$$

Where:

- $\Delta\delta$ : The preliminary settling displacement of the bristles (m)
- $\sigma_{ini}$ : The initial stiffness of the system (N/m)
- $\delta_0$ : The equilibrium position of the bristles (m)

In equation (6),  $\delta_0$  is a vector containing the equilibrium configurations of the  $N$  bristles used by the model. The sum of this vector equals zero.

After the preliminary settling of the body, the resulting configuration of the bristles ( $\delta_0$ ) will act as the reference point from which the pre-sliding displacement ( $x_{pre}$ ) and frictional force ( $F_f$ ) are modelled by realization (Fig. 3).

### Realization

When an actuation force is exerted on the sliding body, the bristles start to deflect in the direction of the force. With it, the body is moved as well. The displacement of the body is called the pre-sliding displacement ( $x_{pre}$ ). The deflection of the bristles causes the frictional force to accumulate counteracting the actuation force. By considering the state of each bristle at a certain time interval a summation can be made of the deflections of the bristles. By multiplying this summation by the stiffness of the bristles the friction force is obtained. This process is called realization since after each time interval ( $dt$ ) the state of each bristle is considered.

The accumulation of the friction force is modelled by realization according to the following formula:

$$\left. \begin{aligned} F_f &= S + P \\ S &= \sigma_b \sum_{i=1}^{n_c} (\delta_{0,i} + x_{pre}) \\ P &= \sigma_b \cdot n_d \cdot \delta_{max} \end{aligned} \right\} \quad (7)$$

Where:

$$N = n_c + n_d \quad (8)$$

- $F_f$ : The friction force ( $N$ )  
 $x_{pre}$ : The pre-sliding displacement of the body ( $m$ )  
 $\delta_{max}$ : The maximum deflection of the bristles ( $m$ )  
 $n_c$ : The number of connected bristles (-)  
 $n_d$ : The number of disconnected bristles (-)

In formula (7) the first term ( $S$ ) represents the force to elastically shear the molecular bonds represented by the bristles. The second term ( $P$ ) represents the force required to displace the softer material, which is transferred due to adhesion, from the pathway of the displacing body.

When all the bristles are connected ( $\delta_{0,i} + \delta_x \leq \delta_{max}$ ), the displacement is purely elastic and the system is in the fully elastic region. Therefore, all the bristles can be considered to form one spring with a stiffness which equals the system's initial stiffness ( $\sigma_{ini}$ ). In this way stiction is modelled and equation (7) turns into a simple spring force formula:

$$F_f = \sigma_{ini} \cdot x_{pre} \quad (9)$$

Due to the varying pre-tension of the bristles, the bristles start to disconnect successively after a certain displacement ( $\delta_{0,i} + \delta_x > \delta_{max}$ ). Hence, the bristles that have disconnected ( $n_d$ ) will generate a constant friction force that corresponds to the second term in Equation (7). The need for this second term in the model is explained by considering the case where a single bristle is used to model the pre-sliding regime (i.e. a linear model). When an actuation force causes the bristles to reach its maximum deflection, the system leaves the pre-sliding regime and enters the sliding regime. At this boundary the single bristle generates a friction force that equals the Coulomb friction force while sliding. When the second term would be absent in the model, it would mean that, at this boundary, the friction force generated by the bristle equals zero. This results in a discontinuous transition from the pre-sliding regime to the sliding regime.

In practice, not every time a molecular bond is disconnected material will be transferred due to adhesion. However, in this model one bristle represents many molecular bonds. Hence, by averaging it is possible to assign a constant resulting friction force to each bristle. This force then represents the average force that is generated by many molecular bonds for

pushing the transmitted material from the sliding body's pathway.

From the point that the first bristle has disconnected ( $N = n_c + n_d$ ) the system's total stiffness will vary depending on the pre-sliding displacement. This results in a nonlinear accumulation of the friction force according to formula (7). The process of the successively disconnecting of the bristles, and therefore the loss of stiffness, continues until all the bonds have disconnected. When this has happened, the system has entered the sliding regime and all the bristles together are generating a constant friction force that equals the Coulomb friction force:

$$F_c = \sigma_{ini} \cdot \delta_{max} \quad (10)$$

Where:

- $F_c$ : The coulomb friction force ( $N$ )

In the pre-sliding regime hysteresis only occurs in the plastic-elastic region ( $N = n_c + n_d$ ). Once the actuation force has disappeared, the bristles that are still connected after the pre-sliding displacement will pull back the body to a state free of internal stress. The distance over which the body is pulled back by the bristles is called the relaxation displacement ( $x_{rel}$ ) and equals:

$$x_{rel} = \frac{F_f}{n_c \cdot \sigma_b} + \Delta\delta \quad (11)$$

Where:

- $x_{rel}$ : The relaxation displacement ( $m$ )  
 $\Delta\delta$ : from equation (5)

In equation (11), the first term represents the relaxation displacement that results from the summation of the stiffness of the connected bristles. In the second term,  $\Delta\delta$  represents the settling of the connected bristles to a state free of internal stress. The bristles that have disconnected during the pre-sliding displacement ( $n_d$ ) will not help to pull back the body to its initial equilibrium position. As a result the initial position will never be reached. In practice, the latter is caused due to hysteresis. The position of the sliding body after hysteresis has occurred now becomes:

$$x = x_0 + x_{pre} - x_{rel} \quad (12)$$

Where:

- $x$ : The global position of the sliding body ( $m$ )  
 $x_0$ : The initial position of the body ( $m$ )

When an equilibrium position has been reached, the disconnected bristles will reconnect. We propose that at this point the disconnected bristles are still fully stretched. Hence,

the bristles are reconnected in the direction that leads to a decrease in strain for the bristle. This is done according to the following formula:

$$\delta_{x,i} = \delta_{\max} - \text{sgn}(\dot{\delta}_{\max}) \cdot \text{norm}(\mu_2, \sigma_2) \quad (13)$$

Where:

*sgn*: The direction of the of the pre-sliding displacement (-)

After being reconnected by the distribution function, the reconnected bristles pull back the body to a state free of internal stress according to Equations 5 and 6.

By proposing that only the bristles that are connected cause the relaxation displacement, the model implies that the larger the pre-sliding displacement the larger the relaxation displacement. After all, when the body is moved over an increasing pre-sliding distance the connected bristles become more deflected and therefore the relaxation displacement will be larger. In addition, by proposing that the number of the bristles is dependent on the normal load of the interface according to equation (2) the system's initial stiffness will be dependent on the normal load as well. The validation of these implications will be the subject of the next section. Finally, since the model is only position dependent and therefore a static model, no damping has to be included in order to prevent limit cycling.

#### Relation to the Bristle model

The new model is related to the Bristle model [12] in the sense that pliable bristles are being used to model the molecular contacts between the contacting surfaces. In addition, the Bristle model also uses a random distribution for reconnection of the bristles. However, differences can be distinguished in comparison to the study published by Haessig and Friedland [12].

The bristles in the Bristle model directly reconnect when the maximum deflection is reached. The new model uses a different approach. The bristles in the new model remain disconnected until an equilibrium position is found by the bristles that are still connected. Furthermore, it is not clear whether the bristles in the Bristle model are placed randomly while initializing as is done in the new model. In addition the Bristle model uses a uniform distribution where the new model uses a normal distribution. The Bristle model is a dynamic model since the stiffness of the bristles is velocity dependent. This is not the case with the new model that is purely position dependent. Finally, the Bristle model is not a continuous model since it uses a velocity bandwidth. When the velocity is within this bandwidth the model is modelling the pre-sliding regime using more bristles than while modelling the sliding regime. As a result there is a sudden discontinuous drop in friction force when the velocity crosses the boundary of this bandwidth. In this way stick-slip is modelled. The new model only considers the pre-sliding regime, which is the friction that is generated

within the Bristle model's velocity bandwidth. Therefore the new model does not consider stick-slip.

#### IV. MEASUREMENT SETUP: PARAMETER ESTIMATION & VALIDATION OF THEORETICAL BACKGROUND.

The new model requires three parameters that have to be determined from experimental data. These are; the bristle stiffness ( $\sigma_b$ ), the maximum deflection of the bristles ( $\delta_{\max}$ ) and the Coulomb friction coefficient ( $\mu_c$ ). In addition, the proposal that a proportional relation between the normal load acting on the interface and the initial stiffness exists should be validated. Furthermore, the proposal that a relation between the magnitude of the pre-sliding displacement and the relaxation displacement exists should be validated as well.

To our knowledge, except for the Coulomb friction coefficient, no literature or empirical data about the parameters, and proposed relations are known. Therefore, a measurement setup has been built.

In this section the measurement setup, the method for obtaining the required parameters and the validation of the relations by experiments are discussed. The results of the experiments are presented at the end of this section.



Figure 4: From the notes of Da Vinci (1452-1519) [1]. This measurement setup is the first attempt, currently known, at friction estimation in sliding contacts. From the results of the experiments, his classic friction laws were postulated.

#### Measurement setup

In short, the experiments are simple tests of pushing a solid body over a ground surface. The measurement setup strongly resembles the setup as described in Da Vinci's notes on friction (Fig. 4). However, our setup is capable of measuring subnanoscale displacements and applying microNewton forces. Thereby it is capable of providing accurate insight in microscale frictional behaviour. The measurement setup (Fig. 5a & 5b) consists of three main parts; a ground surface (A), sliding body (B), and an actuation system (C). The ground surface consists of a plate made of high carbon steel (C45) with a honed finishing. A mass, made from bearing bronze (Rg7), is placed on top of the ground surface. This combination of C45-steel and Rg7-bronze is commonly used in many mechanical systems with metal to metal contacts. Furthermore, the mass is connected to a linear guidance mechanism (D), consisting of two 0.2 mm wire springs, in order to obtain a pure linear motion in the longitudinal direction. The actuation system consists of a piezo stack actuator ( $range = 30 \mu m$ ) on which a stiff spring ( $k = 116.04 N/mm$ ) is mounted. When the piezo is elongated the free

end of the spring pushes against the sliding mass resulting in actuation of the mass and simultaneously compression of the spring. The displacement of the mass and the elongation of the piezo are measured by two capacitive sensors with subnanoscale accuracy. By subtracting the position of the piezo actuator ( $x_{piezo}$ ) from the position of the mass ( $x_{mass}$ ), the compression of the spring is obtained. Hence, the friction force can be calculated from multiplying the compression of the spring by its stiffness according to the following equation:

$$F_{act}(t) = k_{spring} \cdot (x(t)_{piezo} - x(t)_{mass}) \quad (14)$$

$$F_{act} = F_f$$

Where:

- $F_{act}$ : The actuation force (N)
- $k_{spring}$ : The spring stiffness (N/m)
- $x_{piezo}$ : The global position of the piezo actuator's free end (m)
- $x_{mass}$ : The global position of the sliding mass (m)

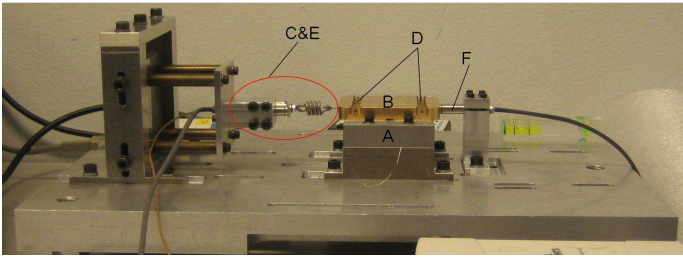


Figure 5a: Measurement setup used for parameter estimation and validation of theoretical background.

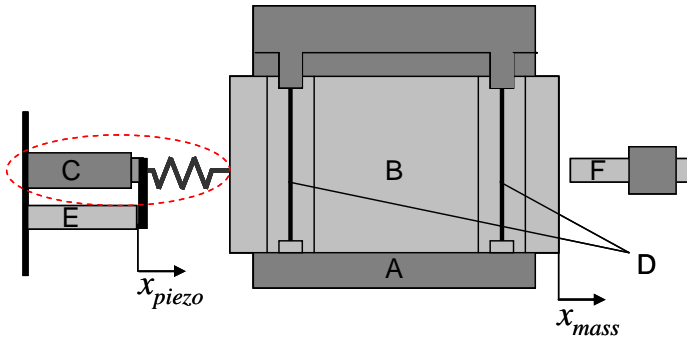


Figure 5b: Schematic representation of measurement setup (Top view). A) Ground surface, B) Sliding body, C) Actuation system consisting of piezo stack actuator with spring, D) linear guidance consisting of two 0.2 mm wire springs, E) Capacitive sensor measuring piezo elongation ( $x_{piezo}$ ), F) Capacitive sensor measuring the sliding body's displacement ( $x_{mass}$ ).

## Method

In order to validate the proposed relations and to obtain the required model parameters, three types of experiments have

been carried out. From the output of the sensors and the spring stiffness the force-displacement behaviour of the system and the position of the mass with respect to the time can be determined. Hence, the required model parameters can be obtained from the plots. By varying the mass of the sliding body and the rate at which the piezo actuator elongates, the frictional behaviour for different circumstances can be investigated.

### Experiments 1

In this experiment, the Coulomb friction force coefficient for the steel-bronze sliding contact is determined. The sliding body is simply pushed over the ground surface and the friction force is calculated according to equation (14). Since the mass of the sliding body is known, the friction coefficient can be calculated according to the following equations:

$$\left. \begin{aligned} \mu_C &= \frac{F_C}{F_n} \\ F_n &= m \cdot g \end{aligned} \right\} \quad (15)$$

Where:

- $m$ : The mass of the sliding body (kg)
- $g$ : The gravitational acceleration ( $m/s^2$ )

The experiment is carried out for three masses of 0.352 kg, 0.522 kg and 0.690 kg after which an averaged value for the Coulomb friction coefficient will be calculated.

### Experiments 2

In this experiment the system's initial stiffness for five masses of the sliding body will be determined. Furthermore, the maximum deflection of the bristles will be determined. From the values found for the system's initial stiffness, the proposed relation between the initial stiffness and the normal load of the interface will be validated.

The values that are obtained from the results of the experiments are validated as follows:

The number of bristles used by the model is determined according to:

$$N = c \cdot \mu_C \cdot F_n \quad (16)$$

Furthermore, from the Coulomb friction law follows:

$$\mu_C \cdot F_n = F_C \quad (17)$$

By substituting equation (10) into equation (17) one obtains:

$$\mu_C \cdot F_n = \sigma_{ini} \cdot \delta_{max} = F_C \quad (18)$$

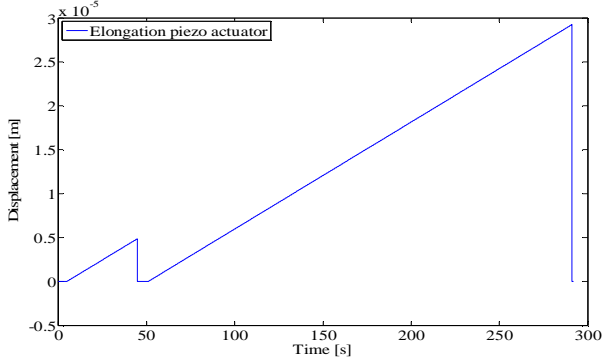


Figure 6: Cutoff values for Experiments 2. The piezo actuator elongates two times. The first peak pushes the mass to a reference position. The second run the actuator elongates to its maximum elongation while pushing the mass from the pre-sliding regime into the sliding regime.

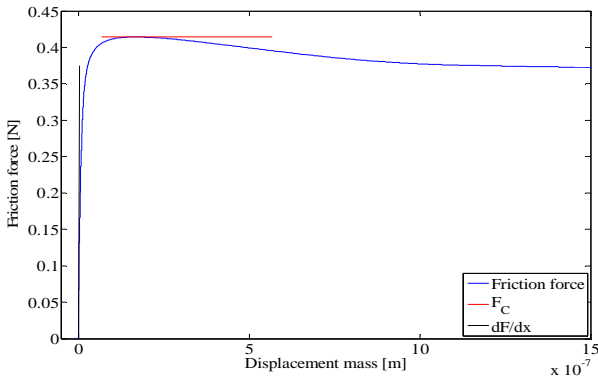


Figure 7: Force-displacement curve obtained from Experiments 2. The systems initial stiffness is determined from the slope of the tangent ( $dF/dx$ ) in the origin of the curve (black line). The Coulomb friction force ( $F_C$ ) is determined from the point where the slope of the tangent becomes zero (red line).

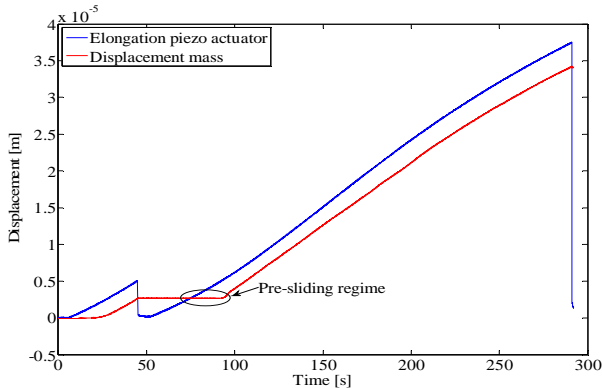


Figure 8: Displacement-time curve obtained from Experiment 2. The blue line represents the elongation of the piezo actuator with respect to time. The red line represents the position of the mass with respect to time. At the point where the red and blue lines cross in the ellipse, indicating the pre-sliding regime, the piezo has reached the mass (reference point). From here the friction force starts to accumulate.

In equation (18) two parameters are unknown  $\delta_{\max}$  and  $\sigma_{\text{ini}}$ . The Coulomb friction coefficient is estimated in Experiment 1. By determining the system's initial stiffness for the different masses, the proposed proportional relation between the initial stiffness and the normal load can be validated. In addition, when the initial stiffness is known, the value for  $\delta_{\max}$  can be calculated. By comparing the calculated values of the maximum bristle deflection with the experimentally found values, the model can be partially validated.

During the experiments, the piezo actuator pushes the sliding body two times from the pre-sliding regime into the sliding regime (Fig. 6). The first peak in Figure 8 brings the sliding body to a reference point. At this point the exact location of the mass is known together with the exact elongation of the piezo actuator. Therefore, this point can act as the origin of the force displacement curve which will be determined from the second run of the piezo actuator (second peak of Fig. 8). After all, when the piezo actuator reaches the reference point, there is contact between the spring and the sliding body while the force exerted on the sliding body equals zero. From the accompanying force displacement curve the system's initial stiffness can be obtained.

We propose that when the system is in stationary equilibrium the maximum number of molecular bonds is formed and the system possesses its maximum stiffness. In the model, this total stiffness corresponds to the sum of the stiffness of all the bristles being used. From the slope of the tangent in the origin of the force-displacement curve (Fig. 7) the system's initial stiffness ( $\sigma_{\text{ini}}$ ) can be derived. By determining the point where the tangent to the force-displacement curve equals zero (i.e. the system is in the sliding regime), the system's maximum pre-sliding displacement and the magnitude of the Coulomb friction while sliding can be determined.

The maximum bristle deflection ( $\delta_{\max}$ ) is derived from the mass' displacement-time curve (Fig. 8). We propose that, when the system returns from the sliding regime to the pre-sliding regime, the stretched bristles reconnect and start pulling the body back to a state free of internal stress. Since all the bristles are stretched up to their maximum deflection, the relaxation displacement can maximally be the distance from the ultimate deflection to the neutral position (upright) and therefore the maximum deflection of a single bristle. By measuring the relaxation displacement of the mass once the actuation force is removed the maximum deflection for a single bristle can be determined by approach.

The experiments have been carried out for five masses of 0.352 kg, 0.419 kg, 0.459 kg, 0.563 kg and 0.690 kg. In addition, each experiment has been carried out for two piezo elongation rates ( $dx/dt$ ) of  $8.25 \times 10^{-8}$  m/s and  $1.65 \times 10^{-8}$  m/s and is repeated for five times.

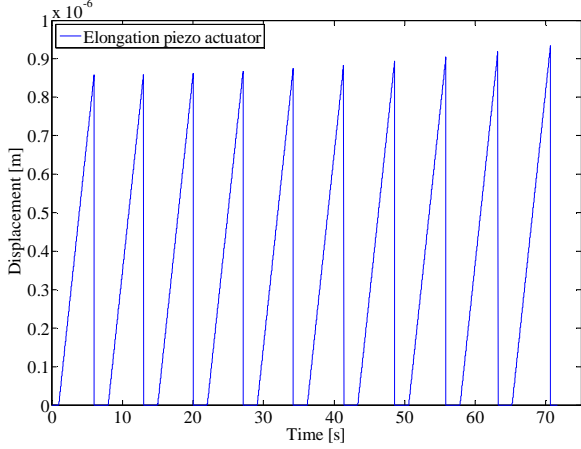


Figure 9: The elongation of the piezo actuator for 10 consecutive iterations with respect to time (Experiments 3). The increase of the increments is determined according to Equation 19.

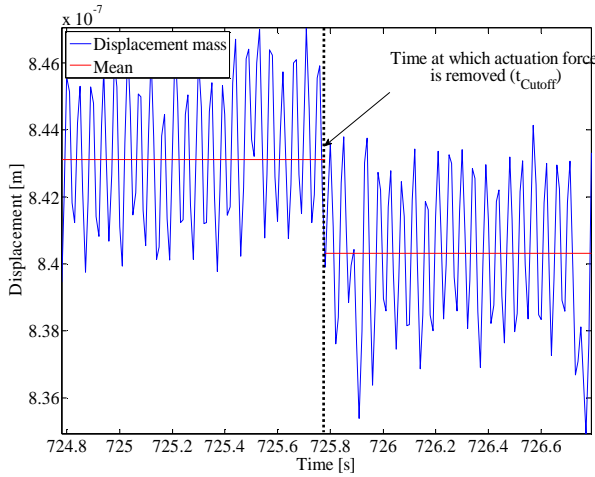


Figure 10: Visualization of relaxation displacement after the piezo actuator has reached its cutoff value. The red line represents the mean value of the noisy signals over a predefined domain before and after the actuation force is removed (Experiments 3).

Table 1: Coulomb friction force ( $F_C$ ) and Coulomb friction coefficient ( $\mu_C$ ) for three masses ( $m$ ) of the sliding body. The Coulomb friction force and the Coulomb friction coefficient are determined by averaging the results of five experiments carried out for each mass (Experiments 1).

$m$ (kg)	$F_C$ (N)	$\mu_C$ (-)
0.352	0.255	0.074
0.522	0.325	0.059
0.690	0.385	0.057

### Experiments 3

In these experiments, the assumption of a relation between the increase of pre-sliding displacement and the increase of relaxation displacement is validated. During the experiments the sliding body is iterative actuated by an increasing force which pushes it further into the pre-sliding regime (i.e. increasing pre-sliding displacement) (Fig. 9). By measuring the relaxation displacement after each iteration, the relaxation displacement belonging to preceding pre-sliding displacement can be determined (Fig 10). After each iteration, the cutoff value is increased according to Equation (19):

$$x_{cut\ off, i} = dx \cdot \sum_{i=1}^{30} i \quad (19)$$

Where:

$x_{cutoff}$ : The elongation of the piezo actuator for iteration  $i$  ( $m$ )  
 $dx$ : The piezo actuator increment for each sample ( $m/sample$ )

In equation (19) the cutoff value ( $x_{cutoff}$ ) represents the elongation at which the actuation of the sliding body by the piezo actuator is cut off. At this point the piezo retracts to its initial position ( $0\ m$ ) and the relaxation displacement of the mass is measured. In the formula,  $dx$  represents the increment of the piezo actuator for each sample ( $dt$ ). By increasing the increment, the rate ( $dx/dt$ ) at which the piezo actuator elongates is increased as well. In this way the influence of velocity on the relaxation displacement can be investigated

The experiments have been carried out for three masses of 0.352 kg, 0.522, kg and 0.690 kg and three increments of  $0.51e-9\ m$ ,  $0.825e-9\ m$  and  $1.65e-9\ m$ .

### Results

Below the results of the three experiments are presented.

#### Experiments 1

The estimated Coulomb friction coefficient has a magnitude between 0.074 and 0.057 (Table 1). The average Coulomb friction coefficient which will be used in the model is determined at 0.0633.

#### Experiments 2

The results of Experiments 2 show that, for an elongation rate of the piezo of  $dt/dx = 8.25e-8\ m/s$ , the system's initial stiffness increases when the mass of the sliding body increases. For the experiments with a rate of  $dt/dx = 1.65e-7\ m/s$ , a decrease in stiffness can be distinguished (Fig. 11). The slopes of the curves amount to  $1.424e6\ N/(m \cdot kg)$  and  $-1.900e6\ N/(m \cdot kg)$  respectively. The mean value of the initial stiffness for all the experiments carried out, amounts to  $2.2173e07\ N/m$

In Figure 12, a decrease in relaxation displacement with respect to the mass of the sliding body can be distinguished. Furthermore, a difference in magnitude of the relaxation

displacement with respect to the piezo's elongation rate used can be distinguished. The means of the relaxation displacement find itself between  $2.277e-08$  m and  $1.278e-09$  m with a slope of  $-2.4969e-9$  m/kg for the experiment with an piezo elongation rate of  $dx/dt = 8.25e-8$  m/s. For the experiment with a rate of  $dx/dt = 1.65e-7$  m/s, the means if the relaxation displacement find itself between  $2.055e-8$  m and  $6.235e-9$  m with a slope of  $-3.5776e-9$  m/kg. The mean for all the relaxation displacements measured during the experiments amounts to  $1.5584e-8$  m.

The values for the initial stiffness from the experiments are inserted in equation (18). Hence, the maximum deflection for the bristles is calculated according to the Coulomb friction force found in Experiments 1. This is done for two masses of the sliding body of 0.352 (kg) and 0.690 (kg) and two elongation rates of  $dx/dt = 8.25e-8$  m/s and  $dx/dt = 1.65e-7$  m/s. The results are presented in Table 2a and 2b.

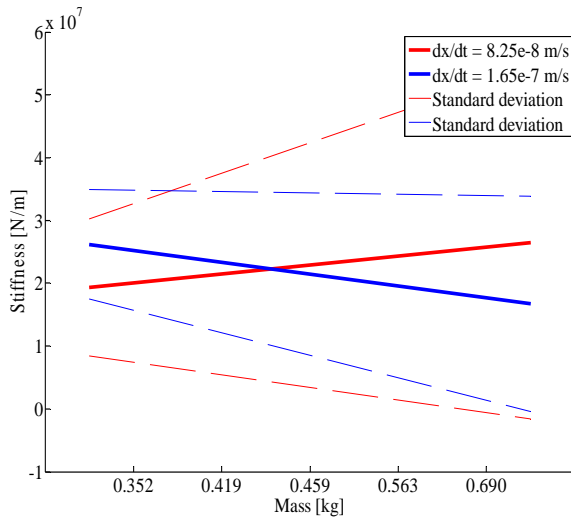


Figure 11: Initial stiffness of the system for five different masses and two piezo actuator elongation rates ( $dx/dt$ ). The initial stiffness increases when the mass increases for an elongation rate of  $8.25e-8$  m/s (red line) while it decreases for a rate of  $1.65e-7$  m/s. The dashed lines represent a standard deviation of  $\sigma$  from the mean (solid lines) (Experiments 2)

Table 2a: Partial validation of the maximum deflection of the bristles ( $\delta_{max}$ ) according to equation (18) for an elongation rate of  $dx/dt = 8.25e-8$  m/s. The measured values for the system initial stiffness ( $\sigma_{ini}$ ) and the Coulomb friction ( $F_C$ ) are inserted in Equation 18 and the relaxation displacement ( $\delta_{max}$ ) is calculated for comparison with the measured value.

$m$ (kg)	$F_C$ (N)	$\sigma_{ini}$ (N/m) (Measured)	$\delta_{max}$ (m) (Calculated)	$\delta_{max}$ (m) (Measured)
0.352	0.255	$2.004e7$	$1.27e-8$	$2.278e-8$
0.690	0.385	$2.574e7$	$1.50e-8$	$1.278e-8$

### Experiments 3

The results of Experiments 3 show that for each mass of the sliding body the relaxation distance increases when the pre-sliding distance increases (Fig 13). The slopes of the curves in the figure have a magnitude of  $0.3060$  m/m,  $0.3036$  m/m and  $0.2987$  m/m for a mass of the sliding body of 0.325 kg, 0.522 kg and 0.690 kg, respectively. The mean of all the relaxation displacements measured during the experiments amounts to  $4.3005e-9$  m.

Figure 14 shows a fluctuation in the magnitude of the relaxation displacement with respect to the increase of the elongation rate. The mean values of the relaxation displacements are  $5.3170e-9$  m,  $4.0045e-9$  m and  $4.3005e-9$  m for the elongation rates of  $dx/dt = 5.10e-8$  m/s,  $dx/dt = 8.25e-8$  m/s and  $dx/dt = 1.65e-7$  m/s respectively. The slopes of the curves amount to respectively  $0.1456$  m/m,  $0.1263$  m/m and  $0.3028$  m/m. The mean of all the relaxation displacements measured during the experiments amounts to  $4.5407e-9$  m.

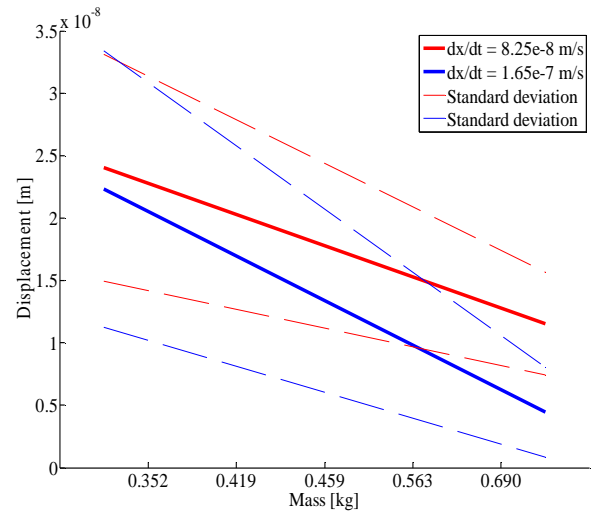


Figure 12: Relaxation displacement of the sliding body when returning from the sliding regime. The experiment has been carried out for five masses each for two different piezo elongation rates ( $dx/dt$ ). For both rates the relaxation displacement decreases when the mass of the sliding body increases. The dashed lines represent the standard deviation of  $\sigma$  from the mean (solid lines) (Experiments 2).

Table 2b: Partial validation of the maximum deflection of the bristles ( $\delta_{max}$ ) according to equation (18) for a elongation rate of  $dx/dt = 1.65e-7$  m/s. The measured values for the system initial stiffness ( $\sigma_{ini}$ ) and the Coulomb friction ( $F_C$ ) are inserted in Equation 18 and the relaxation displacement ( $\delta_{max}$ ) is calculated for comparison with the measured value

$m$ (kg)	$F_C$ (N)	$\sigma_{ini}$ (N/m) (Measured)	$\delta_{max}$ (m) (Calculated)	$\delta_{max}$ (m) (Measured)
0.352	0.255	$2.526e7$	$1.01e-8$	$2.055e-8$
0.690	0.385	$1.766e7$	$2.18e-8$	$6.235e-9$

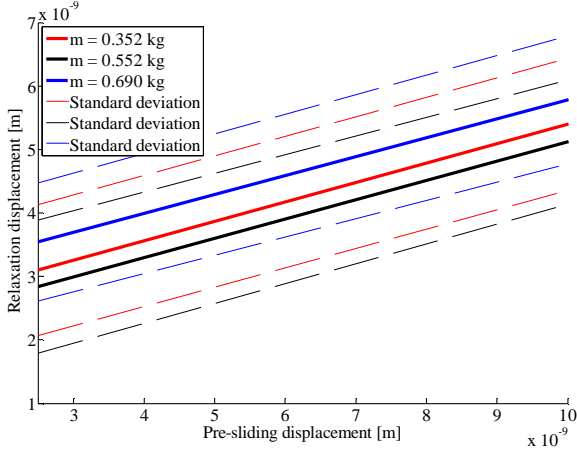


Figure 13: Relation between the pre-sliding displacement ( $x_{pre}$ ) and relaxation displacement ( $x_{rel}$ ) in the pre-sliding regime for three masses ( $m$ ) (Experiment 1). The relaxation displacement ( $y$ -axis) increases when the pre-sliding displacement ( $x$ -axis) increases. The dashed lines represent the standard deviation of  $\sigma$  from the mean (solid lines) (Experiments 3).

## V. SIMULATIONS

From the experiments described in the previous section the model's parameters are obtained. The values of the experimental parameters that will be used for determination of the model parameters are listed Table 3.

The system's initial stiffness is determined from the mean of the initial stiffness found in Experiments 2 and amounts to  $2.2173e07$  N/m (Fig. 11). The maximum deflection of the bristles ( $\delta_{max}$ ) is determined from the mean of the relaxation displacements found in Experiments 2 and amounts to  $1.5584e-8$  m (Fig 12). The magnitude of the average relaxation displacement ( $x_{rel}$ ) is determined from the average of the two mean values found in experiment 3 and amounts to  $4.4206e-9$  m. The Coulomb friction coefficient is determined from the mean of the values found in Experiments 1 and amounts to 0.063.

From the experimentally found values the other model parameters have to be determined. The number of bristles to be used by the model is determined according to equation (2):

$$N = c \cdot \mu_c \cdot F_n$$

In the simulations, the value for  $c$  is chosen to be 500. In this way the minimum amount of bristles used by the model is about 100 for the mass of 0.352 kg. The choice for a minimum of 100 bristles to be used by the model originates from a trade off between the required nonlinearity of the model and the computational effort required to model the 100 bristles by realization. Nevertheless, good results were obtained by using an amount of 10 bristles. The bristle stiffness ( $\sigma_b$ ) is determined according to the following equation:

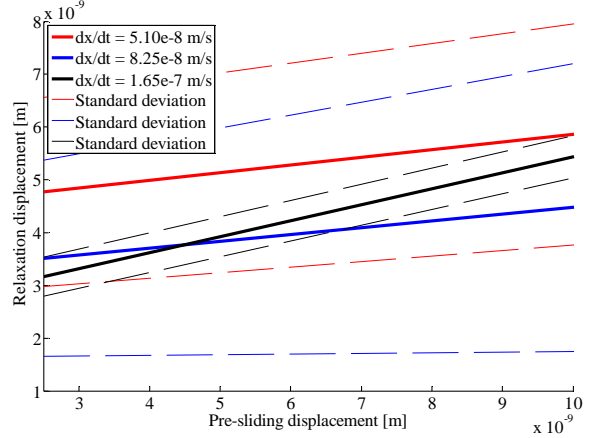


Figure 14: Relation for three actuator elongation rates ( $dx/dt$ ) between the pre-sliding displacement ( $x_{pre}$ ) and relaxation displacement ( $x_{rel}$ ) in the sliding regime. For all three rates, the relaxation displacement ( $y$ -axis) increases when the pre-sliding displacement ( $x$ -axis) increases. The dashed lines represent the standard deviation of  $\sigma$  from the mean (solid lines) (Experiments 3).

$$\left. \begin{aligned} \sigma_b &= \frac{\sigma_{ini}}{N} \\ \sigma_{ini} &= \frac{\mu_c \cdot F_n}{\delta_{max}} \end{aligned} \right\} \quad (20)$$

The mean of the distribution function for the initial placement of the bristles ( $\mu_1$ ) is set at 0. In combination with a standard deviation ( $\sigma_1$ ) of  $2 \cdot \delta_{max}/3$ , 99.7% of the bristles will be placed with an initial deflection between 0 and  $\delta_{max}$  m. The mean value for the reconnection of the bristles ( $\mu_2$ ) is obtained from the averaged value of the relaxation displacement of the bristles  $\delta_{rel}$ . The accompanying standard deviation ( $\sigma_2$ ) is chosen to be  $1/3$  of the mean value. Here 99.7% will be reattached within a range of  $x_{rel}$  m. The latter has no physical background or experimental validation. Nevertheless, it seems plausible to assume that the relaxation displacement of the disconnected bristles is proportional to the average relaxation of the sliding body. Hence, the distribution of the connected and reconnected bristles at the new stationary equilibrium is similar to the initial distribution that is obtained in the initialization process.

### Simulation 1

In this simulation the parameters from Table 3 and 4 are used to simulate Experiments 1 for three different masses. For comparison, from the empirical data of three different masses, the force-displacement curve has been determined. The data is filtered by a low pass filter in order to obtain a good qualitative behaviour (Fig. 15).

Figure 15 shows that the qualitative behaviour of the model corresponds to the behaviour of the experimental data. A distinction in initial stiffness can be observed and both the

model and the empirical data show a nonlinear transition from the pre-sliding regime to the sliding regime. In addition both the model and the empirical data show that the range of the pre-sliding regime (marked by the vertical lines in Figure 15) is indifferent of mass. The quantitative behaviour shows a deviation from the experimental data. The Coulomb friction force found by the model has a magnitude that is within 17 % off from the experimental data for all three experiments. The range of the simulated pre-sliding regime is about  $9.25e-8$  m shorter than the range found in the experiments.

Table 3: Experimentally found parameters for the system's averaged initial stiffness ( $\sigma_{ini}$ ), the averaged maximum deflection of the bristles ( $\delta_{max}$ ), the averaged relaxation displacement of the sliding body ( $x_{rel}$ ) and the averaged Coulomb friction coefficient ( $\mu_C$ ).

$\sigma_{ini}$	2.2173e7 (N/m)
$\delta_{max}$	1.5584e-8 (m)
$x_{rel}$	4.4206e-9 (m)
$\mu_C$	0.0633 (-)

Table 4: Means ( $\mu_1, \mu_2$ ) and standard deviations ( $\sigma_1, \sigma_2$ ) for the initial distribution function and reconnection distribution function.

$\mu_1$	0 (m)
$\sigma_1$	$(2 \cdot \delta_{max})/3$ (m)
$\mu_2$	$x_{rel}$ (m)
$\sigma_2$	$x_{rel}/3$ (m)

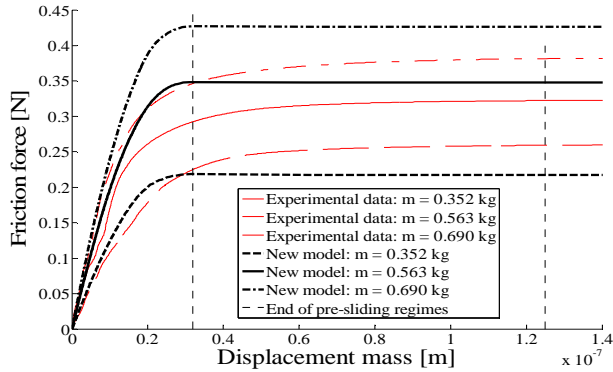


Figure 15: Result simulation 1. The red curves represent the force-displacement curves as obtained by the new model. For comparison the experimental data of three different masses are depicted by the red lines. The vertical dashed lines represent the boundary between the pre-sliding regimes and the sliding regimes.

### Comparison with Dahl's and LuGre model

In order to estimate the model's accuracy and efficiency in simulating the pre-sliding regime, the model is compared with two other models. The Dahl model [7] is one of the first models that represent friction as a combination of elastic and plastic motion. It is a dynamic model and therefore it uses a state variable involving time. The LuGre [8] model is, like the new

model, a bristle model. It is formulated in order to improve the efficiency of the Dahl model and in order to include lubrication influences. Like the Dahl model it is a dynamic model which uses a differential state equation. The parameters used for the simulations are listed in the Table 5a and 5b.

Figure 16 shows a difference of factor 9 between the curves modelled by the Dahl model and the experimental data. The LuGre model resulted in even larger deviations from the experimental data. Therefore, the results of the LuGre model have been left out of consideration. The Coulomb friction force as calculated by the Dahl model amounts to  $0.02759$  N for the sliding body with mass  $0.352$  kg. The length of the pre-sliding regime as calculated by the Dahl model amounts to  $2.7e-7$  m which is about  $1.45e-7$  m longer than the results from the experimental data. Furthermore, the Dahl model does not make a distinction between the initial stiffness with respect to the normal load. The LuGre model does, but the magnitude of stiffness could not be determined. The required computational effort is much higher for the dynamic models. The computational effort required for the new model is about 90 and 60 times lower with respect to the Dahl model and the LuGre model, respectively (Table 6).

Table 5a: Model parameters for simulations of three masses by the Dahl model.  $\sigma_0$  represents the initial stiffness of the model,  $\sigma_1$  is a shape determining factor and  $F_C$  the Coulomb friction force while sliding. The Coulomb friction is given as input for each simulation of mass (m).

m (kg)	0.352	0.522	0.690
$\sigma_0$ (N/m)	2.2173e7	2.2173e7	2.2173e7
$\sigma_1$ (-)	25	25	25
$F_C$ (N)	0.2596	0.3229	0.3828

Table 5b: Model parameters for simulations of three masses by the LuGre model.  $\sigma_0$  represents the initial stiffness of the model,  $\sigma_1$  is the damping coefficient,  $\sigma_2$  the viscous friction coefficient,  $v_s$  the Stribeck velocity,  $F_s$  the static friction and  $F_C$  the Coulomb friction while sliding. The static friction is given as input for each simulation of mass (m).

m (kg)	0.352	0.522	0.690
$\sigma_0$ (N/m)	2.2173e7	2.2173e7	2.2173e7
$\sigma_1$ (Ns/m)	$\sqrt{2.2173e7}$	$\sqrt{2.2173e7}$	$\sqrt{2.2173e7}$
$\sigma_2$ (Ns/m)	0.4	0.4	0.4
$v_s$ (m/s)	$8.25e-8$	$8.25e-8$	$8.25e-8$
$F_s$ (N)	0.2596	0.3229	0.3828
$F_C$ (N)	$F_s/1,5$	$F_s/1,5$	$F_s/1,5$

Table 6: Computational effort required to simulate the force-displacement curve of Experiments 3 for the sliding body with a mass of  $m = 0.352$  kg. The simulations were performed on a HP xw4600 Workstation (3.16 GHz)

Model name	Computer time (s)
New model	0.33
Dahl model	29.1
LuGre model	19.55

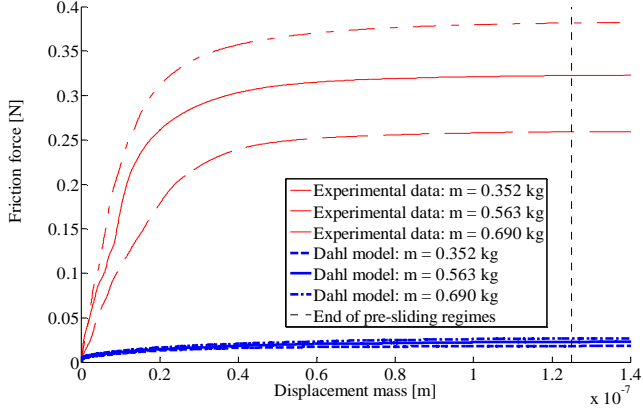


Figure 16: Simulation of force-displacement curve by the Dahl model. The vertical line represents the boundary between the pre-sliding and the sliding regime. The simulation by the Dahl model is still in the pre-sliding regime.

### Data fit for the new model.

Both the Dahl and the LuGre model require the Coulomb friction force for sliding as an input value. For the simulations this input value equals the Coulomb friction force as obtained from the experimental data.

In Figure 17 the results for a simulation by the new model with a data fit similar to those for the models of the previous paragraph is presented. For the data fit the Coulomb friction force is given as a model parameter. The magnitudes are 0.2596 N, 0.3229 N and 0.3828 N for a mass of the sliding body of 0.352 kg, 0.522 kg and 0.690 kg, respectively. Hence, the number of bristles to be used and the bristle stiffness are calculated according to:

$$\begin{aligned}
 N &= c \cdot F_C \\
 \sigma_{ini} &= \frac{F_C}{\delta_{max}} \\
 \sigma_b &= \frac{\sigma_{ini}}{N}
 \end{aligned} \tag{21}$$

In equation (21) the maximum deflection is chosen to fit the curve of the experimental data for the mass of 0.352 kg optimally. The maximum deflection found amounts to 2.500e-8 m. Next, the simulations were carried out for the other two masses while keeping the maximum deflection constant. In Figure 17 the simulation has been carried out ten times for each mass. The latter results in a varying force accumulation

Figure 17 shows that the Coulomb friction force modelled by the new model meet together with the magnitude of the Coulomb friction force found from the experimental data. The pre-sliding regime modelled by the new model has become larger with respect to the results of Simulation 1 but it is still 7.25-8 m off from the experimental data.

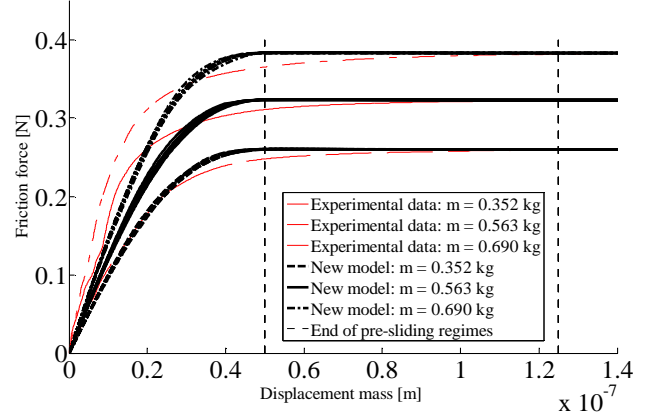


Figure 17: Simulation of the experimental data by means of a data fit of the Coulomb friction force. The simulation has been carried out for 10 consecutive runs.

### Simulation 2

In this simulation two iterations from the experimental data of Experiments 2 are simulated. In the simulation the mass is actuated twice by an actuation force. In Figure 18 the experimental data is presented together with a simulation using the estimated parameters from Simulation 1 and a simulation with the parameters found by the data fit of the previous paragraph.

Figure 18 shows that both simulations simulate the qualitative behaviour of the experimental data. Due to the strong filtering of the experimental data, no judgement about the quantitative behaviour can be made. Nevertheless, hysteresis is modelled by both simulations.

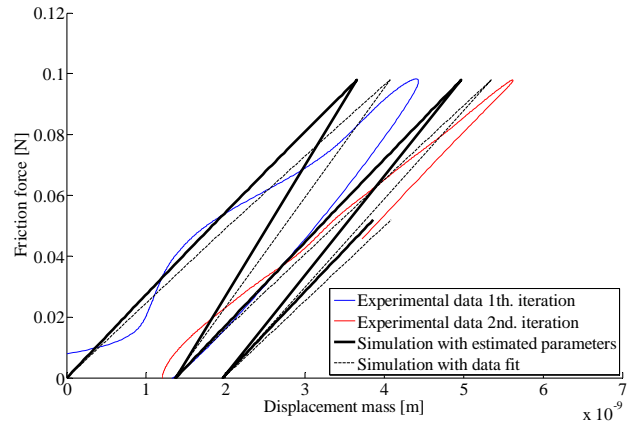


Figure 18: Simulation of 2 iterations of the force-displacement curve of Experiment 3. The solid black line represents the simulation using the estimated parameters. The dashed line represents the simulation with the fitted parameters.

## VI. DISCUSSION

The objective of this research was to formulate a new model for the pre-sliding regime of dry friction and to validate the model by experiments. In order to do so, a measurement setup has been built and simulations on experimental data were performed. In this section, after a general discussion of the research, the results and observations from this research are discussed according to the structure of the sections of this paper.

### General

The focus on friction analysis generally lies upon the analysis of dynamic friction. This is why there is a vast amount of dynamic friction models in contrast with a few models suited for static friction analysis. Nevertheless, current dynamic models incorporate analysis in the pre-sliding regime in order to model stick-slip behaviour. However, in all the models the pre-sliding regime is still considered to be velocity dependent due to the differential state equation used by the models. The new model is a static model which means that it lacks a time dependent state variable. This leads to fewer requirements for computational effort and thereby enhances efficiency. In addition, the numerical integration algorithms required for the dynamic models become inaccurate when the velocity reaches near static conditions. This results in inaccurate modelling of friction. The new model is not troubled by calculations that become stuck. However, due to the lack of a time dependent state variable, the new model is not suited for analysis of the sliding-regime. In the sliding regime velocity dependent influences, like viscous friction and lubrication effects play a leading part. Therefore, for analysis of the sliding regime, a dynamic model is required. Nevertheless, the proposed model has a continuous transition to the sliding regime. This makes the model suited for implementation in dynamic models and thereby enhances the effectiveness of the dynamic model in modelling the pre-sliding regime.

### Theoretical background

The theoretical background is based upon the assumption of the absence of ploughing. In practice there will always be some ploughing involved in dry metal to metal contacts, even if they have run in properly. For example, contaminations due to corrosion and wear cause the smoothed surface to be roughened up which can lead to ploughing effects. However, the influence of the ploughing effect is considered to be minor and random and is overcome due to the presence of the distribution function implemented in the model.

### The new model

The initialization process of the model is considered as a tool in order to create the random pre-tension in the bristles that, based on the theoretical background, should be present in the model prior to running a simulation. The process does not have a firm physical background. However, it can be interpreted by considering the placement of a body with a certain mass on a

ground surface. Suppose that the body is placed on the ground surface and no external forces other than the normal force are acting on the body. Due to the weight of the body, the molecular bonds at the interface of the contacting surfaces are being deformed. Hence, the elastic deformations of the molecular bonds cause an internal stress to arise at the interface between the ground surface and the sliding body. However, since no actuation force is acting on the body, the molecular bonds will settle until equilibrium of forces is reached. In other words, the mass will displace until the summation of the strain in all the molecular bond equals zero. This settling displacement corresponds to  $\Delta\delta$  in Equation (6) in the model.

Current bristle models propose that the pre-sliding and sliding regime of friction are characterised by the continuous forming and breaking of molecular bonds. The new model differs from this assumption by assuming that once a bond is broken it will not reconnect immediately. In the new model we proposed that the bristles only will reconnect when a stationary equilibrium has been obtained where no internal stress at the interface is present (i.e. after settling). It could very well be that in the sliding regime this assumption does not hold. However, this is not investigated in this research

### Experiments

The experiments carried out in this research are drawn up in order to approach static conditions. In order to do so, the sample rate and elongation increment of the piezo stack actuator are kept as low as possible. The maximum elongation rate ( $dx/dt$ ) for the piezo during the experiments amounts to  $1.65e-7$  m/s, which can be considered to be near zero. This is why inertia influences, if present, are not considered in the experiments.

Furthermore, from the experiments no velocity dependent influences can be distinguished. Figure 13 points out that the relaxation displacement is indifferent of the mass of the sliding body and the sample rate at which the actuation force is applied. There is a slight difference in magnitude but this difference falls within a standard deviation of one  $\sigma$  of the mean of the experimental results. In addition, Figure 14 points out that the relaxation displacement is not influenced by the elongation rate of the piezo for very small velocities. Again, there is a difference in the magnitude and slope of the curves representing the elongation rates. However, since the difference is mainly within standard deviation of one  $\sigma$  of the results, this difference is not significant. Both observations are in congruence with the model's theoretical background by representing the pre-sliding frictional forces as elastic forces which are not influenced by inertia effects. However, further research, using higher elongation rates of the piezo, should be performed in order to determine to what extent inertia influences the frictional behaviour in the pre-sliding regime for higher actuation rates.

From Experiments 2 no relation between the mass of the sliding body and the initial stiffness could be validated (Fig. 11). However, due to the large standard deviations of the experimental results the assumption is neither invalidated.

Figure 12 shows a decrease of the relaxation displacement with respect to the mass of the sliding body. The cause of this phenomenon is unknown. However, the phenomenon is not incorporated in the model since the decrease is not significant due to the large standard deviation in the experimental results.

The model is partially validated by substituting the values found by the experiments in Equation (18). However, due to the large scatter in the experimental results it is only possible to validate the order of magnitude of the parameters used by the model. The results from the validation give a plausible indication that the order of magnitude of the estimated parameters is correct. Nevertheless, more research should be carried out using very accurate force sensors instead of the combination of a piezo and spring with displacement sensors.

Considering the standard deviations in Figures 11, 12 & 14, one can conclude that there is a considerable dispersion in the results of the experiments. This can be due to several causes. First of all, the sensors register noise. Therefore, the data has to be filtered prior to be analysed. Filtering enhances the acquiring of qualitative data but on the other hand it deteriorates the acquiring of quantitative data. Due to the filtering data can be lost and therefore a trade off has to be made between the amount of filtering and the acquiring of useful data. Furthermore, the capacitive sensors suffer from drift. This means that over time the reference position as recorded by the sensors fluctuates. The latter is visualised in Figure 8. Here, the blue line, representing the sensor measuring the elongation of the piezo actuator, has a slight curve. The line should be linear since the piezo actuator's input (Fig. 6) is linear. Finally, although the sliding mass is guided by a linear guidance, some disturbances in the motion of the mass could be present. Causes of the disturbances can be misalignment of the actuation system, different pre-tension in the wire springs and disturbances introduced by the fixation of the wire springs.

The above can be considered to be disturbing factors for the acquiring of accurate data and the large dispersion that can be noticed in the results. The noise and filtering especially influence the determination of the force-displacement curves for the experiments. The actuation force exerted by the piezo-spring combination is determined according to the output of two sensors. Therefore, the estimation suffers from twice the noise and filtering as for determination of the displacement-time curves which are determined by the output of one sensor. Furthermore, the drift introduces inaccuracies to the calculation of the initial stiffness. Since the determination of the force-displacement takes place over a considerable time interval the drift in the sensors causes the reference point to fluctuate. This results in a drift of the origin during the measurements, which in turn results in inaccurate estimation of the friction force. Nevertheless, a good qualitative characteristic of the frictional behaviour in the pre-sliding regime could be achieved.

For the determination of the relaxation displacement, the influences of noise, filtering and drift are less drastically. Since this parameter is determined from the output of one sensor, noise and filtering effects are less disturbing. In addition, the

time interval over which the relaxation displacement is calculated is very short so drift of the sensors does not influence the outcome of the measurement. Therefore, a good qualitative and quantitative behaviour of the relaxation displacement could be obtained.

## Simulations

The simulations show that the qualitative behaviour of the pre-sliding regime is modelled more accurate in comparison with the Dahl and LuGre model. The Coulomb friction force calculated by the new model deviates for a maximum of 17 percent from the Coulomb friction force obtained from the experimental data. The results obtained from simulations using the Dahl and LuGre model deviate more than a factor 9 from the experimental results. The reason for this difference in magnitude is probably the result of the low velocity of the sliding mass during the experiments. The low velocity causes problems in the numerical integration process of the models and results in inaccurate estimation of friction in the pre-sliding regime.

The difference between the range of the pre-sliding regime found by the model and the range obtained by the experiments is due to the parameter used for the maximum deflection of the bristles. The range of the pre-sliding regime found by the model can maximally be twice the magnitude of the maximum deflection of one bristle. The experimental results show that the value used for the maximum deflection should be higher. However, in the model the estimation of the boundary between the pre-sliding and the sliding regime can be determined very accurate by considering the point where the last bristle has disconnected. In the experimental data this boundary is determined by considering the point where the slope of the force displacement becomes zero. Due to the strong filtering it is very good possible that this point is displaced by smoothening of the sensors' output signals.

In the transition from pre-sliding to sliding friction, a peak force can be distinguished (Fig. 7). The Coulomb friction while sliding is lower than this peak force. The decrease in friction force from this peak force to the Coulomb friction force while sliding is not incorporated in the new model because it is a dynamic phenomenon that can be modelled by the Stribeck effect [3].

Since little research on the pre-sliding regime is performed, it is not possible to obtain analytical data from literature. This makes it difficult to validate the model or compare it to other models in static conditions. In this research the new model is validated on modelling the force-displacement curves obtained from experimental data from the experiments performed. Due to the inaccuracy in the estimation of the friction force, it is not sure that the analytical data obtained resembles the actual situation. Nevertheless, since a good qualitative result could be achieved, a partial validation of the qualitative behaviour of the model for the bronze to steel contact could be made.

Finally, the parameters used by this model currently have to be obtained empirically. More research is required in order to

obtain more insight in the relation between the material properties and the model's parameters. This clears the way for the formulation of a general model suited for pre-sliding friction estimation in many types of materials.

## VII. CONCLUSION

A static friction model, representing clusters of molecular bonds by pliable bristles has been formulated. The model is capable of modelling stiction, pre-sliding displacement, hysteresis and randomness of friction.

Experiments show that the proposed theoretical background of the model is plausible.

A relation between an increase of the pre-sliding displacement and the increase of the relaxation displacement is validated by experiments. Furthermore, a proportional relation between the initial stiffness of the system and the normal force acting on the interface of the contacting surfaces could not be invalidated. The experiments point out that, for near static situations, the proposal of friction only to be dependent on displacement is plausible.

The model is partially validated by comparing the calculated maximum bristle deflection with the experimentally obtained maximum deflection of the bristles. The order of magnitude found for the maximum deflection amounts to  $1e-8$  m. The system's initial stiffness found by the experiments has a magnitude in the order of  $1e7$  N/m. The latter agrees with the magnitude calculated by the model with respect to the experimentally determined maximum deflection of the bristles.

In simulations, the model proves to be a factor 9 more accurate in estimating the Coulomb friction force of the experimental data than the LuGre and Dahl model. In addition, the model proves to be 60 and 90 times faster in simulating the pre-sliding regime than respectively the LuGre and Dahl model.

## NOMENCLATURE

$dx/dt:$	Elongation rate of the piezo actuator ( $m/s$ )
$\delta_{mi}:$	Initial placement of the bristles ( $m$ )
$\delta_{max}:$	Maximum deflection of the bristles ( $m$ )
$\delta_n:$	Pre-sliding displacement of the bristles ( $m$ )
$\delta_0:$	Equilibrium position of the bristles ( $m$ )
$\delta_{max}:$	Relaxation displacement of the bristles in the pre-sliding regime. ( $m$ )
$\Delta\delta:$	Preliminary displacement of the bristles ( $m$ )
$F_{act}:$	Actuation force ( $N$ )
$F_C:$	Coulomb friction force ( $N$ )
$F_f:$	Friction force ( $N$ )
$F_{int}:$	Internal stress ( $N$ )
$k_{spring}:$	Spring stiffness ( $N/m$ )
$\mu:$	Mean value of the distribution function ( $m$ )
$\mu_C:$	Coulomb friction coefficient
$N:$	Total number of bristles used by the model (-)
$n_c:$	Number of connected bristles (-)
$n_b:$	Number of disconnected bristles (-)
$\sigma:$	Standard deviation distribution function ( $m$ )
$\sigma_b:$	Bristle stiffness ( $N/m$ )
$\sigma_{mi}:$	Initial stiffness of the system ( $N/m$ )
$x_{mass}:$	Global position of the sliding mass ( $m$ )

$x_{piezo}:$	Global position of the piezo's free end ( $m$ )
$x_{rel}:$	Relaxation displacement of the sliding body ( $m$ )

## REFERENCES

1. A. van Beek, Advanced Engineering Design - Lifetime performance and reliability. 2006.
2. M.J. Appels, Suitability of friction models for accurate modelling of dry friction in statically balanced mechanisms. 2009, Delft University of Technology: Delft.
3. H. Olsson, et al., Friction Models and Friction Compensation. 1997.
4. U. Parlitz, et al., Identification of pre-sliding friction dynamics. Chaos, 2004. 14(2): p. 420-430.
5. P. Dupont, B. Armstrong-Hélouvy, and V. Hayward, Elastoplastic Friction Model: Contact Compliance and Stiction. AACC, 2000.
6. B. Armstrong-Hélouvy, P. Dupont, and C.C.d. Wit, A Survey of Models, Analysis Tools and Compensation Methods for the Control of Machines with Friction. Automatica, 1994. 30(7): p. 1083-1138.
7. P. R. Dahl, A Solid Friction Model. 1968, The Aerospace Corporation: Los Angeles, California.
8. C. Canudas de Wit, et al., A New Model for Control of Systems with Friction. IEEE Transactions on Automatic Control, 1995. 40(3): p. 419-425.
9. V. Lampaert, J. Swevers, and F. Al-Bender, Modification of the Leuven Integrated Friction Model Structure. IEEE Transactions on Automatic Control, 2002. 47(4): p. 683-687.
10. F.P. Bowden, J. Moore, and D. tabor, The ploughing and adhesion of sliding materials. Journal of Applied Physics, 1943. 14: p. 80-91.
11. K. Kendall, Molecular adhesion and its applications. 2004, Birmingham: Kluwer Academic Publishers.
12. D. A. Haessig and B. Friedland, On the Modeling and Simulation of Friction. Transactions of the ASME, 1991. 113: p. 354-362.
13. F.P. Bowden, D.T., Mechanism of metallic friction. Nature, 1942. 150(August 15): p. 3.

## Appendix A – Measurement setup

This appendix discusses the measurement setup used during the experiments. In Section A.1 calculations that have been made prior to manufacturing the measurement setup are presented. Section A.2 discusses the materials used and contains the specifications of the spring that is used in the actuator system. Furthermore it contains the drawings in Section A.3 and pictures of the measurement setup in Section A.4.

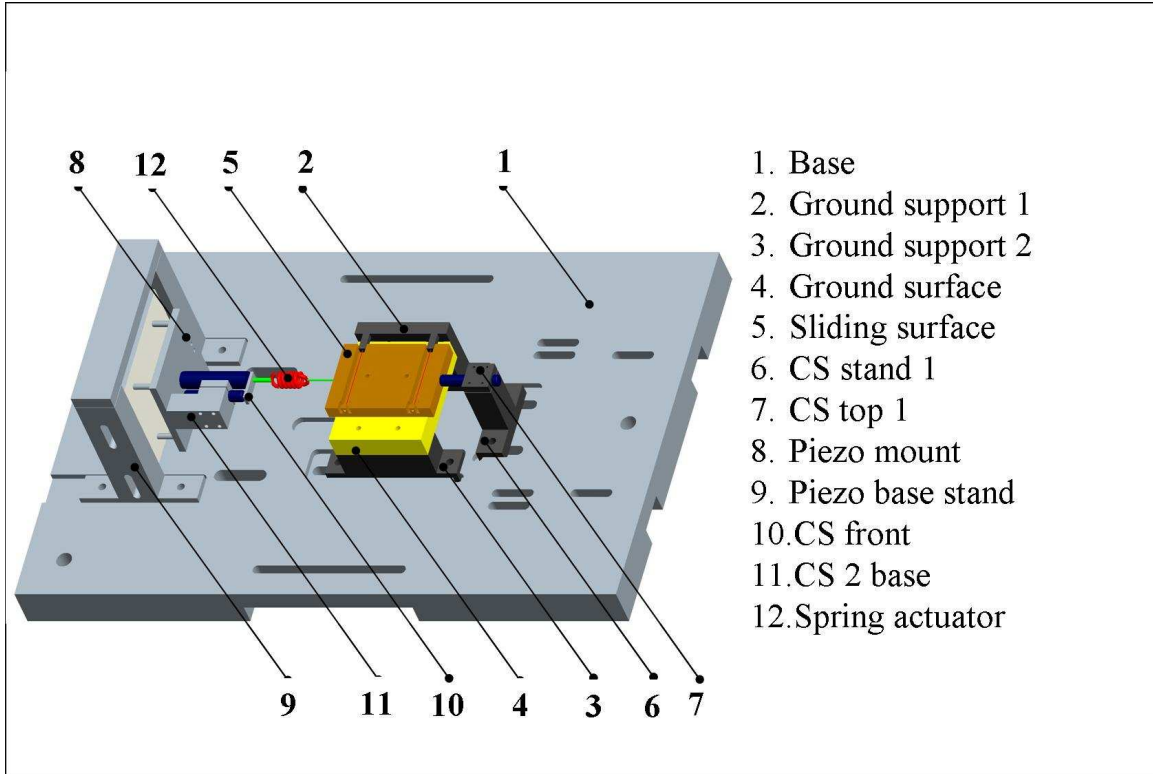


Figure 1: Pro Engineer picture of the measurement setup.

### A.1 Calculations

#### Linear guidance

The linear guidance is used in order to obtain a purely linear motion in the longitudinal direction. Inaccuracies, caused by for example misalignment of the piezo-spring actuator, can cause the mass to rotate around its central axis (perpendicular to the ground surface). The rotation introduces inaccuracies to the measurements since the surface that is facing the capacitive sensor will slant. The linear guidance is implemented in order to prevent the mass from rotating around its vertical axis.

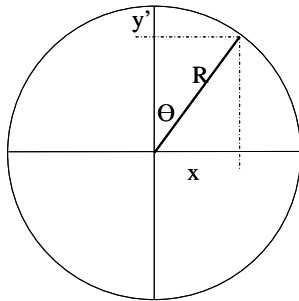
The presence of the linear guidance prevents the mass from rotation but it introduces a lateral movement. It is important to minimize the lateral movement in such a way that it does not influence the measurements of the sensor. The latter is done by making the maximal lateral displacement that will occur during the experiments smaller than the accuracy of the sensor.

Ideally the line of action of the actuation force should be exactly at half the length of the wire spring. Therefore the demand that the lateral displacement should be smaller than  $1e-10$  in combination with a line of action crossing the wire spring at half its length determine the width of sliding body.

#### Determination of length of wire springs

By estimation, the maximum range of the pre-sliding regime will be maximally several micrometers. The sensors have a resolution in the order of  $1e-9$  m. By choosing the maximum admissible lateral

displacement of mass in the order of  $1e-10$ , the lateral motion will not influence the measurements by the capacitive sensor.



$$\left. \begin{array}{l} 1) \quad x = R \sin \theta \\ 2) \quad y' = R(1 - \cos \theta) \end{array} \right\} \frac{x}{y'} = \frac{\sin \theta}{(1 - \cos \theta)} \rightarrow \theta = 2 \tan^{-1} \left( \frac{x}{y'} \right)$$

Substitution:

$$R = \frac{x}{\sin \theta} = \frac{x}{\sin \left( 2 \tan^{-1} \left( \frac{x}{y'} \right) \right)}$$

Where:

- $x$ : The longitudinal displacement off the sliding body ( $m$ )
- $R$ : The length of the wire springs ( $m$ )
- $\theta$ : Deflection angle of the wire springs (Rad)
- $y'$ : The lateral displacement ( $m$ )

For a maximum longitudinal displacement ( $x$ ) of  $5e-6 \text{ m}$  and a maximal lateral displacement ( $y'$ ) of  $2.5e-10 \text{ m}$  the above results in a spring length ( $R$ ) of exactly  $0.05 \text{ m}$ .

*Determination of properties of the wire springs*

From [Koster, Constructies voor het nauwkeurig positioneren en bewegen] the following equations are obtained for calculation of the properties of the wire spring:

$$\text{Axial stiffness (N/m)} \quad \frac{EA}{l} = \frac{E \pi d^2}{4l}$$

$$\text{Perpendicular stiffness (N/m)} \quad \frac{72EI}{5l^3} \approx 0.6 \frac{Ed^4}{l^3}$$

$$\text{Bendingstress (N)} \quad \frac{3Edz}{l^2}$$

$$\text{Buckle load (N)} \quad \frac{4\pi^2 EI}{l^2}$$

Where:

- $E$ : The modulus of elasticity ( $Pa$ )
- $A$ : The cross sectional area of the wire ( $m^2$ )
- $l$ : The length of the wire spring ( $m$ )
- $d$ : The diameter of the wire ( $m$ )
- $z$ : The longitudinal displacement of the sliding body

When implementing the above equations in Matlab for a stainless steel wire spring with a length of  $0.05 \text{ m}$  and a diameter of  $0.2 \text{ mm}$  the following properties were obtained.

- Axial stiffness ( $c_x$ ):  $1.2566e5 \text{ N/m}$
- Perpendicular stiffness ( $c_z$ ):  $1.5360 \text{ N/m}$
- Bendingstress ( $\sigma_\psi$ ):  $2.4000e5 \text{ N}$
- Maximum buckle load ( $F_k$ ):  $0.2481 \text{ N}$

The Matlab-file for calculation of the wire spring properties is presented below:

```

%% Calculation of properties of the wire springs
clc; clear all

% length
l = 0.05; % m

% Diameter
d = 0.2e-3; % m

% Modulus of elasticity stainless steel
E_ss = 200e9; % Pa

% Density stainless steel
ro_ss = 7800; % kg/m^3

% Cross sectional area
A = pi*(0.5*d)^2; % m^2

% mass
m = ro_ss*A*l; % kg

% inertia
Inertia = (pi*r^4)/4; % m^4

% Maximum longitudinal displacement
z_max = 5e-6; % m

% Perpendicular stiffness
c_x = E_ss*A/l; % N/m

% Axial stiffness
c_z = 0.6*((E_ss*d^4)/l^3); % N/m
c_z_2 = (72/5)*((E_ss*Inertia)/l^3); % N/m

% Maximum bendingstress
s_psi = (3*E_ss*d*z_max)/l^2; % N

% Maximum buckle load
F_k = (4*pi^2*E_ss*Inertia)/l^2; % N

```

*Calculation of maximum spring force at maximum longitudinal displacement.*

When implementing the perpendicular stiffness obtained in the calculations below, the maximum actuation force absorbed by the wire springs can be calculated according to:

$$\begin{aligned}
 dx_{\max} &= 5e^{-6}m \\
 c_z &= 1.5360 \text{ N/m} \\
 F_v &= 2 \cdot c_z \cdot dx_{\max} \\
 F_v &= 2 \cdot 1.5360 \cdot 5e^{-6} = 1.536e^{-5}N
 \end{aligned}$$

Where:

$dx_{\max}$ : The maximum longitudinal displacement ( $m$ )  
 $c_z$ : The stiffness of the wire spring ( $N/m$ )  
 $F_v$ : The spring force at  $x = dx_{\max}$  ( $N$ )

The maximum actuation force ( $F_v$ ) absorbed by the wire springs is very small and therefore can be ignored in the calculation of the force-displacement curve obtained by the experiments.

*Determination of maximum angle of misalignment of the actuation system*

The maximum force that can be generated by the piezo-spring combination amounts to 3 N. Considering the maximum buckle load of the wire springs in combination with the maximum actuation force that can be generated by the actuation system the maximum angle of misalignment of the actuation system can be determined:

$$F_{act} = 3N$$

$$F_k = 0.2481 N$$

$$dx = 5.0 \cdot 10^{-6} m$$

$$F_y = F_{act} \sin \alpha$$

$$\alpha_{max} = \sin^{-1} \left( \frac{F_y}{F_{act}} \right) - dx = \sin^{-1} \left( \frac{0.2481}{3} \right) - 5.0 \cdot 10^{-6} = 7.12^\circ$$

Where:

$F_{act}$ : The actuation force (N)

$F_k$ : The buckling load (N)

$F_y$ : The lateral force due to misalignment of the piezo (N)

$\alpha_{max}$ : The maximum angle of misalignment (rad)

When considering a maximum displacement of the sliding body of 5  $\mu m$  the maximum angle of misalignment for the actuation system ( $\alpha_{max}$ ) is determined at 7.12°.

## A.2 Material properties

The material properties of the materials used in this measurement setup are:

Name (werkstof nr.)	Part	Modulus of elasticity	Coefficient of thermal expansion	density
AL7075 (3.4365)	All	72000 Mpa	23.5 $\mu m m^{-1} K^{-1}$	2810 kg m <sup>-3</sup>
C45 (1.0503)	Ground surface	205000 Mpa	11.5 $\mu m m^{-1} K^{-1}$	7850 kg m <sup>-3</sup>
Rg7 (2.1090)	Sliding body	102000 Mpa	18.0 $\mu m m^{-1} K^{-1}$	8800 kg m <sup>-3</sup>

When measuring at nano-scale, temperature influences from the surroundings and deflections of the structure due to the load can not be ignored. In this paragraph the influence of temperature differences on the expansion of the materials is determined. Furthermore the minimum thickness of the base plate is determined.

### Determination of the influence of temperature differences

Due to temperature differences the materials used in the measurement setup will expand or shrink. This will have its effect on the output of the capacitive sensors. In order to minimize the influences of the temperature differences the following can be done:

- Compensation of the output of the sensors for the temperature differences measured during the experiments. This requires a highly accurate thermometer and all the materials thermal expansion coefficients to be known.
- The use of as little as possible different materials. If all the materials have the same thermal expansion coefficient, the temperature differences will not influence the output of the sensors.
- When using different materials; choose the materials carefully. When the differences in expansion coefficients are small. The influence of temperature differences can be neglected since they will be smaller than the sensor resolution.

The best option would be to use only one material for the measurement setup. However, since the material of the sliding body will be bronze and the material of the ground surface of high carbon steels this is not an option. Since all the sensors will be mounted on the base which is made of AL7075 aluminium, only the influence of temperature on the aluminium and bronze sliding body should be determined. This is done as follows according to the equation for the coefficient of thermal expansion:

$$\alpha = \frac{1}{l_0} \frac{dl}{dT}$$

Where:

$\alpha$ : The Coefficient of thermal expansion ( $mK^{-1}m^{-1}$ )

$l_0$ : The length of the material in direction of expansion ( $m$ )

$T$ : The temperature ( $^{\circ}$ )

From this equation the influence of a temperature change of 1 degree on the distance between the sensor and the sliding body is determined.

$$dT (\alpha_{base} \cdot l_{base} - \alpha_{mass} \cdot l_{mass}) = dx$$

$$(23.5e^{-6} \cdot 70e^{-3} - 18e^{-6} \cdot 40e^{-3}) = 7.2e^{-7} m$$

The calculated change of distance for 1 degree of temperature change ( $7.2e-7 m$ ) between the sensor and the measured surface of the mass will certainly be measured. Therefore it is necessary to keep the experiments over a short interval. The temperature drops over the short interval will be very small and therefore they will not influence the outcome of the experiment.

**Determination of minimal thickness base plate.**

From the equation for the deflection of a beam and that is clamped on both ends the maximum thickness for the aluminium base plate can be determined according to:

$$w = \frac{1}{48} \frac{Fl^3}{EI} =$$

$$I_{doorsnede} = \frac{b \cdot h^3}{12} =$$

$$h = \sqrt[3]{\frac{F_n \cdot l^3}{4 \cdot E \cdot b \cdot w}} =$$

Where:

- $w$ : The deflection of the beam in the middle between the clamped points ( $m$ )
- $F_n$ : The resultant of the normal loads of the beam at  $\frac{1}{2} l$  ( $N$ )
- $E$ : The modulus of elasticity of AL7075 ( $Pa$ )
- $I$ : The inertia of mass ( $m^4$ )
- $b$ : The width of the beam ( $m$ )
- $h$ : The thickness of the beam ( $m$ )

Since only the mass of the sliding body will change during the experiments the difference between the lightest and heaviest mass is the only resultant normal force that is influencing the measurement output of the sensors. The lightest mass has a weight of 0.352  $kg$  while the heaviest has a weight of 0.690  $kg$ . Therefore  $F_n$  will be:

$$F_n = g \cdot dm$$

$$F_n = 9.81 \cdot (0.690 - 0.352) = 3.32N$$

Where:

- $g$ : The gravitational acceleration ( $m/s^2$ )
- $dm$ : The maximum change of mass ( $kg$ )

The supports of the base plate are located at a distance of 0.4  $m$  from each other. Therefore  $l$  will be 0.4  $m$ .

The centre of mass of the sliding body is located at  $\frac{29}{50}$  of  $l$ . Therefore  $F_n$  will be:

$$\frac{29}{50} \cdot 0.4 \cdot 3.32 = 0.2 \cdot F_n$$

$$F_n = 3.85N$$

When implementing the above in Matlab the following for a maximum allowable deflection of  $1e-10$   $m$  the value for the thickness of the base plate is obtained.

$$h = 0.0153 m.$$

The Matlab-file is presented below.

```

%% Calculation minimum thickness base plate
clc; clear all;

% Modulus of elasticity
E = 0.72e9; % GPa

% Maximum allowable deflection
w_max = 1e-10; % m

% Length base
l = 0.4; % m

% Width base
b = 0.240; % m

% Normal load by mass
F_n = 3.85; % N

% Minimum thickness
h = ((F_n*l^3)/(4*E*b*w_max))^(1/3) % m

```

### Frictional coefficient steel on bronze

The SKF catalogue ‘SKF spherical plain bearings and rod ends’ gives the following guidelines for the frictional coefficients for not lubricated metal-metal sliding bearings.

Sliding contact surface combination	Coefficient of friction $\mu$	
	min	max
Steel-on-steel	0,08	0,20
Steel-on-bronze	0,10	0,25
Steel/sinter bronze composite	0,05	0,25
Steel/PTFE fabric	0,03	0,15
Steel/PTFE composite	0,05	0,20

Figure 2: Coefficients of friction for dry sliding contacts.  
From [www.skf.com](http://www.skf.com).

**Spring specifications**

The specifications of the spring used in the actuation system are presented below. The spring is designed in such a way that it generates a maximum force of 3 N at a compression of 30  $\mu\text{m}$ .

		<b>Verenfabriek Roveron B.V.</b>				
		Graafstroomstraat 15-17				
		3044 AN Rotterdam				
		The Netherlands				
Tel:	+31-(0)10-4152577	Date:	11-11-2009			
Fax:	+31-(0)10-4379801	Time:	15:17:11			
E-mail:	info@roveron.nl	Initials:				
<b>Spring Type</b> Round Wire Compression			<b>Calculated Data</b>			
Designed To:	EN 13906-1: 2002	Solid Length:	15,00	mm		
Tolerance Standard:	DIN 2095 / 2096	Min. Length (static):	16,22	mm		
		Min. Length (dynamic):	16,82	mm		
		Solid Load:	290,09	N		
		Solid Stress:	449,14	N/mm <sup>2</sup>		
		Stress Factor:	1,41			
		Active Coils:	4,00			
		Spring Index:	3,80			
		Helix Angle:	5,98	Deg		
		Buckling Possible:	Not Applicable			
		Buckling Definite:	Not Applicable			
		Spring Pitch:	3,13	mm		
		Inside Diameter:	7,00	mm		
		Outside Diameter::	12,00	mm		
		Wire Length:	179,93	mm		
		Weight / 100:	0,693	Kg		
		Natural Freq:	150672	RPM		
<b>Material</b>						
EN 10270 P11 Patented Carbon						
Youngs Mod (E):	206000	N/mm <sup>2</sup>				
Rigidity Mod (G):	81500	N/mm <sup>2</sup>				
Density:	,00000785	Kg/mm <sup>3</sup>				
Unprestress:	0-45	%				
Prestress:	45-56	%				
<b>End Type:</b> Closed and Ground						
Dead Coils:	2,00					
Tip Thickness:	50,00	%				
End Fixation:	Fixation not known					
<b>Design Parameters</b>						
Wire Diameter:	2,50	mm				
Mean Coil Dia.	9,50	mm				
Total Coils:	6,00					
Spring Rate:	116,04	N/mm	(Calculated)			
Free Length:	17,50	mm				
<b>Stress Data</b>						
			Operating Positions			
	Lower Tensile	Solid	% Tensile	1	2	3
SL	1460	31 U	0 U	0 U	0 U	0 U
SM	1690	27 U	0 U	0 U	0 U	0 U
DM	1690	27 U	0 U	0 U	0 U	0 U
SH	1900	24 U	0 U	0 U	0 U	0 U
DH	1900	24 U	0 U	0 U	0 U	0 U
Specified						
<b>Operating Data</b>						
			Operating Positions			
			1	2	3	
Length (mm)			17,47	17,48	17,47	
Load (N)			3,00	2,90	3,10	
Deflection (mm)			0,0259	0,0250	0,0267	
Stress (N/mm <sup>2</sup> )			5	4	5	
Stress % Solid			1	1	1	
Load Tol. Grade 1 (N)			32,62	32,62	32,62	
Load Tol. Grade 2 (N)			51,78	51,78	51,78	
Load Tol. Grade 3 (N)			82,85	82,85	82,85	
O.D. Expansion (mm)			0,000247	0,000238	0,000255	

Software Copyright © 2002-2008 Institute of Spring Technology, Sheffield, UK (V7.50)

Figure 3: Properties of the actuation spring

### A.3 Drawings

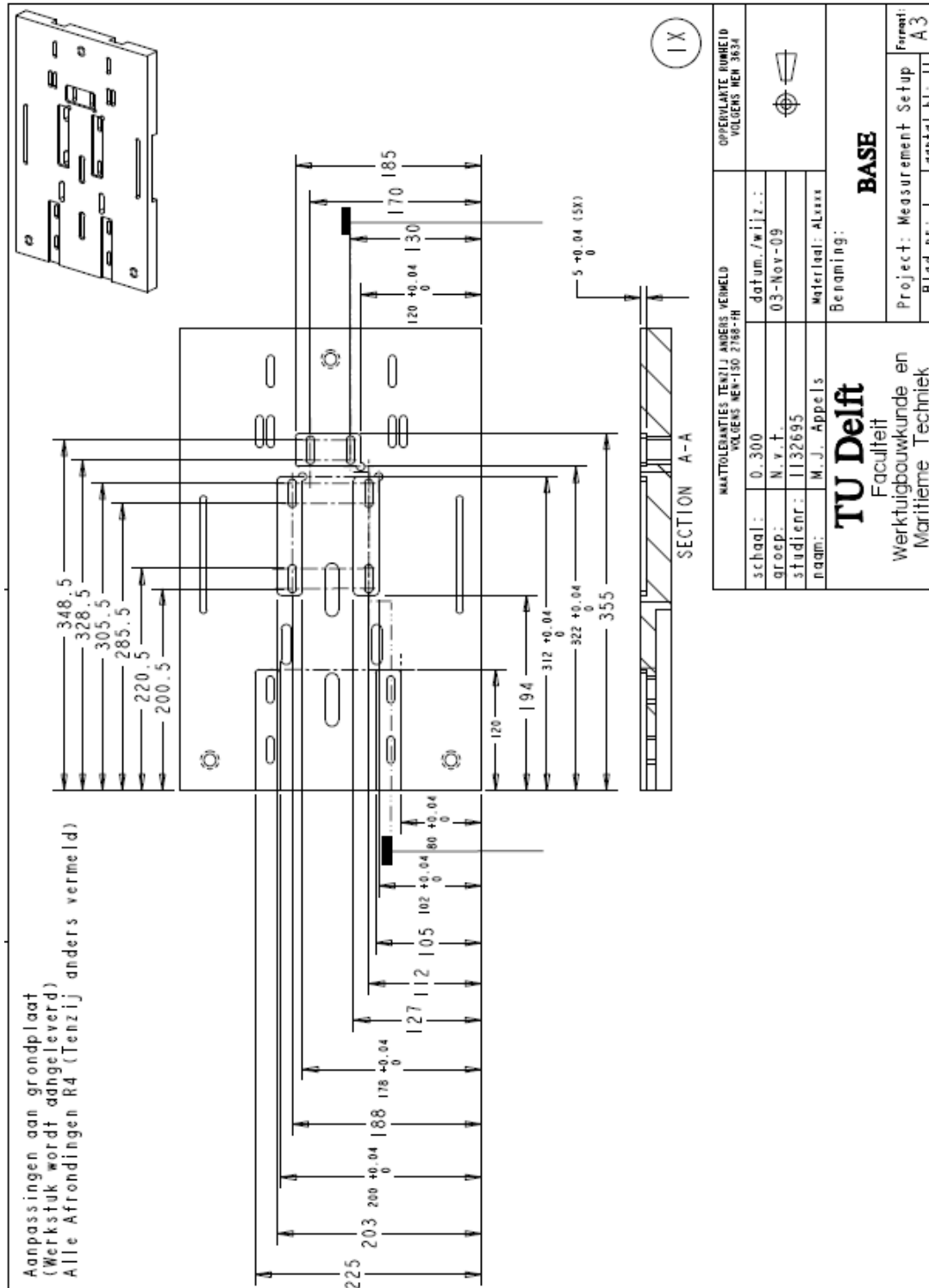
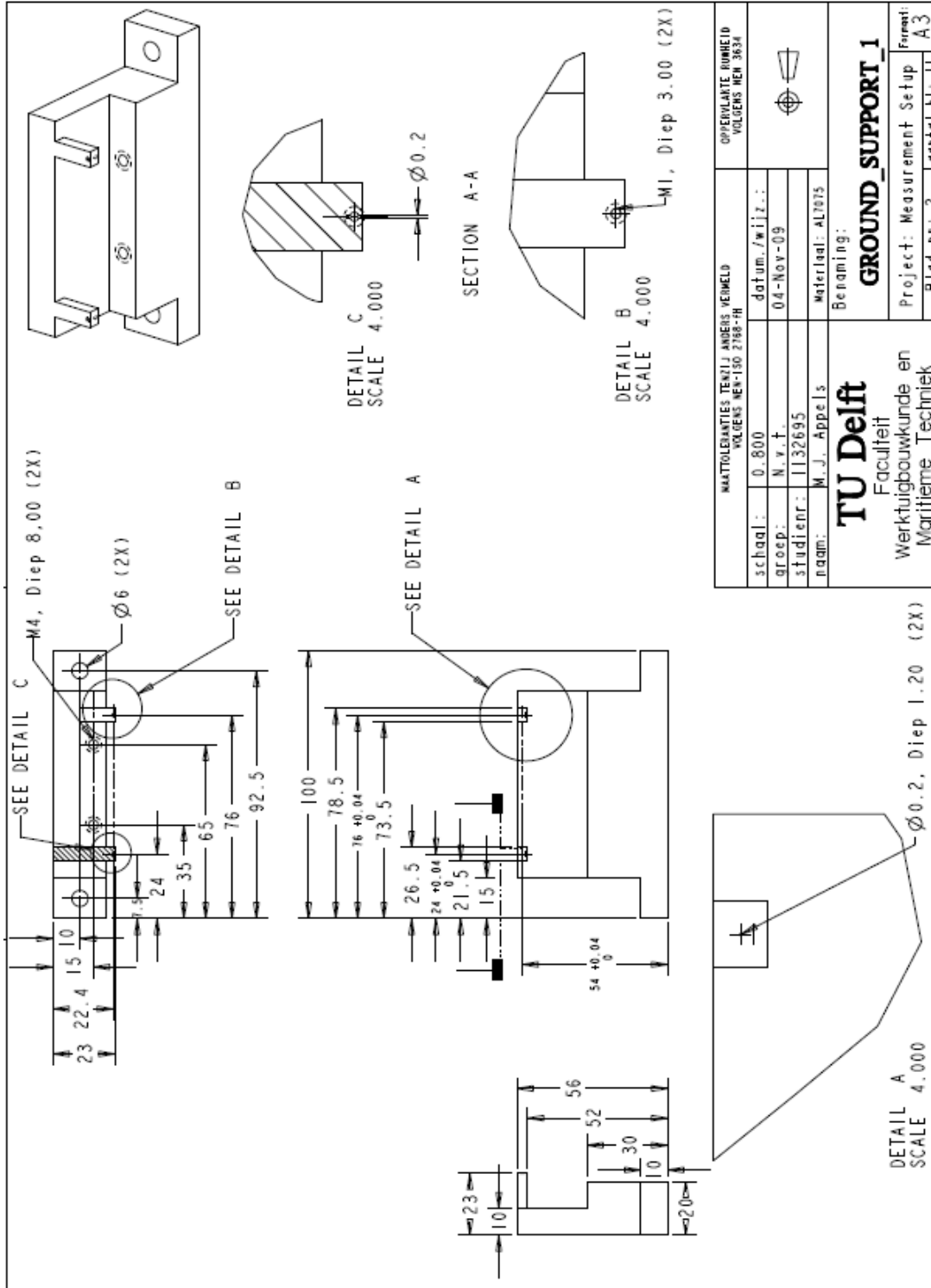


Figure 4: Pro Engineer drawing of the Base



MAATTOEGELIJKHEID TENZIJ ANDERS VERMELD VOLGENS NEN-ISO 2768-MS		OPPERVLAKTE RUWHEID VOLGENS NEN 3654	
schaal:	0.800	datum./wijz.:	
groep:	N.v.t.	04-Nov-09	
studienr.:	1132695	material:	AL7075
naam:	M.J. Appels	Benaming:	<b>GROUND_SUPPORT_1</b>
TU Delft Faculteit Werktuigbouwkunde en Maritieme Techniek		Project:	Measurement Setup
		Blad nr.:	2
		Formaat:	A3
		aanb. nr.:	2
		aanb. bl.:	11

Figure 5: Pro Engineer drawing of Ground support

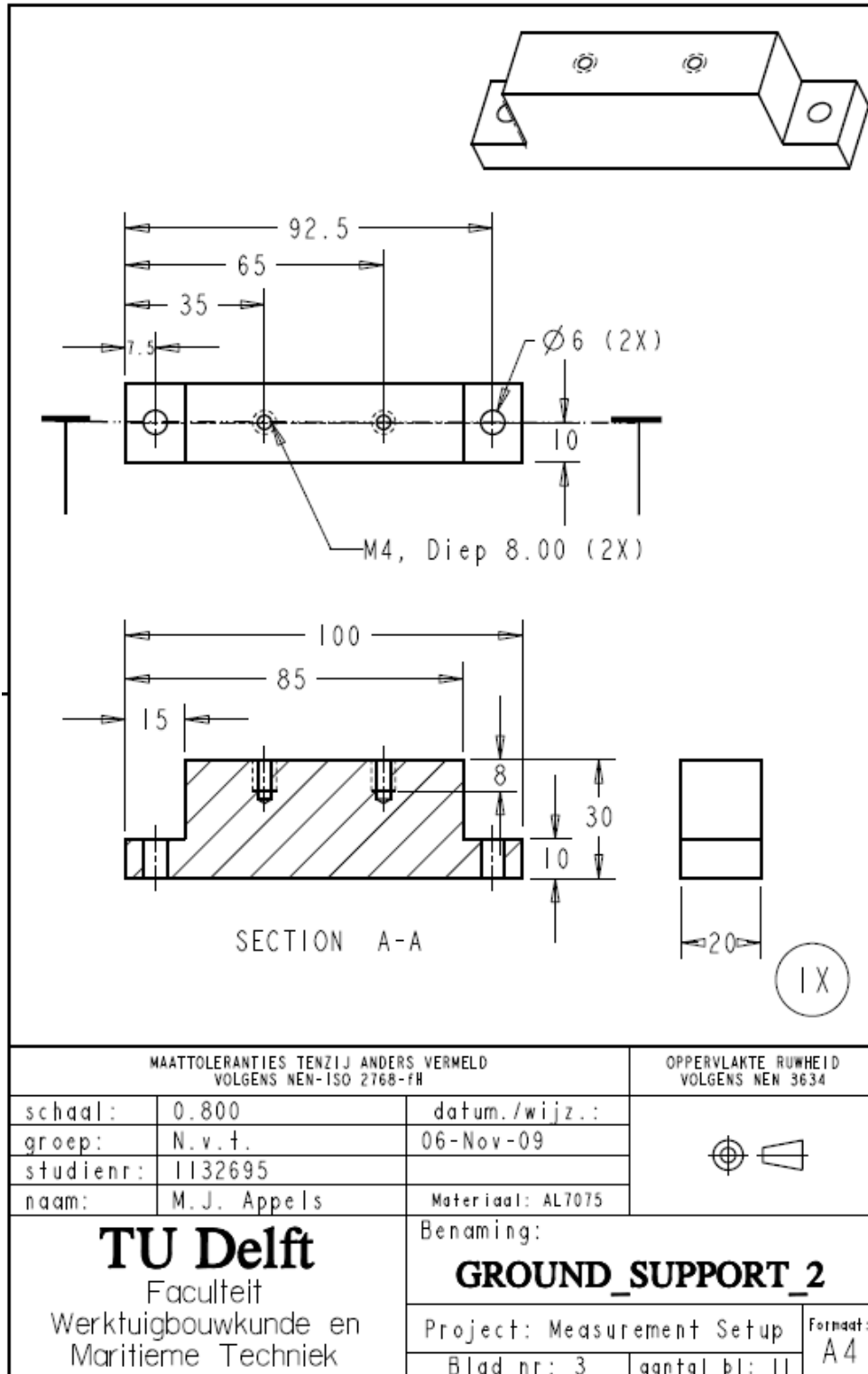


Figure 6: Pro Engineer drawing of Ground support 2

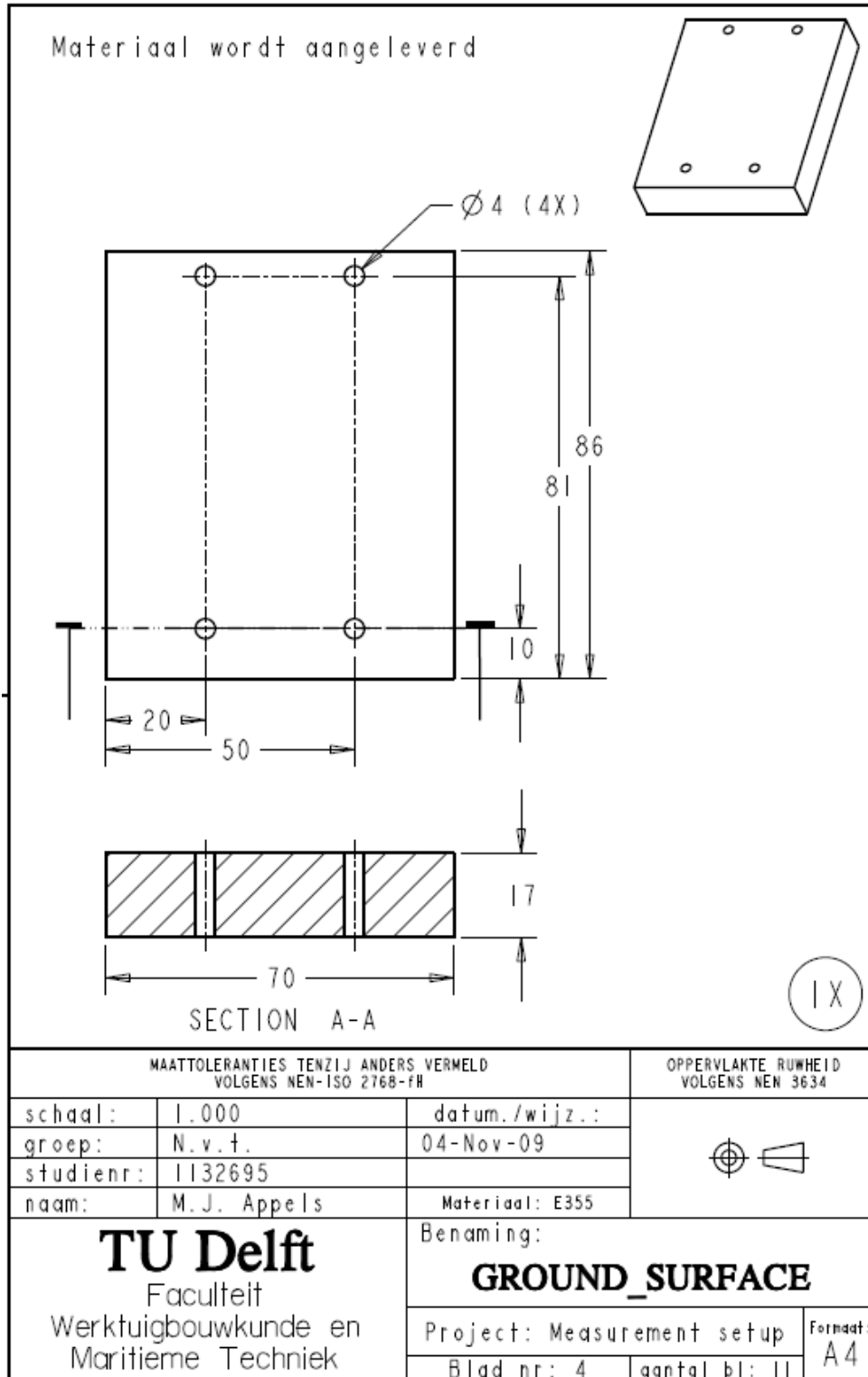


Figure 7: Pro Engineer drawing of the Ground surface



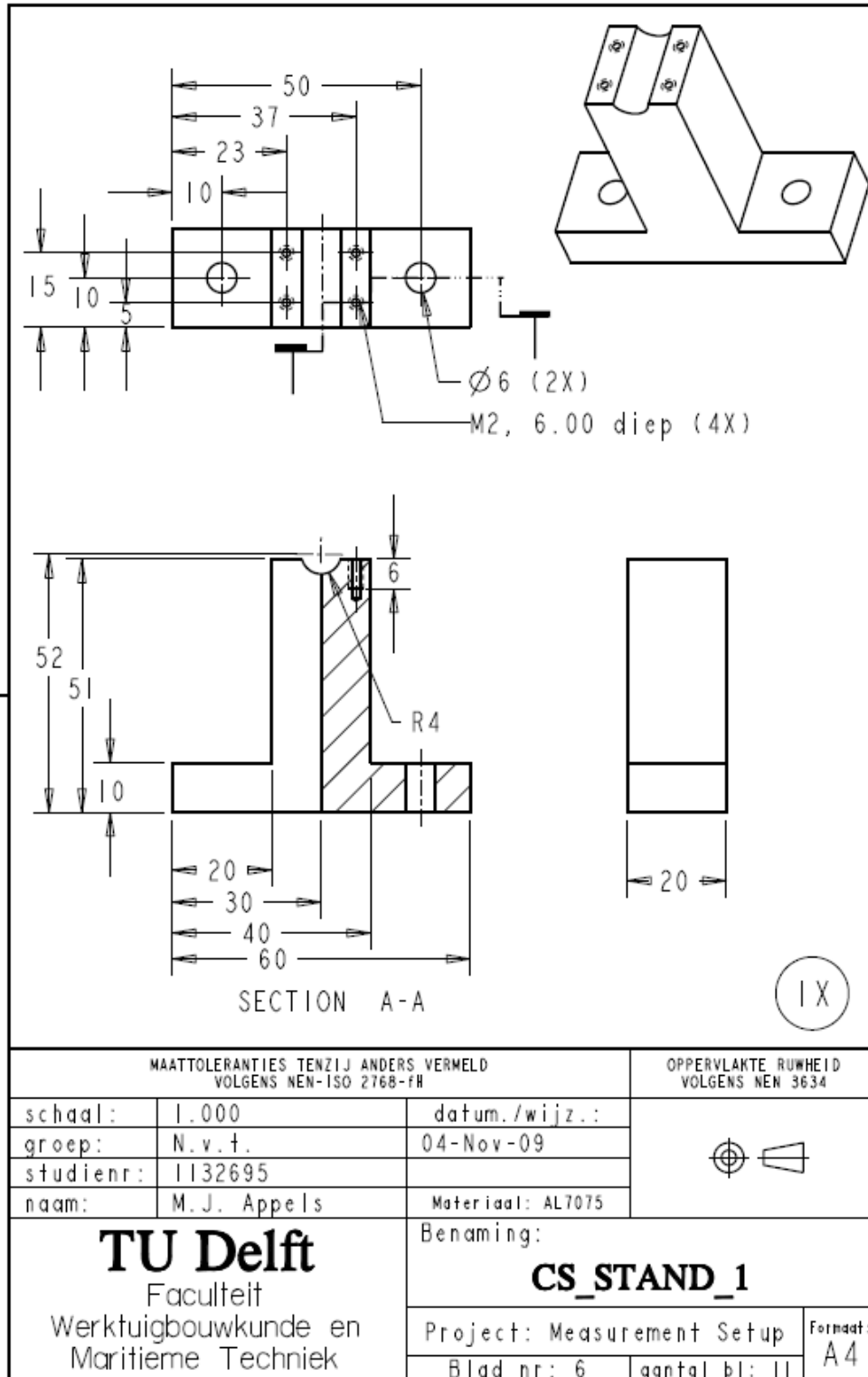


Figure 9: Pro Engineer drawing of the stand of the capacitive sensor measuring the displacement of the sliding body.

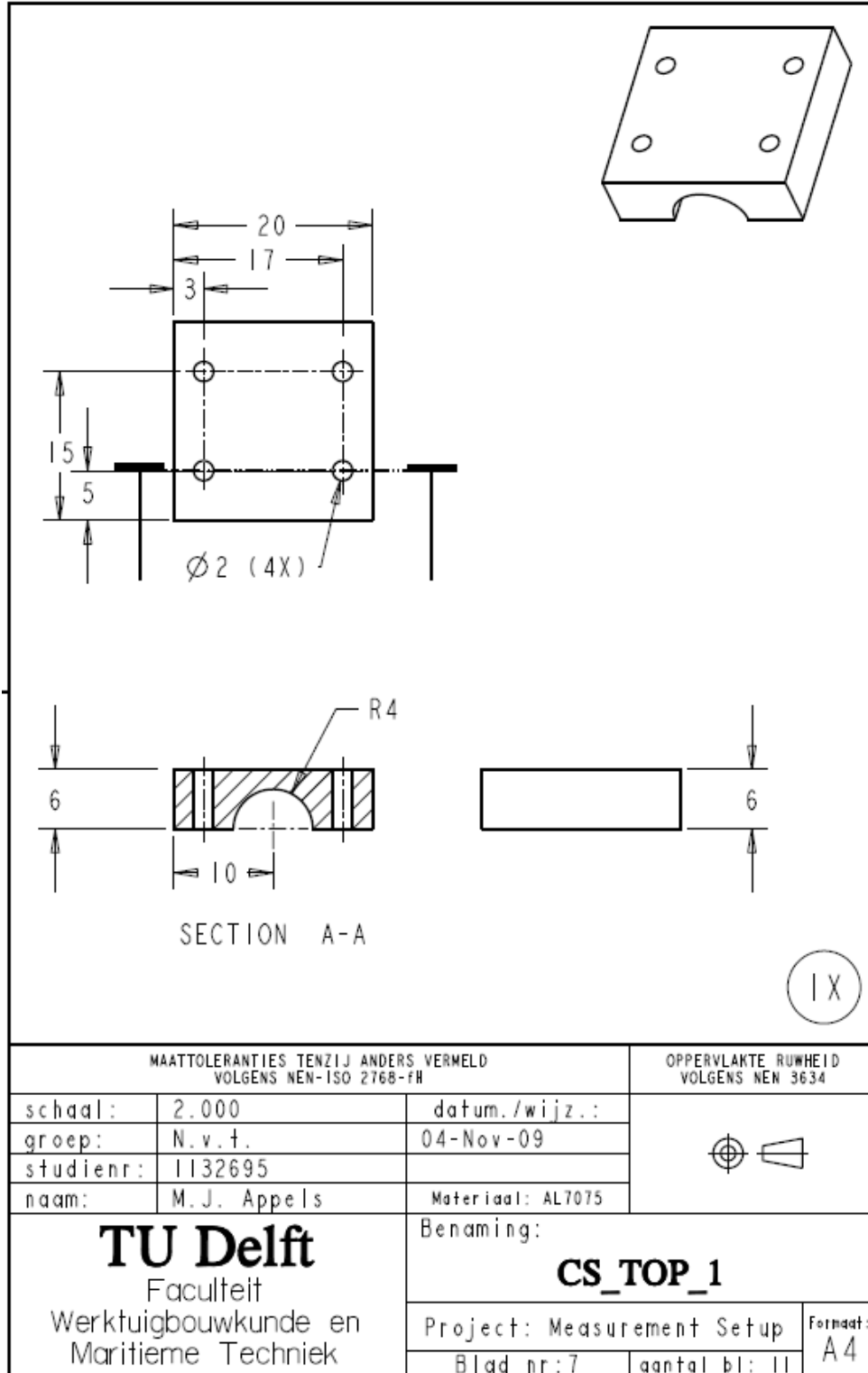


Figure 10: Pro Engineer drawing of the top of the stand of the capacitive sensor measuring the displacement of the sliding body.

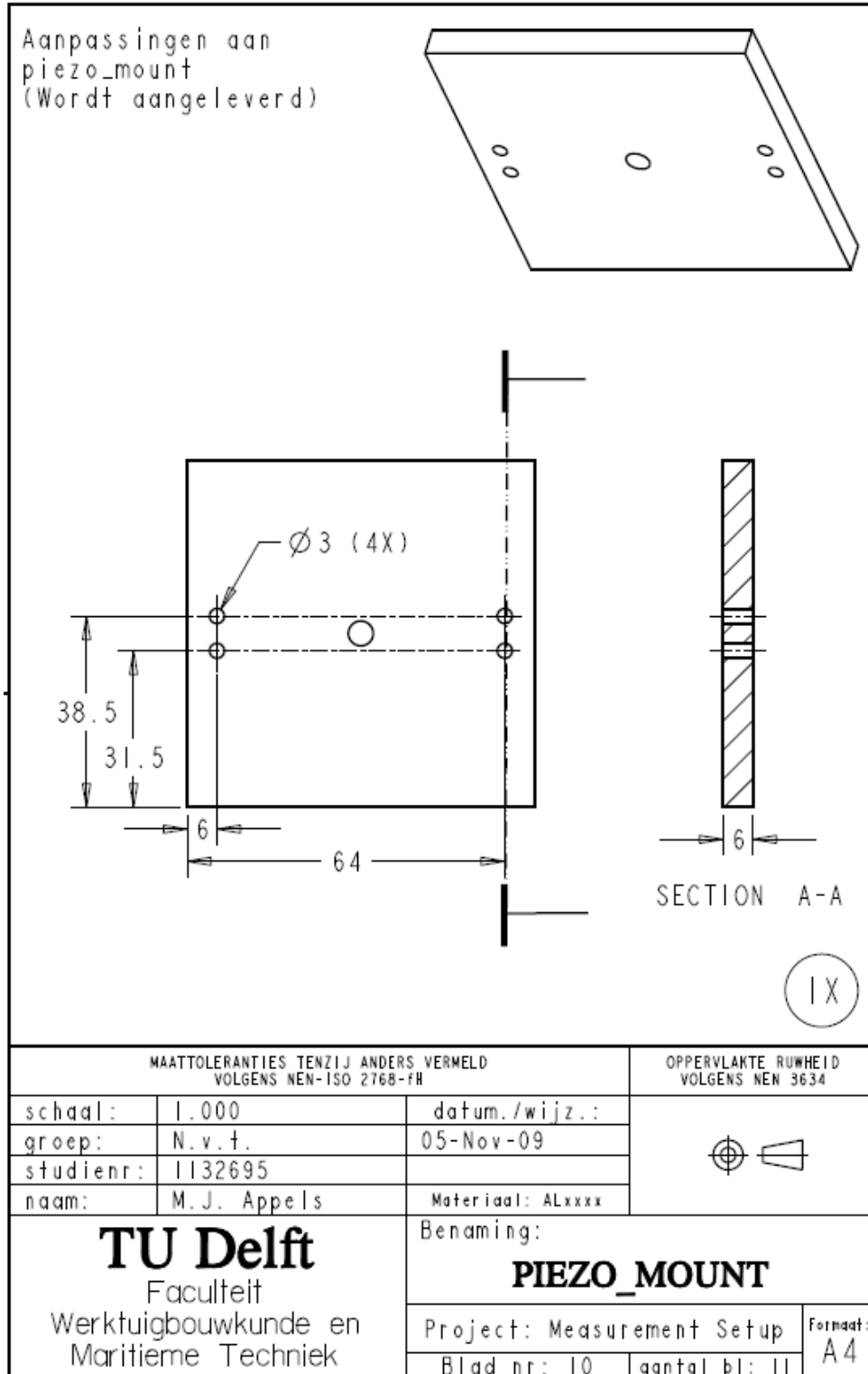


Figure 11: Pro Engineer drawing of the piezo mount.

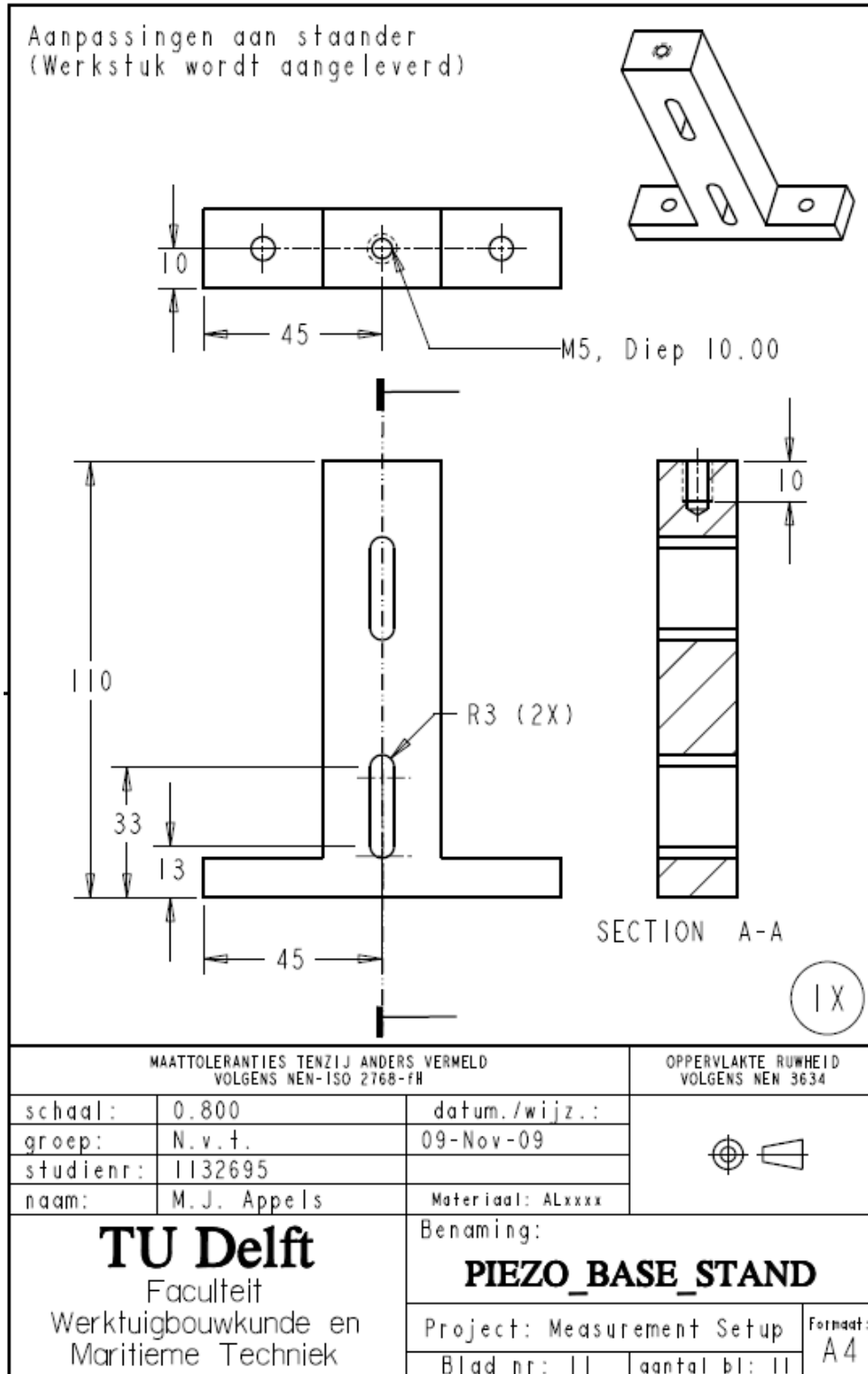


Figure 12: Pro Engineer drawing of the piezo base stand

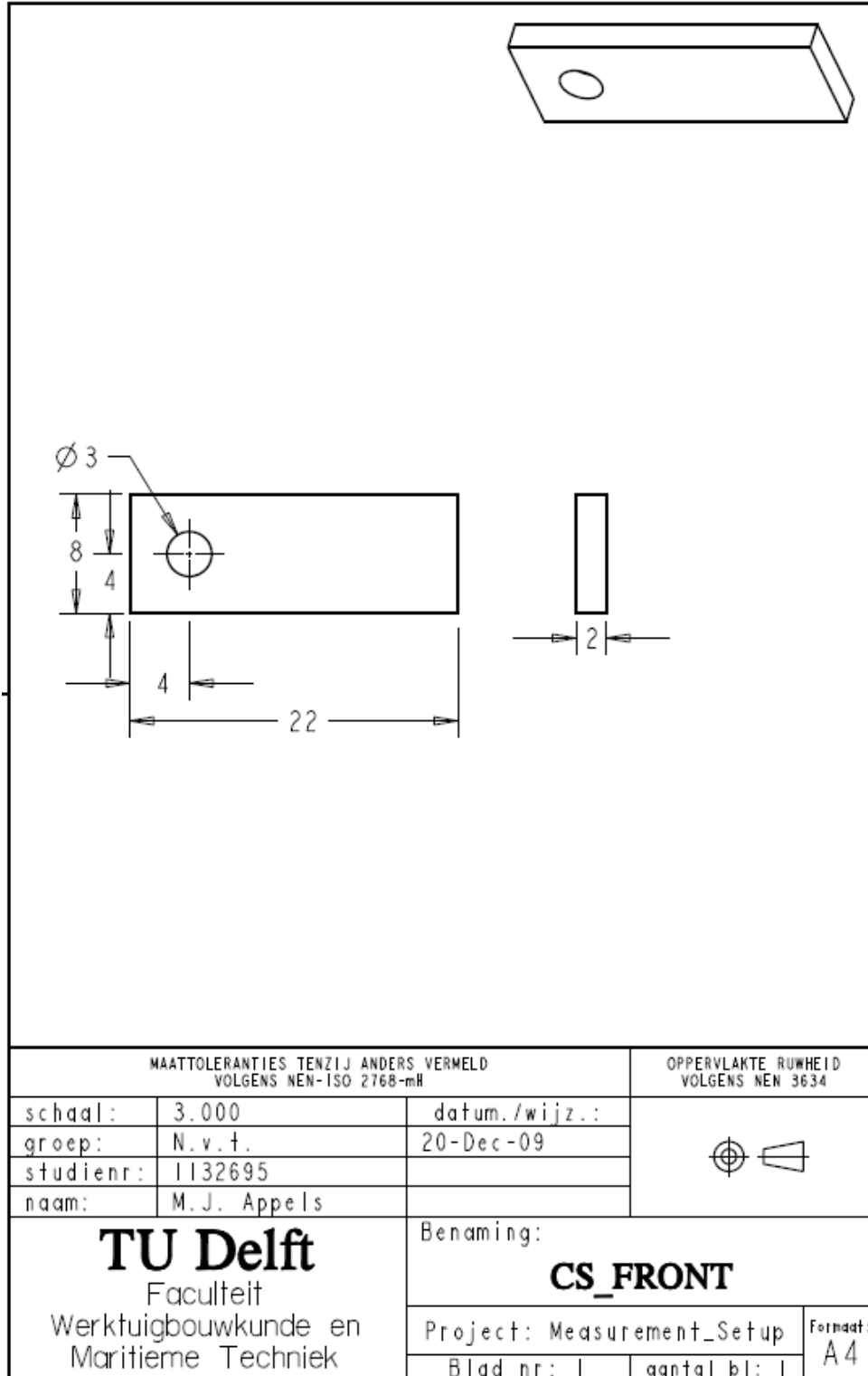


Figure 13: Pro Engineer drawing of the front of the capacitive sensor for measuring piezo elongation.

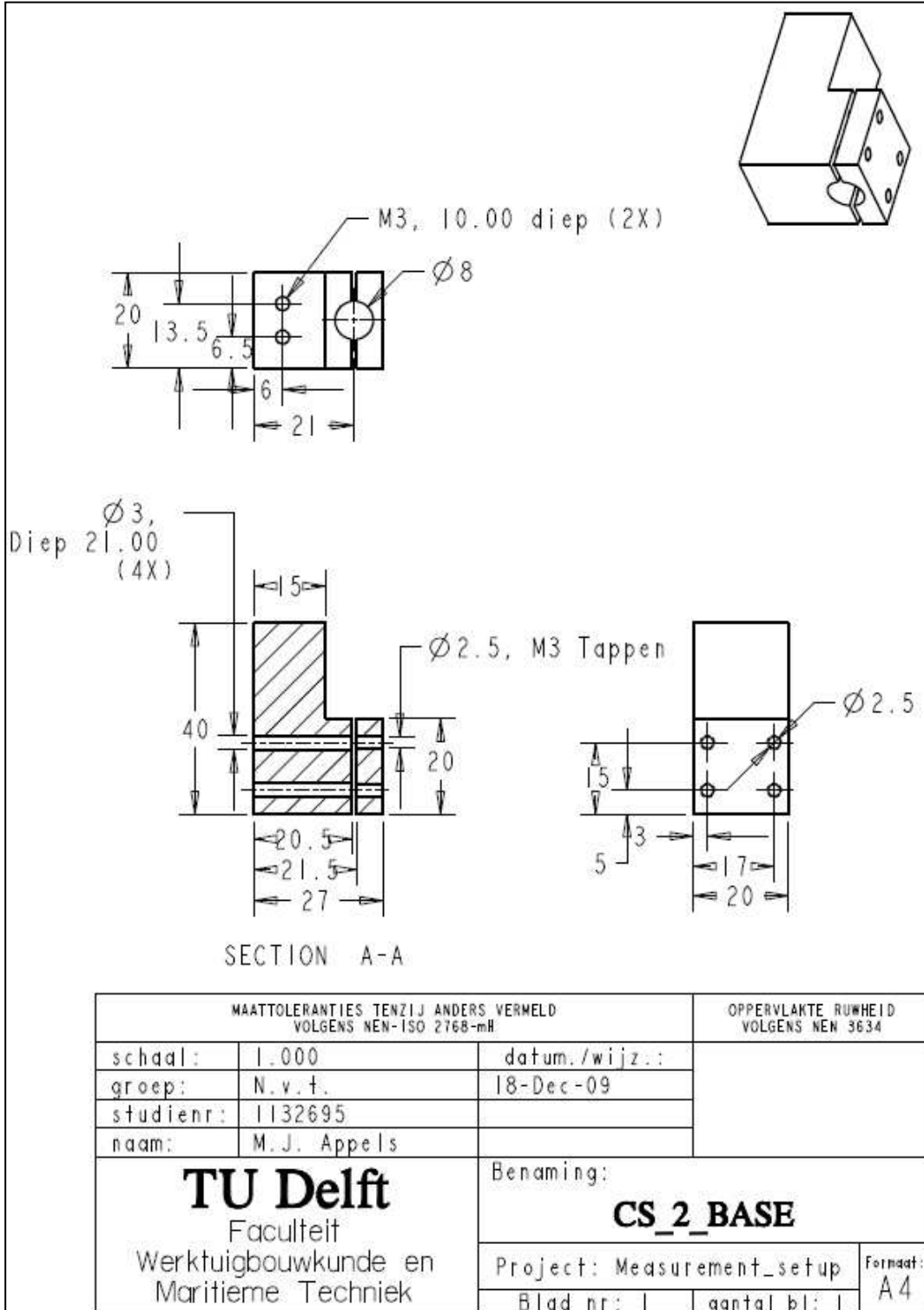


Figure 14: Pro Engineer drawing of the stand of the capacitive sensor measuring the elongation of the piezo.

## A.4 Photo's

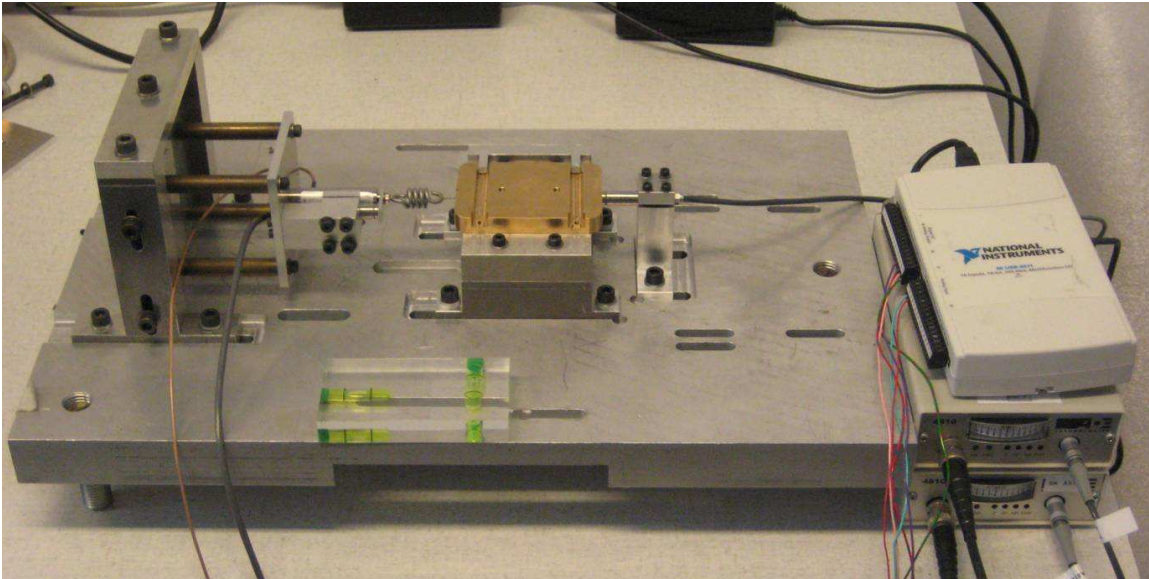


Figure 15: Measurement setup. On the right 2 microsense 4810 amplifiers with on top the NI A/D converter.

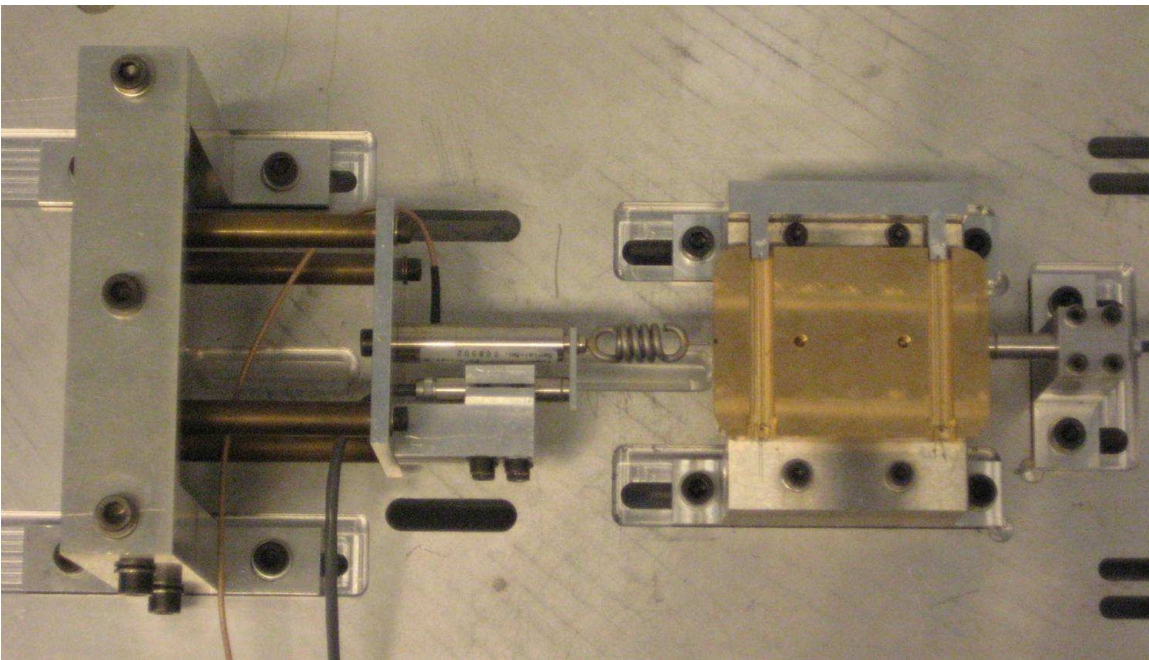


Figure 16: Top view of the measuring setup. From left to right; the piezo base stand, the piezo stack actuator with spring (with capacitive sensor below), the sliding body on top of the ground surface and the stand with the capacitive sensor measuring the displacement of the sliding body.

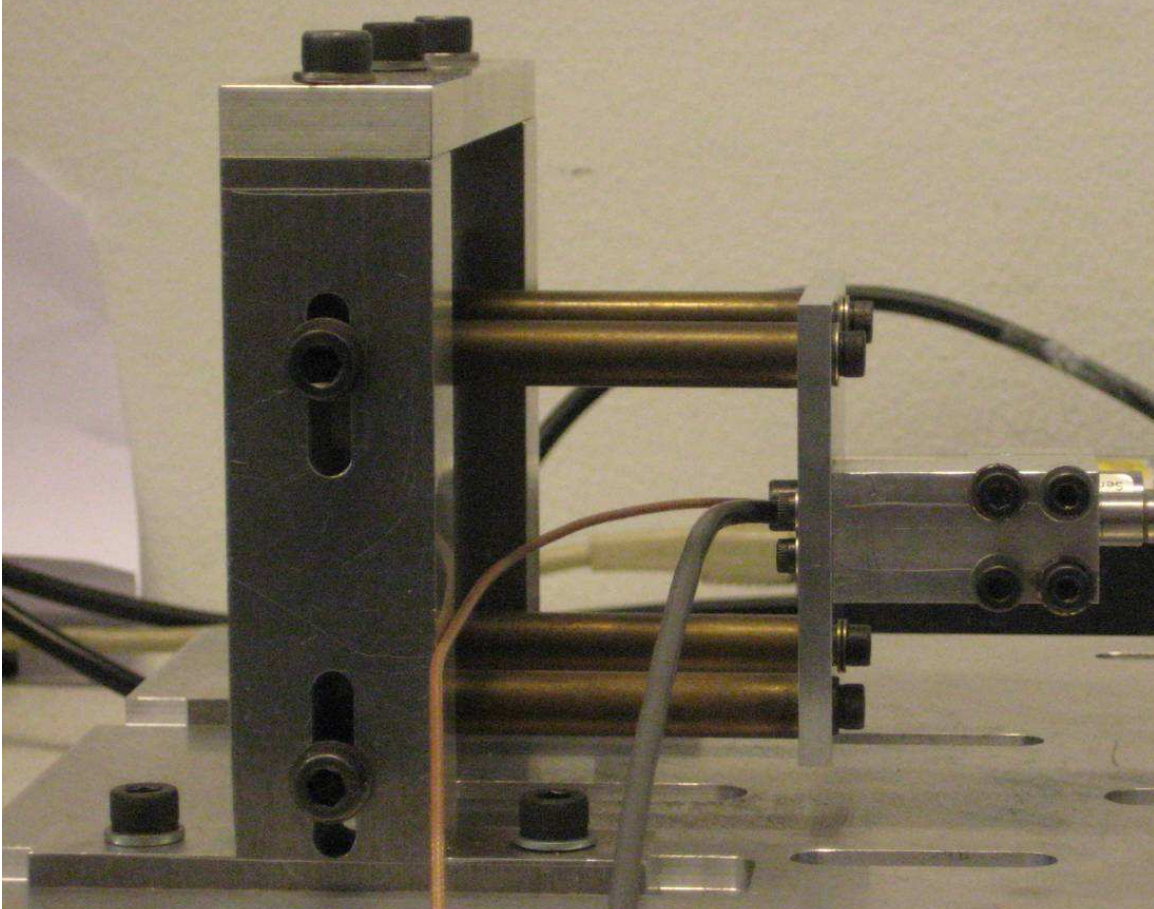


Figure 17: Piezo base stand with the stand holding the capacitive sensor measuring the piezo elongation.

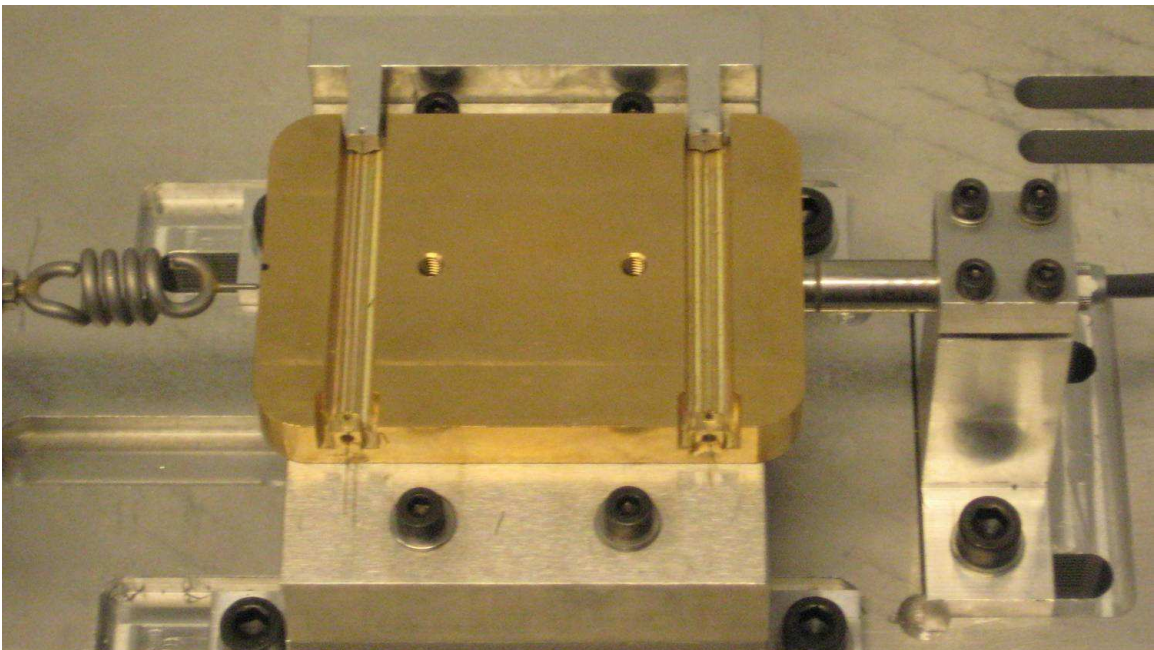


Figure 18: Sliding body with linear guidance.

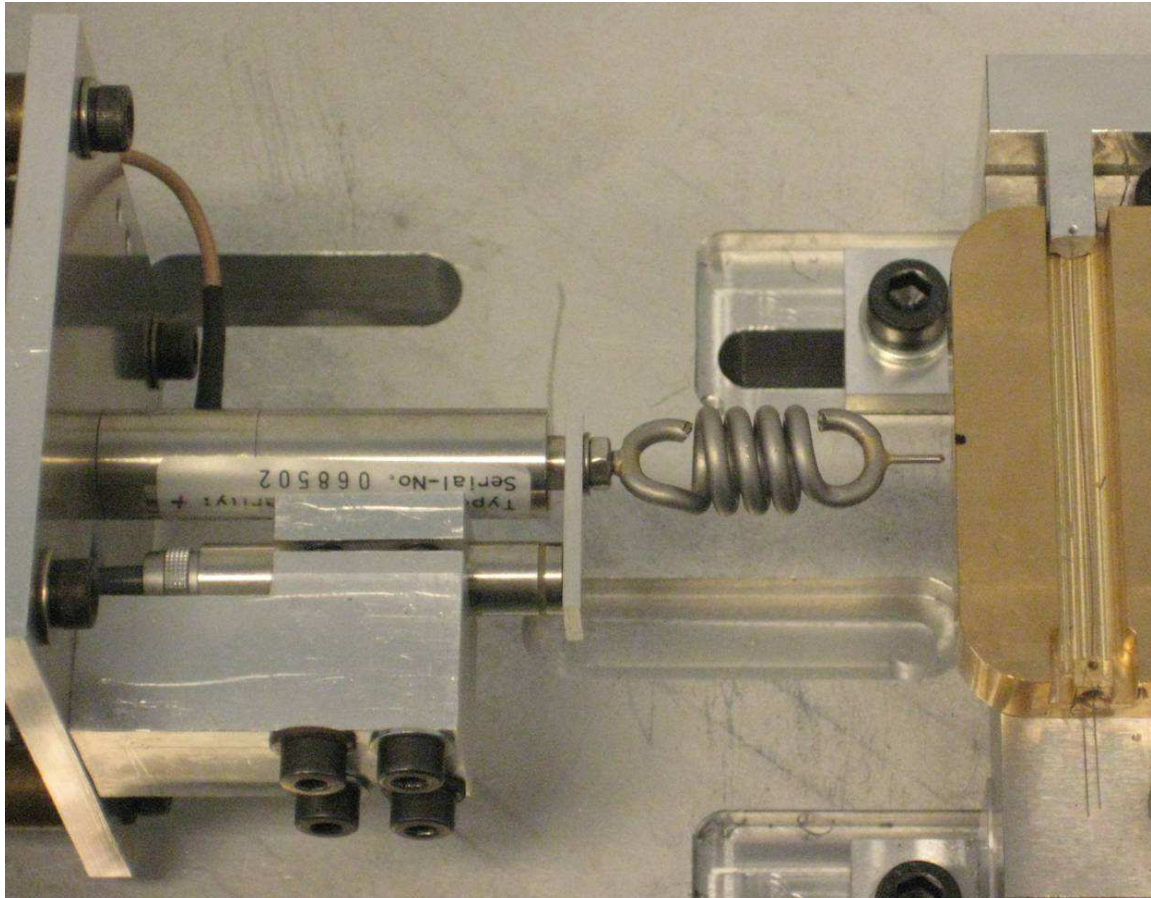


Figure 19: Piezo stack actuator with spring and capacitive sensor below

## Appendix B – Measurement equipment

In this section the technical specifications of the capacitive sensors, the piezo stack actuator, their amplifiers, the a/d converter and the computer used for the experiments are presented.

### B.1 Capacitive position sensors

4810

#### Non-Contact Capacitance Gauging Instrument & Series 2800 Capacitive Probes



**Description**

The 4810 is a single channel instrument that provides an analog display of probe displacement on the front panel. The 4810 provides analog output via a BNC jack on the front panel for easy connection to oscilloscopes, spectrum analyzers or computer based A/D boards. The 4810, along with the 2800 series family of standard and custom probes, uses an advanced capacitive gauging technology to provide exceptional resolution, large operating ranges and large standoff distances. The large, easy-to-read front panel display makes the 4810 an ideal production tool for operations requiring visual verification of measurements.

**Applications**

- Non-contact, non-destructive measurements
- Precision dimensional gauging
- X-Y positioning
- Real-time in-process measurements
- Slide and spindle runout
- In-process sheet thickness
- Vibration analysis
- Servo-loop positioning systems
- Wear measurements
- Precision alignment
- Ultra high vacuum measurements
- Ultra high stability
- Go/no go gauging

**Features**

Sub nanometer resolution for ultra-precise measurements

Exceptional temperature stability for a wide variety of environmental measurement applications

Wide variety of precision capacitive sensors for measuring even the most difficult size and shape target

Standard analog outputs for easy connection to A/D boards

Large standoff distances allow safe gauging of delicate parts

Superior price/performance

Patented PhaseLock™ probe driver circuitry for improved accuracy on ungrounded targets and applications such as thickness

Selectable filters for maximum resolution: 10 Hz, 100 Hz, 1 kHz, 10 kHz

Probes are interchangeable with straightforward recalibration

Portable, lightweight

**Laser calibration**

High-precision individual unit calibration at factory using ADE-developed laser interferometry system. Calibration traceable to NIST. Performance graph included.

**Options**

**Operating ranges**

- Operating ranges can be user specified to optimize resolution for a specific application.
- Optional “driven target” mode significantly improves resolution.
- Optional Ultra High stability system for the most demanding long term measurements

**Series 2800 probes**

ADE Technologies has developed a new, lower cost family of high performance capacitive sensors providing a greater temperature stability and measurement linearity.

Measurement ranges from 20 microns to 2 millimeters are available in standard products. Custom probe configurations are available to meet unique applications requirements.

- ▲ Sub nanometer resolution for ultra-precise measurements
- ▲ Exceptional temperature stability
- ▲ Wide variety of precision capacitive sensors available
- ▲ Standard analog outputs for easy connection to A/D boards
- ▲ Large standoff distances allow safe gauging of delicate parts
- ▲ Superior price and performance
- ▲ Portable, lightweight



[www.adetech.com](http://www.adetech.com)



## B.2 Piezo Stack Actuator



### P-840 · P-841 Preloaded Piezo Actuators Optional with Integrated Position Sensor



- Outstanding Lifetime Due to PICMA® Piezo Ceramic Stacks
- Travel Range to 90 µm
- Compact Case
- Pushing Forces to 1000 N
- Pulling Forces to 50 N
- Sub-Millisecond Response
- Sub-Nanometer Resolution
- Option: Ball Tip, Vacuum Version

© Physik Instrumente (PI) GmbH & Co. KG 2008. Subject to change without notice. All data are representative of any new release. The newest information for data sheets is available for download at www.pi.ws. Call 506.444.4444 for more information.

The P-840 and P-841 series translators are high-resolution linear actuators for static and dynamic applications. They provide sub-millisecond response and sub-nanometer resolution.

#### Application Examples

- Static and dynamic Precision positioning
- Disc-drive-testing
- Adaptronics
- Smart structures
- Active vibration control
- Switches
- Laser tuning
- Patch-Clamp
- Nanotechnology

#### Design

These translators are equipped with highly reliable multilayer piezo ceramic stacks protected by a non-magnetic stainless steel case with internal spring preload. The preload makes them ideal for dynamic applications and for tensile loads as well.

#### Ceramic Insulated Piezo Actuators Provide Long Lifetime

Highest possible reliability is assured by the use of award-winning PICMA® multilayer piezo actuators. PICMA® actuators are the only actuators on the market with ceramic-only insulation, which makes them resistant to ambient humidity and leakage-current failures. They are thus far superior to conventional actuators in reliability and lifetime.

#### Optimum UHV Compatibility - Minimum Outgassing

The lack of polymer insulation and the high Curie temperature make for optimal ultra-high-vacuum compatibility (no outgassing / high bakeout temperatures, up to 150 °C).

#### Mounting

Mounting is at the foot, with push/pull forces of less than 5 N, the actuator can be held by clamping the case. The optional ball tip (P-840.95) is intended to decouple torque and off-center forces from the piezo ceramic. The magnetic adapter P-176.20 is to be screwed into the top piece in order to provide magnetic coupling.

Read details in Mounting and Handling Guidelines (p. 1-67).

#### High Accuracy in Closed-Loop Operation

The standard model P-840 is designed for open-loop positioning. Version P-841 with integrated high-resolution strain gauge position sensors provides high precision for closed-loop operation (further details see p. 2-199).

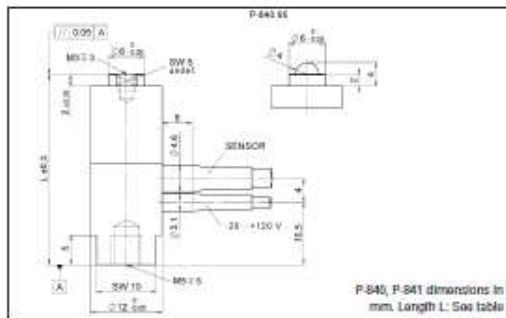
#### Piezo Drivers, Controllers & Amplifiers

High-resolution amplifiers and servo-control electronics, both

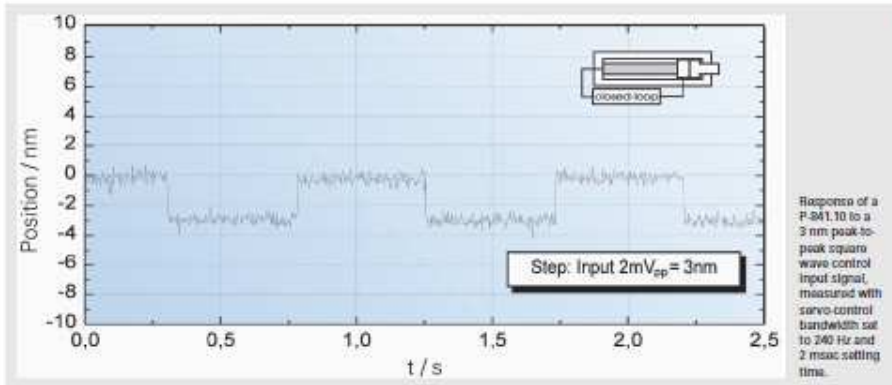
#### Ordering Information

- P-840.10**  
Preloaded Piezo Actuator,  
15 µm Travel range
- P-840.20**  
Preloaded Piezo Actuator,  
30 µm Travel range
- P-840.30**  
Preloaded Piezo Actuator,  
45 µm Travel range
- P-840.40**  
Preloaded Piezo Actuator,  
60 µm Travel range
- P-840.60**  
Preloaded Piezo Actuator,  
90 µm Travel range
- P-841.10**  
Preloaded Piezo Actuator with  
SGS-Sensor, 15 µm Travel range
- P-841.20**  
Preloaded Piezo Actuator with  
SGS-Sensor, 30 µm Travel range
- P-841.30**  
Preloaded Piezo Actuator with  
SGS-Sensor, 45 µm Travel range
- P-841.40**  
Preloaded Piezo Actuator with  
SGS-Sensor, 60 µm Travel range
- P-841.60**  
Preloaded Piezo Actuator with  
SGS-Sensor, 90 µm Travel range

digital and analog, are described in the "Piezo Drivers / Servo Controllers" (see p. 2-99) section.



P-840, P-841 dimensions in mm. Length L: See table



Response of a P-841.10 to a 3 nm peak-to-peak square wave control input signal, measured with servo control bandwidth set to 240 Hz and 2 msec settling time.

Linear Actuators & Motors

- PiezoWalk® Motors / Actuators
- PILine® Ultrasonic Motors
- DC-Servo & Stepper Actuators
- Piezo Actuators & Components
- Isolated / Piezoelectric Actuators
- Stipitraget Stack Actuators
- Patches/Stacks/Tubes/Shear

Nanopositioning / Piezoelectrics

Nanonstrlogy

Micropositioning

Index

Technical Data

Model	P-841.10 P-840.10	P-841.20 P-840.20	P-841.30 P-840.30	P-841.40 P-840.40	P-841.60 P-840.60	Units
Open-loop travel @ 0 to 100 V	15	30	45	60	90	µm ±20 %
Closed-loop travel	15 / -	30 / -	45 / -	60 / -	90 / -	µm
Integrated feedback sensor*	SGS / -					
Closed-loop / open-loop resolution**	0.3 / 0.15	0.6 / 0.3	0.9 / 0.45	1.2 / 0.6	1.8 / 0.9	nm
Static large-signal stiffness***	57	27	19	15	10	N/µm ±20 %
Pushing forces to: 1000 N	1000	1000	1000	1000	1000	N
Pulling forces to: 50 N	50	50	50	50	50	N
Max. torque limit (on tip)	0.35	0.35	0.35	0.35	0.35	Nm
Electrical capacitance	1.5	3.0	4.5	6.0	9.0	µF ±20 %
Dynamic operating current coefficient (DOCC)	12.5	12.5	12.5	12.5	12.5	µA / (Hz · µm)
Unloaded resonant frequency fo	18	14	10	8.5	6	kHz ±20 %
Operating temperature	-20 to +80	°C				
Voltage connection	LEMO	LEMO	LEMO	LEMO	LEMO	
Sensor connection	LEMO	LEMO	LEMO	LEMO	LEMO	
Mass without cables	20	25	45	54	62	g ±5 %
Material: case, end pieces	N-S	N-S	N-S	N-S	N-S	
Length L	32	50	68	86	122	mm ±0.3

\*Closed loop models can attain linearity up to 0.15% and are shipped with performance reports.  
 \*\*Resolution of piezo actuators is not limited by stiction or friction. Value given is noise equivalent motion with E-503 amplifier. (p. 2-146)  
 \*\*\*Dynamic small signal stiffness is ~ 30% higher.  
 Recommended amplifiers / controllers:  
 Single channel: E-610 servo controller / amplifier (p. 2-110), E-625 servo controller, bench-top (p. 2-114), E-621 controller module (p. 2-160)  
 Single channel: modular piezo controller system E-500 (p. 2-142) with amplifier module E-505 (high-power) (p. 2-147) and E-509 controller (p. 2-152) (optional)  
 Multi-channel: modular piezo controller system E-500 (p. 2-142) with amplifier module E-503 (three channels) (p. 2-146) or E-505 (1 per axis, high-power) (p. 2-147) and E-509 controller (p. 2-152) (optional)

3.2. E-505 Amplifier Module for LVPZTs

E-505

**Function:**

The E-505 LVPZT Amplifier Module is a single-channel amplifier for low-voltage PZTs. The E-505.00 and E-505.10 models available differ in their peak power and their small-signal bandwidth: while the E-505.00 can output and sink a peak current of 2000 mA with a small-signal bandwidth of > 5 kHz, the E-505.10 can output and sink a peak current of 10 A with >10 kHz. The output voltage ranges from -20 to +120 volts adapted to the nominal operating voltage range of PI LVPZTs.

The amplifier is designed for static and dynamic operations of low-voltage PZTs. The modules deliver an average output power of 30 Watts for dynamic applications.

Up to three E-505 modules can be installed in the E-500 mother chassis and one E-505 can be installed in the E-501 chassis.

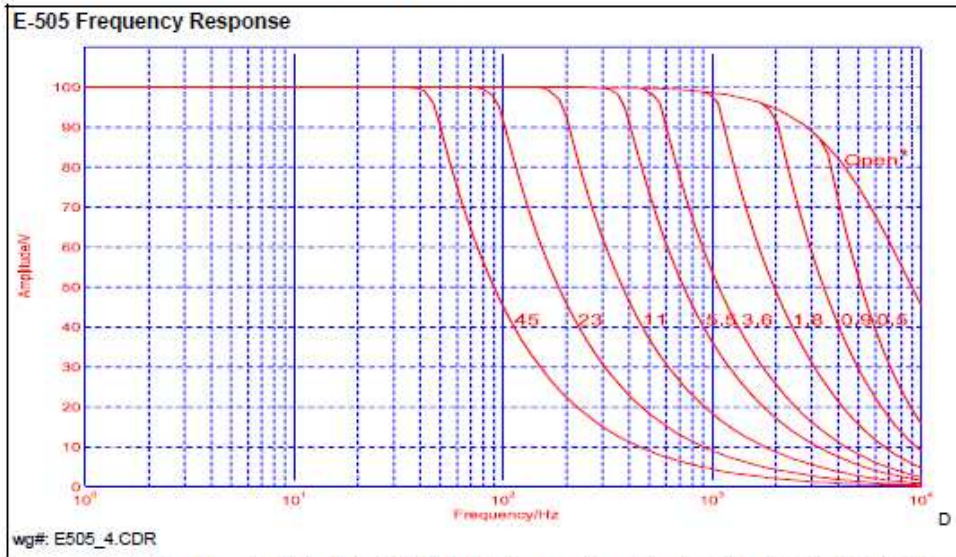
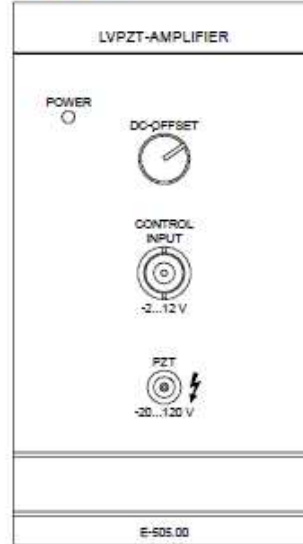
Output voltages can be controlled either via the 10-turn manual potentiometers located at the front panel or by analog input signals (DC or AC) applied to the BNC input connectors.

Multiplying by the gain factor of 10 results in an output voltage range from -20 to +120 volts. The DC offset potentiometer is active at the same time. Internally it produces an offset voltage from 0 to 10 volts to the input signal.

Analog control signals can be generated by external sources or by E-515 or E-516 Display and Interface module.

**Front Panel Elements:**

- 10-turn potentiometers for DC-Offset
- Control input sockets (BNC)
- PZT-voltage power output (-20 to +120V)



\*Small-signal bandwidth for E-505.00. Note that the small-signal bandwidth for E-505.10 is 10 kHz instead.

## E-500 Series PZT Servo Controllers

## User Manual PZ 62E

## E-505 Specifications:

Model	E-505.00	E-505.10
Function:	DC-Amplifier for LVPZTs	
Channels:	1	
Output voltage range:	-20 to +120 V	
Polarity:	positive	
Maximum output power:	30 W per channel (average) 200 W per channel (peak, for 5 ms)	30 W per channel (average) 1 kW per channel (peak, for 150 $\mu$ s)
Maximum output current:	300 mA (> 5 ms) 2000 mA (< 5 ms, peak)	300 mA (> 5 ms) 10 A (< 150 $\mu$ s, peak)
Current limitation:	short circuit proof	
Control voltage input range:	-2 V to +12 V	
Input impedance:	> 100 kOhm	
Voltage gain:	10 $\pm$ 0.1	
DC offset setting:	0 to 100 V with 10-turn pot.	
Output voltage socket*:	LEMO ERA.00.250.CTL	
Signal Input sockets:	BNC	
Main connector (for mother board):	32 pin DIN 41612, male	
Operating voltages:	requires E-530 or E-531 power supply (+33, -33, +127 V)	
Operating temperature range:	+5°C to +50°C, (over 40°C, max. av. power derated 10%)	
Output voltage temperature stability**:	< 0.02% per °C	
Weight:	0.9 kg	
Module size:	Width 2.8"(14HP), depth 160 mm	

\*With E-505.10, keep the cable length as short as possible and/or increase the conductor cross-section of the cable due to the voltage drop at 10 A output current.

\*\*Compared to the E-505.00, the noise level of the E-505.10 is slightly increased due to its high bandwidth.

## E-505 Pin Assignment (32 pin connector, DIN 41612, male)

Row	PIN a	PIN c
2	Power Fail	OUT: ch1 (BNC+Bias)
4	IN: ch1	OUT: ch1 (monitor)
6	PZT GND	PZT GND
8	OUT: PZT	OUT: PZT
10	n.c.	n.c.
12	n.c.	n.c.
14	internal use, Bus_A	internal use, Bus_B
16	internal use, Bus_Vcc	internal use, Bus_GND
18	n.c.	n.c.
20	n.c.	n.c.
22	GND (measurement)	GND (measurement)
24	GND (power)	GND (power)
26	IN: +27V	IN: +27 V
28	IN: -33V	OUT: -10 V
30	IN: +127V	IN: +127 V
32	GND (chassis)	GND (chassis)

### B.3 A/D Converter



Technical Sales  
 Netherlands  
 0348 433 486  
 info.netherlands@ni.com

#### NI USB-6211

#### 16-Bit, 250 kS/s M Series Multifunction DAQ, Bus-Powered

- 16 analog inputs (16-bit, 250 kS/s)
- 2 analog outputs (16-bit, 250 kS/s); 4 digital inputs; 4 digital outputs; 32-bit counters
- Bus-powered USB for high mobility; built-in signal connectivity
- NI signal streaming for sustained high-speed data streams over USB; OEM version available
- Compatible with LabVIEW, LabWindows™/CVI, and Measurement Studio for Visual Studio .NET
- NI-DAQmx driver software and NI LabVIEW SignalExpress LE interactive data-logging software



#### Specifications

##### Specifications Documents

- Detailed Specifications
- Data Sheet

##### Specifications Summary

##### Specifications Summary

General	
Product Name	USB-6211
Product Family	Multifunction Data Acquisition
Form Factor	USB
Operating System/Target	Windows , Linux , Mac OS
DAQ Product Family	M Series
Measurement Type	Voltage
RoHS Compliant	Yes
Analog Input	
Channels	16 , 8

Single-Ended Channels	16
Differential Channels	8
Resolution	16 bits
Sample Rate	250 kS/s
Max Voltage	10 V
Maximum Voltage Range	10 V , -10 V
Maximum Voltage Range Accuracy	2.69 mV
Maximum Voltage Range Sensitivity	91.6 $\mu$ V
Minimum Voltage Range	200 mV , -200 mV
Minimum Voltage Range Accuracy	0.088 mV
Minimum Voltage Range Sensitivity	4.8 $\mu$ V
Number of Ranges	4
Simultaneous Sampling	No
On-Board Memory	4096 samples
<b>Analog Output</b>	
Channels	2
Resolution	16 bits
Max Voltage	10 V
Maximum Voltage Range	10 V , -10 V
Maximum Voltage Range Accuracy	3.512 mV
Minimum Voltage Range	10 V , -10 V
Minimum Voltage Range Accuracy	3.512 mV
Update Rate	250 kS/s
Current Drive Single	2 mA
Current Drive All	4 mA
<b>Digital I/O</b>	
Bidirectional Channels	0
Input-Only Channels	4
Output-Only Channels	4
Number of Channels	0 , 4 , 4
Timing	Software

## B.4 Software

The computer used for measuring the sensor output and for actuation of the piezo stack actuator:

Type	Asus EEE PC 1000H
Intel CPU & Chipset	Intel Atom N270
Memory	1 Gb
Harddisk	160 GB

The software used for the data acquisition and the actuation of the piezo:

- National instruments Labview 8.2.1

## B.5 Wiring scheme

The wiring scheme for the measurement equipment is presented in the figure below. The A/D converter provides the input voltage for the piezo stack actuator and in the mean time it acquires the output voltages of the sensors. The sensors are interconnected as a master slave system. The master sensor, measuring the displacement of the mass, has a phase of  $0^\circ$ . The slave sensor, measuring the elongation of piezo has a phase shift of  $180^\circ$  with respect to the master sensor. In this way the sampling frequencies of the sensors, which are set at 1 kHz, do not influence each other.

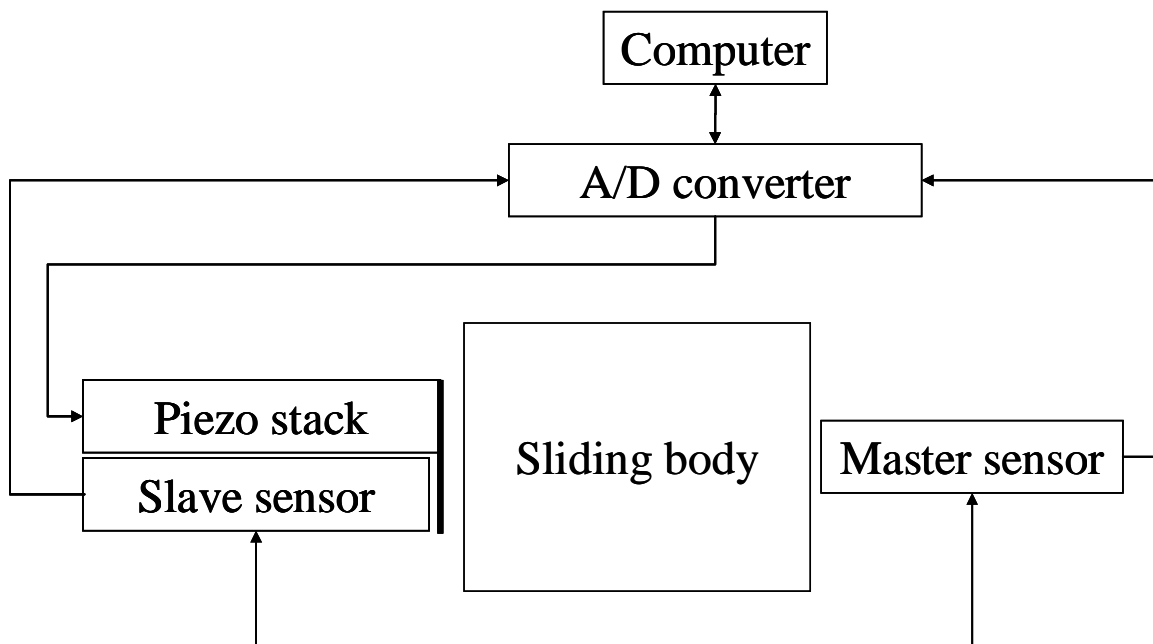


Figure 20: Wiring scheme for measurement equipment.

## Appendix C - Data analysis

In this section all the Matlab files used for the data analysis of the experiments and the files used for the simulations are presented. In the files information about the files and calculations is presented in the green font color. Further information about the calculations can be obtained from the help function of Matlab.

### C.1 Experiments 2

#### Experiments 2 stiffness estimation.m

```
% M.J. Appels (Student)
% Delft University of Technology
% Faculty of mechanical engineering
% Department of Biomechanical Engineering
% email: m.j.appels@gmail.com

% In this file the data is processed and a displacement-time curve is
% constructed from the sensor's output. Hence, the reference point can be
% determined and the system's initial stiffness can be determined.

%% Load data
load 'H:\Desktop\Data Analysis (01-02-10)\Metingen2\Metingen2-
7\20100111170909.txt'
RawData = X20100111170909;

%% Compensate drift sensor

% linear fit of stationary measurement (centred and scaled)
mu = 28141;
sigma = 16247;

pm_1 = -0.00056099;
pm_2 = 0.00051319;
pm_3 = 0.0095918;
pm_4 = 6.9166;

ps_1 = -0.0095176;
ps_2 = 0.014322;
ps_3 = -0.02235;
ps_4 = 1.3287;

% Compensation of output data sensors
for j = 1:length(RawData)

    z =(j - mu)/sigma;

    ys = ps_1*z^3 + ps_2*z^2 + ps_3*z + ps_4;
    ym = pm_1*z^3 + pm_2*z^2 + pm_3*z + pm_4;

    RawData(j,2) = RawData(j,2) - ys;
    RawData(j,3) = RawData(j,3) - ym;

end

%% Determination of time displacement curve

% Rename data
Actuator1 = RawData(:,1);
Slave1 = RawData(:,2);
Master1 = RawData(:,3);

% Conversion factor Master sensor (Mass)
a = -2.505888839e-6;
% Conversion factor Slave sensor (Piezo)
```

```

b = 4.925016622e-6;

% Initialize data by setting initial displacements to zero
Actuator = Actuator1 - Actuator1(1,1);
Slave = Slavel - Slavel(1,1);
Master = Master1 - Master1(1,1);

% Displacements
Disp_Mass = Master.*a;
Disp_Piezo = Slave.*b;

% Convert samples to time
Time = 0:dt:(length(RawData)*dt-dt);

% Stepsize
dt = 10e-3; % [V]

% Plot Displacement Time
figure('name', 'Position vs. Time mass')
plot(Time, Disp_Piezo, 'b')
hold on
plot(Time, Disp_Mass, 'r')
legend('Elongation piezo actuator', 'Displacement mass', 'location',
'NorthWest')
xlabel('Time [s]')
ylabel('Displacement [m]')

%% Stiffness estimation

% Implement time at which reference point is reached by piezo
t = input('Time where actuation start(s): t = ');

% Close displacement-time curve
close all

% Define range for stiffness calculation
Sample_start = 900;
Sample_stop = 200;
Domain = 50;
r1 = t*100 ;
r2 = r1 + Sample_stop + 600;

% Spring stiffness (N/m)
k_spring = 116.04e3;

% Calculation of actuation force
F_Actuation = -k_spring.*(Disp_Mass - Disp_Piezo);

% Determine stiffness
A1 = mean(Disp_Mass(r1:r1 + Domain));
A2 = mean(Disp_Mass(r1:r1 + Sample_stop + Domain));
B1 = mean(F_Actuation(r1:r1 + Domain));
B2 = mean(F_Actuation(r1:r1 + Sample_stop + Domain));

Stiffness = (B2-B1)/(A2-A1)

```

### Experiments 2\_stiffness.m

```

% M.J. Appels (Student)
% Delft University of Technology
% Faculty of mechanical engineering
% Department of Biomechanical Engineering
% email: m.j.appels@gmail.com

```

```

% In this file an statistic analysis is performed on the initial stiffness
determined by the previous file.

clc; clear all; close all

% load stiffness from experiments
load Initial_Stiffness2.mat

Initial_Stiffness2 = data;

% Check for missing data
for n = 1:length(Initial_Stiffness2)
Relaxation_Displacement2NaNCount(1,n) = sum(isnan(Initial_Stiffness2(:,n)));
end

% Outliers
% Select experiment for analysis
r1 = 1;
r2 = 10;

% Start analysis
for n = r1:r2
IS = Initial_Stiffness2(:,n);

% Remove missing values
IS = IS(~isnan(IS));

bin_IS = hist(IS);
NIS = max(bin_IS);
muIS = mean(IS);
sigmaIS = std(IS);

% Remove outliers
outliers = (IS - muIS) > 2*sigmaIS;
ISm = IS; % Copy c3 to c3m
ISm(outliers) = NaN; % Add NaN values
ISm = ISm(~isnan(ISm));

% Smoothing data
span = 3; % Size of the averaging window
window = ones(span,1)/span;
smoothed_ISm = convn(ISm>window,'same');

% Summarizing data

% Measures of location
x1(n,1) = mean(IS);
x1m(n,1) = mean(ISm);
x1s_m(n,1) = mean(smoothed_ISm);

dx2(n,1) = std(IS);
dx2m(n,1) = std(ISm);
dx2s_m(n,1) = std(smoothed_ISm);

dx3(n,1) = var(IS);
dx3m(n,1) = var(ISm);
dx3s_m(n,1) = var(smoothed_ISm);
end

% Remove outliers from mean values
mux1 = mean(x1);
sigmax1 = std(x1);

outliers = (x1 - mux1) > 2*sigmax1;
x1m = x1; % Copy c3 to c3m
x1m(outliers) = NaN; % Add NaN values
x1m = x1m(~isnan(x1m));

```

```

% Remove outliers from standard deviation
mudx2 = mean(dx2);
sigmadx2 = std(dx2);

outliers = (dx2 - mudx2) > 2*sigmadx2;
dx2m = dx2; % Copy c3 to c3m
dx2m(outliers) = NaN; % Add NaN values
dx2m = dx2m(~isnan(dx2m));

% Means of the experiments
x1 = num2str(x1);
x1m = num2str(x1m);
x1s_m = num2str(x1s_m);

% Standard deviation from the mean
dx2 = num2str(dx2);
dx2m = num2str(dx2m);
dx2s_m = num2str(dx2s_m);

% Variance
dx3 = num2str(dx3);
dx3m = num2str(dx3m);
dx3s_m = num2str(dx3s_m);

```

### Relaxation analysis Experiments 2

The relaxation analysis uses the same algorithm as is used for the initial stiffness estimation. A matrix consisting of all the relaxation displacements measured during the experiments is loaded into the workspace of the program after which a statistic analysis is run.

## C.2 Experiments 3

### Experiments 3 relaxation estimation.m

```

% M.J. Appels (Student)
% Delft University of Technology
% Faculty of mechanical engineering
% Department of Biomechanical Engineering
% email: m.j.appels@gmail.com

% In this file the relaxation displacements are determined from
% experiments 3. Furthermore a statistic analysis on the results is
% performed

clc; %clear all; close all;

%% Load data into workspace
load 'O:\Weekend 22-02-10\Metingen5\dv 1 mV\20100205132830_0690kg.txt'
RawData = X20100205132830_0690kg;

% Determine samples at which actuation force is cut off
for w = 1:length(RawData)-1

    D(w,1) = abs(RawData((w+1),1) - RawData(w,1));

    I = find(D > 0.1);
end

% Rename data
Actuator1 = RawData(:,1);
Slave1 = RawData(:,2);
Master1 = RawData(:,3);

% Conversion factor Master sensor (Mass)

```

```

a = -2.505888839e-6;
% Conversion factor Slave sensor (Piezo)
b = 4.925016622e-6;

% Initialize data by setting initial displacements to zero
Actuator = Actuator1 - Actuator1(1,1);
Slave = Slavel - Slavel(1,1);
Master = Master1 - Master1(1,1);

for jj = 1:length(I)
    H(jj,1) = RawData(I(jj),1);
end

% Domain for relaxation analysis
d1 = 12;
d2 = 100;

% Determine relaxation displacement for each iteration
kk = 1;
for n = 1:10:401
    k = 1;
    for nn = 0:1:9
        H(k, kk) = I(n + nn,1);

        % Calculate mean of noise signal before (M1) and after (M2) cut off
        M1 = mean(Disp_Mass((H(k, kk)-d1):H(k, kk),1));
        M2 = mean(Disp_Mass(H(k, kk):(H(k, kk)+d2),1));

        % Determine relaxation displacement
        Relaxation_Displacement5(k, kk) = M1-M2;

        % Remove incorrect measurements
        if Relaxation_Displacement5(k, kk) <= 0
            Relaxation_Displacement5(k, kk) = NaN;
        end

        % Plot relaxation displacement on domain [d1 d2]
        figure
        plot(Disp_Mass((H(k, kk)-d1):H(k, kk)+d2,1))
        line([0 d1], [M1 M1], 'color', 'r')
        line([d1 d1+d2], [M2 M2], 'color', 'r')

        k = k + 1;

    % pause(0.05) % Hold figure for 0.05 seconds before closing figure
    close
    end
    kk = kk + 1;
end

% Save results
save Relaxation_Displacement5_031_0352

%% Statistic analysis of the results

% Select experiment for analysis
r1 = 11;
r2 = 41;

% Relaxation_Displacement5 = Relaxation_Displacement5';

for n = r1:r2

IS = Relaxation_Displacement5(:,n);

% Remove missing values
IS = IS(~isnan(IS));

```

```

bin_IS = hist(IS);
NIS = max(bin_IS);
muIS = mean(IS);
sigmaIS = std(IS);

% Remove outliers
outliers = (IS - muIS) > 2*sigmaIS;
ISm = IS; % Copy c3 to c3m
ISm(outliers) = NaN; % Add NaN values
ISm = ISm(~isnan(ISm));

%% Smoothing data
span = 3; % Size of the averaging window
window = ones(span,1)/span;
smoothed_ISm = convn(ISm,window,'same');

%% Summarizing data

% Measures of location
x1(n,1) = mean(IS);
x1m(n,1) = mean(ISm);
x1s_m(n,1) = mean(smoothed_ISm);

dx2(n,1) = std(IS);
dx2m(n,1) = std(ISm);
dx2s_m(n,1) = std(smoothed_ISm);

dx3(n,1) = var(IS);
dx3m(n,1) = var(ISm);
dx3s_m(n,1) = var(smoothed_ISm);
end

%% Remove outliers from mean values
mux1 = mean(x1);
sigmax1 = std(x1);

% Remove outliers from standard deviation
mudx2 = mean(dx2);
sigmadx2 = std(dx2);

outliers = (dx2 - mudx2) > 2*sigmadx2;
dx2m = dx2; % Copy c3 to c3m
dx2m(outliers) = NaN; % Add NaN values
dx2m = dx2m(~isnan(dx2m));

% Means of the experiments
x1 = num2str(x1);
x1m = num2str(x1m);
x1s_m = num2str(x1s_m);

% Standard deviation from the mean
dx2 = num2str(dx2);
dx2m = num2str(dx2m);
dx2s_m = num2str(dx2s_m);

% Variance
dx3 = num2str(dx3);
dx3m = num2str(dx3m);
dx3s_m = num2str(dx3s_m);

```

### C.3 Simulation 1

Simulation1 extract experimental data.m

```

% M.J. Appels (Student)
% Delft University of Technology
% Faculty of mechanical engineering
% Department of Biomechanical Engineering
% email: m.j.appels@gmail.com

% In this file the data is processed and a force displacement-curve is
% constructed from the sensor output from Experiments 2. Hence, the force
% displacement curve can be compared with the results from the simulation

close all; clc;

%% Simulation1: dv = 1 mV, dt = 10 ms

% Load Experimental data and data from stationary test
load('Stat_Simulation1.mat')
load('Simulation1.mat')

% Initialize data by setting initial displacements to zero
Stat_Simulation1(:,1) = Stat_Simulation1(:,1) - Stat_Simulation1(1,1);
Stat_Simulation1(:,2) = Stat_Simulation1(:,2) - Stat_Simulation1(1,2);
Stat_Simulation1(:,3) = Stat_Simulation1(:,3) - Stat_Simulation1(1,3);

Simulation1(:,1) = Simulation1(:,1) - Simulation1(1,1);
Simulation1(:,2) = Simulation1(:,2) - Simulation1(1,2);
Simulation1(:,3) = Simulation1(:,3) - Simulation1(1,3);

%% Compensate drift sensor

% linear fit of stationary measurement (centered and scaled)
mu = 28141;
sigma = 16247;

pm_1 = -0.00056099;
pm_2 = 0.00051319;
pm_3 = 0.0095918;
pm_4 = 6.9166;

ps_1 = -0.0095176;
ps_2 = 0.014322;
ps_3 = -0.02235;
ps_4 = 1.3287;

% Compensation of output data sensors
for j = 1:length(RawData)

    z = (j - mu)/sigma;

    ys = ps_1*z^3 + ps_2*z^2 + ps_3*z + ps_4;
    ym = pm_1*z^3 + pm_2*z^2 + pm_3*z + pm_4;

    Simulation1_Compensated(j,1) = RawData(j,2) - ys;
    Simulation1_Compensated(j,2) = RawData(j,3) - ym;
End

%% Conversion of output voltage to meters

% Conversion factor Master sensor (Mass)
a = -2.505888839e-6;
% Conversion factor Slave sensor (Piezo)
b = 4.925016622e-6;
% Conversion factor piezo input to output (Piezo)
c = (0.9891).*b/2;

% Conversion of voltages to meters
Disp_Mass = Simulation1_Compensated(:,2).*a;
Disp_Piezo_Sensor = Simulation1_Compensated(:,1).*b;

```

```

Disp_Piezo_input = RawData(:,1)*c;

%% Determination of force displacement curve

% Spring stiffness (N/m)
k_spring = 116.04e3;

% Initialize displacement
Disp_Mass = Disp_Mass - -2.469e-6;
Disp_Piezo_input = RawData(:,1)*c - -2.469e-6;

% Calculation of actuation force
F_Actuation = -k_spring.*(Disp_Mass - Disp_Piezo_input);

% replace negative values of actuation force (i.e. Disp_Mass > Disp_Piezo)
for n = 1:length(RawData)
    if (Disp_Mass(n,1) - Disp_Piezo_input(n,1)) > 0
        F_Actuation(n,1) = 0;
    end
end

% Select domain for simulation of experimental data
r1 = 6000;
r2 = 10350;

% Save data
Simulation1_Data(:,1) = Disp_Mass;
Simulation1_Data(:,2) = Disp_Piezo_input;
Simulation1_Data(:,3) = F_Actuation;
Simulation1_Data(:,4) = RawData(:,2).*b;
save('Simulation1_Data', 'Simulation1_Data')

% Filter data
[B A] = butter(2, 0.01, 'low');
Disp_Mass_Filtered = filtfilt(B ,A , Simulation1_Data(:,1));
F_Actuation_Filtered = filtfilt(B ,A , Simulation1_Data(:,3));

% Plot data for comparison to simulations
figure
hold on
plot(Disp_Mass_Filtered(r1:r2), F_Actuation_Filtered(r1:r2), 'r')

% Plot line indicating end of the experimental data's pre-sliding regime
line([1.25e-7 1.25e-7], [0 0.40], 'color', 'k', 'linestyle', ':')

```

### Simulation 1.m

```

% M.J. Appels (Student)
% Delft University of Technology
% Faculty of mechanical engineering
% Department of Biomechanical Engineering
% email: m.j.appels@gmail.com

% This file contains the simulation of the experimental data from
% Simulations 1. The simulation simulates 3 masses being pushed from the
% pre-sliding regime into the sliding regime. The output is a force-
% displacement curve representing the frictional behaviour in the
% pre-sliding regime.

% Start timer
tic

clc; clear all;

for s = 1:3 % (Loop for consecutive simulation of the 3 masses)
%% Model parameters

```

```

% Maximum deflection of the bristles (m)
d_max = 1.5584e-8;
% d_max = 2.5e-8; % From datafit

% Coulomb frictional coefficient (-)
mu_Coulomb = 0.063; % Obtained from Experiment 1

% Gravitational acceleration (m/s^2)
g = 9.81;

% Mass of sliding body(Kg)
m = [0.352 0.563 0.690];

% Scale factor for the number of bristles to be used. for c = 500 about 100
% bristles will be used for modelling the sliding body with mass m = 0.352
% kg (-)
c = 500;

%% Simulation parameters

% Piezo increment (m)
dx = 0.825e-9;

% Sample time (s)
dt = 10e-3;

% Spring stiffness (N/m)
k = 116.04e3;

%% Initialization

% Determination of number of bristles to be used
N = round(c*mu_Coulomb*g*m(s));
fprintf('1) The model uses a total of %g bristles.\n', N)

% Determine initial_stiffness
sigma_ini = (mu_Coulomb*g*m(s))/d_max;
% sigma_ini = (F_C(s))/d_max % Used for datafit

% Initialize normal distribution for placement of the bristles
% (99,7 of locations within a range of d_max)
mul = 0;
sigma1 = (2/3)*d_max;

% Bristle placement function
[d_w, sigma_b, N] = Initial_bristle_placement(mul, sigma1, sigma_ini,...
    N, d_max);

%% Realization

% Number of iterations (-)
r = 1000;

% Increment of atuation force
dF = 1e-3;

% Initialization of output matrices
F = zeros(r+1, 1);
d_w_eval = zeros(N, r+1);
x_eval = zeros(r+1, 1);
x_eval(1,1) = 0;
F(1,1) = 0;
d_w_eval(:, 1) = d_w;

% Actuation force at t = 0
F_act = 0; % (N)

```

```

% Position sliding body at t = 0
x = 0; % (m)

% Calculation of force-displacement curve for r iterations
for w = 1:1:r % F_act = (w*dF)
    [F_f d_w, x, n_d] = New_model(x, dF, sigma_b, d_w, d_max);
    F(w + 1, 1) = F_f;
    d_w_eval(:, w + 1) = d_w;
    x_eval(w + 1, 1) = x;
end

%% Plot output

% line style for each run
ls2 = '-';
ls1 = '--';
ls3 = '-.';
Ls = [ls1 ;ls2 ; ls3];

% plot simulation in plot containing experimental data. The plot is obtained
% from the m-file: Experiments_2_0_5mv
hold on
plot(x_eval, F, 'k', 'linestyle', Ls(s,:), 'linewidth', 4)

% Clear data from workspace prior to simulation of new mass
clear
end

% Plot line indicating end of the simulated pre-sliding regime and insert
% scaling, labels and legend
line([5.0e-8 5.0e-8], [0 0.40], 'color', 'k', 'linestyle', ':')
axis([0 1.4e-7 0 0.45])
xlabel('Displacement mass [m]')
ylabel('Friction force [N]')
legend('Experimental data, m = 0.352 kg',...
    'Experimental data, m = 0.563 kg',...
    'Experimental data, m = 0.690 kg',...
    'New model, m = 0.352 kg',...
    'New model, m = 0.563 kg',...
    'New model, m = 0.690 kg',...
    'End of pre-sliding regimes',...
    'location', 'EastOutside')

% Stop timer and return computer time
toc
fprintf('\n')

```

### Initial bristle placement.m

```

% M.J. Appels (Student)
% Delft University of Technology
% Faculty of mechanical engineering
% Department of Biomechanical Engineering
% email: m.j.appels@gmail.com

% This file contains the placement algorithm for the initial placement
% of the bristles (d_ini). After the placement the bristles find a state
% free of internal stress (d_0). This point will be the reference point for
% further modelling of the frictional behaviour.
% If during the initializing process one of the bristles is disconnected
% this bristle is replaced by a new randomly chosen bristle and the new
% equilibrium state will be determined. This process continues until an
% equilibrium is obtained where each bristle is connected.

function [d_w, sigma_b, N] = Initial_bristle_placement(mul, sigma1,...
    sigma_ini, N, d_max)

```

```

% Determination of the bristle stiffness (N/m)
sigma_b = sigma_ini/N;

% Placement of the bristles according to normal distribution (m)
d_ini = normrnd(mul, sigma1, N, 1);

% Calculation of internal stress after placement (N/m)
F_int = sigma_b*sum(d_ini);

% Calculation of settling displacement (m)
D_0 = F_int / sigma_ini;

% Configuration of the bristles while internal equilibrium (m)
d_w = d_ini - D_0;

% Check whether all bristles at equilibrium position are connected
N_bonds = 0;
while N_bonds < N
    for q = 1:N
        % When connected
        if abs(d_w(q,1)) <= d_max
            N_bonds = N_bonds + 1;

            % when disconnected
        elseif abs(d_w(q,1)) > d_max
            % reconnect bristle
            d_w(q,1) = random('norm', mul, sigma1, 1, 1);

            % Initial stress (N/m)
            F_int = sigma_b*sum(d_w);

            % Initial relaxation displacement (m)
            D_0 = F_int / sigma_ini;

            % Internal equilibrium
            d_w = d_w - D_0;

            % restart determination of equilibrium configuration
            N_bonds = 0;

        break
    end
end
end

% Check internal equilibrium
F_int = sigma_ini*sum(d_w);
fprintf('2) The bristles are placed and an internal equilibrium has been
obtained.\n')
fprintf('\n')
fprintf('    The internal stress amounts to %e Newtons.\n', F_int)
fprintf('\n')

```

### New\_model.m

```

% M.J. Appels (Student)
% Delft University of Technology
% Faculty of mechanical engineering
% Department of Biomechanical Engineering
% email: m.j.appels@gmail.com

% This file contains the actual friction model.

function [F_f, d_w, x, n_d] = New_model(x, dF, sigma_b, d_w, d_max)

```

```

% Initialization of friction force calculation
d_w_c = zeros(length(d_w),1);
d_w_d = zeros(length(d_w),1);
n_c = 0;
n_d = 0;

% Count bristles that are connected
for e = 1:length(d_w)
    % If connected
    if abs(d_w(e,1)) < d_max
        n_c = n_c + 1;
    % If disconnected
    elseif abs(d_w(e,1)) >= d_max
        n_d = n_d + 1;
    end
end

%% Calculation of pre-sliding displacement and friction force
% The actuation force acts is the input from which the pre-sliding
% displacement and frictionforce are determined.

% return Coulomb friction force over distance x when all bristles have
% disconnected
if n_c == 0
    % Coulomb friction force
    F_f = sigma_b*d_max*n_d;
    % Distance x
    x = 2*x;
else

    % Add increment to pre-sliding displacement related to actuation force
    % and the systems current stiffness
    dx = dF/(n_c*sigma_b);
    % New global position
    x = x + dx;

    % Check wheter bristles are conencted or not
    n_c = 0;
    n_d = 0;
    for q = 1:1:length(d_w)
        % If connected
        if abs(d_w(q,1)) < d_max
            d_w_c(q) = d_w(q,1) + dx;
            d_w(q,1) = d_w(q,1) + dx;
            n_c = n_c + 1;
        % If disconnected
        elseif abs(d_w(q,1)) >= d_max
            d_w_d(q) = d_max;
            d_w(q,1) = d_max;
            n_d = n_d + 1;
        end
    % Calculation friction force (d_w = [d_w_c ; d_w_d])
    F_f = sigma_b*sum(d_w);
    end
end

```

## C.4 Simulation 2

### Simulation2\_extract\_experimental\_data.m

```

% M.J. Appels (Student)
% Delft University of Technology
% Faculty of mechanical engineering
% Department of Biomechanical Engineering
% email: m.j.appels@gmail.com

```

```

% In this file the data is processed and a force displacement-curve is
constructed from the sensor output from Experiments 3. Hence, the force
displacement curve can be compared with the results from the simulation

close all; clear; clc;

%% Simulation2 dv_sample = 0.01 V, dv = 1 mV, dt = 110 ms

% Load Experimental data and data from stationary test
load('Stat_Simulation2.mat')
load('Simulation2.mat')

% Initialize data by setting initial displacements to zero
Stat_Simulation2(:,1) = Stat_Simulation2(:,1) - Stat_Simulation2(1,1);
Stat_Simulation2(:,2) = Stat_Simulation2(:,2) - Stat_Simulation2(1,2);
Stat_Simulation2(:,3) = Stat_Simulation2(:,3) - Stat_Simulation2(1,3);

Simulation2(:,1) = Simulation2(:,1) - Simulation2(1,1);
Simulation2(:,2) = Simulation2(:,2) - Simulation2(1,2);
Simulation2(:,3) = Simulation2(:,3) - Simulation2(1,3);

%% Compensation raw data for drift by stationary measurements

% linear fit of stationary measurement
pm_1 = 5.8642e-7;
pm_2 = -0.23826;
ps_1 = -8.8545e-007;
ps_2 = 0.0016612;

% Compensation of output data sensors
for j = 1:length(Simulation2)
    ys = ps_1*j;
    ym = pm_1*j;

    Simulation2_Compensated(j,1) = Simulation2(j,2) - ys;
    Simulation2_Compensated(j,2) = Simulation2(j,3) - ym;
end

%% Conversion of output voltage to meters

% Conversion factor Master sensor (Mass)
a = -2.505888839e-6;
% Conversion factor Slave sensor (Piezo)
b = 4.925016622e-6;
% Conversion factor piezo input to output (Piezo)
c = (0.19).*b/0.534;

% Conversion of voltages to meters
Disp_Mass = Simulation2_Compensated(:,2).*a;
Disp_Piezo_Sensor = Simulation2_Compensated(:,1).*b;
Disp_Piezo_input = Simulation2(:,1).*c;

%% Determination of force displacement curve

% Spring stiffness (N/m)
k_spring = 116.04e3;

% Initialize displacement
Disp_Mass = Disp_Mass - -8.698e-9;

% Calculation of actuation force
F_Actuation = -k_spring.*(Disp_Mass - Disp_Piezo_input);

% replace negative values of actuation force (i.e. Disp_Mass > Disp_Piezo)
for n = 1:length(Simulation2)
    if (Disp_Mass(n,1) - Disp_Piezo_input(n,1)) > 0

```

```

        F_Actuation(n,1) = 0;
    end
end

% Select domain for simulation of experimental data
r1 = 10;
r2 = 649;
r3 = 649;
r4 = 1216;

% Save data
Simulation2_Data(:,1) = Disp_Mass;
Simulation2_Data(:,2) = Disp_Piezo_input;
Simulation2_Data(:,3) = F_Actuation;
Simulation2_Data(:,4) = Simulation2(:,2).*b;
save('Simulation2_Data', 'Simulation2_Data')

% Filter data
[B A] = butter(2, 0.01, 'low');
Disp_Mass_Filtered = filtfilt(B ,A , Simulation2_Data(:,1));
F_Actuation_Filtered = filtfilt(B ,A , Simulation2_Data(:,3));

% Plot data for comparison to simulations
figure
hold on
plot(Disp_Mass_Filtered(r1:r2), F_Actuation_Filtered(r1:r2))
plot(Disp_Mass_Filtered(r3:r4), F_Actuation_Filtered(r3:r4), 'r')
axis([0 0.7e-8 0 0.12])

```

### Simulation2\_hysteresis.m

```

% M.J. Appels (Student)
% Delft University of Technology
% Faculty of mechanical engineering
% Department of Biomechanical Engineering
% email: m.j.appels@gmail.com

% This file contains the simulation of the experimental data from
% Simulations 2. The simulation simulates a mass of 0.690 kg which is actuated
% twice
% for by a certain force delivered by the piezo actuator in order to
% simulate hysteresis.

% Start timer
tic

clc; clear all;

%% Model parameters

% Maximum deflection of bristle (m)
d_max = 1.55584e-8;

% Average relaxation displacement (m)
x_rel = 4.4206e-9;

% Coulomb frictional coefficient (-)
mu_Coulomb = 0.063;

% Mass of sliding body (Kg)
m = 0.690;

% Gravitational acceleration (m/s^2)
g = 9.81;

% Scale factor for the number of bristles to be used. for c = 500 about 100

```

```

% bristles will be used for modelling the sliding body with mass m = 0.352
% kg (-)
c = 500;

%% Simulation parameters

% Piezo increment (m)
dx = 0.825e-9;

% Sample time (s)
dt = 10e-3;

% Spring stiffness (N/m)
k = 116.04e3;

%% Initialization

% Determination of number of bristles to be used
N = round(c*mu_Coulomb*g*m);
fprintf('1) The model uses a total of %g bristles.\n', N)

% Determine initial_stiffness
sigma_ini = (mu_Coulomb*g*m)/d_max;
% sigma_ini = (F_C)/d_max % Used for datafit

% Initialize normal distribution for placement of the bristles
% (99,7 of locations within a range of d_max)
mu1 = 0;
sigma1 = (2/3)*d_max;

% Initialize normal distribution for reconnection of the bristles
% (99,7 of locations within a range of x_rel)
mu2 = x_rel;
sigma2 = x_rel/3;

% Bristle placement function
[d_w, sigma_b, N] = Initial_bristle_placement(mu1, sigma1, sigma_ini, N, d_max);

%% Realization

% Number of iterations (-)
r = 250;

% Increment of atuation force
dF = 1e-3;

% Initialization of output matrices
F = zeros(r+1, 1);
d_w_eval = zeros(N, r+1);
x_eval = zeros(r+1, 1);
x_eval(1,1) = 0;
F(1,1) = 0;
d_w_eval(:, 1) = d_w;

% Actuation force at t = 0
F_act = 0; % (N)

% Position sliding body at t = 0
x = 0; % (m)

% Calculation of force-displacement curve for r iterations
n = 1;
for w = 1:1:r % F_act = (w*dF)
    [F_f d_w, x, n] = New_model_hysteresis(n, x, dF, sigma_b, d_w, d_max, mu2,
sigma2, sigma_ini);
    F(w + 1, 1) = F_f;
    d_w_eval(:, w + 1) = d_w;
end

```

```

        x_eval(w + 1, 1) = x;
end

%% Plot output

% Initialize plot

% line style for each run
ls2 = '-';
ls1 = '--';
ls3 = '-.';
Ls = [ls1 ;ls2 ; ls3];

% plot simulation in figure containing experimental data. The plot is obtained
% from the m-file: Experiments_2_0_5mv
hold on
title('Simulation of force-displacement curves for three masses')
plot(x_eval, F, 'k', 'linestyle', Ls(1,:), 'linewidth', 2)
legend('Experimental data 1th. cycle', 'Experimental data 2nd. cycle',...
       'Simulation', 'Simulation with datafit' )
xlabel('Displacement mass [m]')
ylabel('Friction force [N]')

% Stop timer and return computer time
toc
fprintf('\n')

```

#### Initial bristle placement.m

See simulation 1

#### New model hysteresis.m

```

% M.J. Appels (Student)
% Delft University of Technology
% Faculty of mechanical engineering
% Department of Biomechanical Engineering
% email: m.j.appels@gmail.com

% This file contains the actual friction model for modelling the hysteresis
% behaviour.

function [F_f, d_w, x, n] = New_model_hysteresis(n, x, dF, sigma_b, d_w,...
        d_max, mu2, sigma2, sigma_ini)

% Initialization of friction force calculation
n_c = 0;
n_d = 0;

% Count bristles that are connected
for e = 1:length(d_w)
    % If connected
    if abs(d_w(e,1)) < d_max
        n_c = n_c + 1;
        % If disconnected
        elseif abs(d_w(e,1)) >= d_max
            n_d = n_d + 1;
    end
end

%% Calculation of pre-sliding displacement and friction force
% The actuation force acts is the input from which the pre-sliding
% displacement and friction force are determined.

```

```

% Return Coulomb friction force over distance x when all bristles are
% disconnected
if n_c == 0
    % Coulomb friction force
    F_f = sigma_b*d_max*n_d;
    % Distance x
    x = 2*x;
else

    % Add increment to pre-sliding displacement related to actuation force
    % and the systems current stiffness
    dx = dF/(n_c*sigma_b);
    % New global position
    x = x + dx;

    % Check wheter bristles are conencted or not
    n_c = 0;
    n_d = 0;
    for q = 1:1:length(d_w)
        % If connected
        if abs(d_w(q,1)) < d_max
            n_c = n_c + 1;
            d_w_c(n_c,1) = d_w(q,1) + dx;
            d_w(q,1) = d_w(q,1) + dx;
            % If disconnected
            elseif abs(d_w(q,1)) >= d_max
                n_d = n_d + 1;
                d_w_d(n_d) = d_max;
                d_w(q,1) = d_max;
            end
        % Calculation friction force
        F_f = sigma_b*sum(d_w);
    end
end

% Remove force when cut-off value is reached and model hysteresis
if F_f >= 0.0982
    disp('cut-off')

    % Count number of iterations (-)
    n = n + 1;

    % Calculation relaxation displacement (m)
    x_rel = F_f/((n_c)*sigma_b);

    % Calculate bristle configuration (m)
    d_w_c = d_w_c - x_rel;

    % Determine internal stress (N)
    F_int = sigma_b*sum(d_w_c);

    % Calculate settling displacement (m)
    D_0 = F_int/(n_c*sigma_b);

    % Compensate relaxation displacement with settling displacement (m)
    x_rel = x_rel - abs(D_0);

    % Calculate compensated bristle configuration (m)
    d_w_c = d_w_c + abs(D_0);

    % Reconnect disconnected bristles according to normal distribution for
    % reconnection (m)
    d_w_d = sign(F_f)*d_max - abs(normrnd(mu2,sigma2,n_d,1));

    % Bristle configuration for output (m)
    d_w = [d_w_c ; d_w_d];

```

```
% Initial stress (N/m)
F_int = sigma_b*sum(d_w);

% Settling displacement after reconnection of the bristles (m)
D_0 = F_int / sigma_ini;

% Internal equilibrium configuration (m)
d_w = d_w - D_0;

% Check internal equilibrium (N)
F_int = sigma_ini*sum(d_w);

fprintf('2) The bristles are placed and an internal equilibrium has been
obtained.\n')
fprintf('\n')
fprintf('    The internal stress amounts to %e Newtons.\n', F_int)

% New global position for new iteration (m)
x = x - x_rel + D_0;

% Initialize friction force for new iteration (N)
F_f = 0;
end
```

## C.5 Comparison to other models

### Dahl model

#### Friction\_model\_parameters.m

```
% M.J. Appels (Student)
% Delft University of Technology
% Faculty of mechanical engineering
% Department of Biomechanical Engineering
% email: m.j.appels@gmail.com

% Friction model parameters from: Haessig and Friedland [8]

%% Simulation parameters

% Mass (kg)
m = 0.690; % (unit mass)
% Springs stiffness (N/m)
K = 116.04e3;
% Spring actuation velocity (m/s)
dy = 8.25e-8;

%% Model parameters

% Dahl model parameters from: Haessig and Friedland (not realistic)
% A good approximation seems to be: sigma_0 = 10^2, alpha = 1, F_c = 1. But
% this is in combination with a higher mass, lower spring stiffness and
% higher actuation velocity.

sigma_0 = 2.2137e07; % Bristle stiffness (N/m)
alpha_1 = 1; % Shape determining parameter (-)
% (Higher alpha results in a sharper bent of the stress-strain curve
% and vice versa)
F_C = 0.3828; % Coulomb friction (N)
```

#### Spring\_mass\_example.m

```
% M.J. Appels (Student)
% Delft University of Technology
% Faculty of mechanical engineering
% Department of Biomechanical Engineering
% email: m.j.appels@gmail.com

% The data for time domain and model parameters are obtained from Haessig
% and Friedland as the formulation for the model. The simulation results
% are identically to those obtained by H&F but some remarks have to be
% made.
% First of all the formulation for the model is a linearised model and not
% the model generally used by others. The parameters chosen are not
% optimal. Much better results can be obtained by the choice for a much
% higher stiffness. But are still not ideal.

% Start timer
tic

clc; clear all;

% Load model parameters
Friction_model_parameters

% Initial input ode23-solver
x_0 = 0;
F_0 = 0;
dx_0 = 0;
```

```

Q_0 = [x_0 ; F_0 ; dx_0 ];

% Timespan (s)
t_0 = 0;
t_end = 5;

% Numerical integration
[T Q] = ode23(@OdeHold, [t_0 t_end], Q_0);

%% Extract Data

% initialize output matrices
x = Q(:,1);
F_f = Q(:,2);
dx = Q(:,3);

% Actuator input position
y = dy.*T;
F_act = (dy.*T-Q(:,1)).*K;

% Position
x_Dahl = Q(:,1);

% velocity
dx_Dahl = Q(:,3);

% Dahl friction force
F_f_Dahl = Q(:,2);

% Filter data
[B A] = butter(2, 0.0001, 'low');
F_f_Dahl = filtfilt(B ,A , F_f_Dahl);

%% Plot Data

% Linestyle for each mass
ls2 = '-';
ls1 = '--';
ls3 = '-.';
Ls = [ls1 ;ls2 ; ls3];

% plot simulation in figure containing experimental data. The plot is obtained
% from the m-file: Experiments_2_0_5mv
hold on
plot(x_Dahl, F_f_Dahl, Cl(3), 'linestyle', Ls(3,:), 'linewidth', 4)
title('Simulation of force-displacement curves (Dahl model)')
axis([0 1.4e-7 0 0.45])
xlabel('Displacement mass [m]')
ylabel('Friction force [N]')
line([1.25e-7 1.25e-7], [0 0.40], 'color', 'k', 'linestyle', ':')
legend('Experimental data, m = 0.352 kg', 'Experimental data, m = 0.563 kg',
'Experimental data, m = 0.690 kg',...
'Dahl model, m = 0.352 kg', 'Dahl model, m = 0.563 kg', 'Dahl model, m =
0.690 kg', 'End of pre-sliding regimes', 'location', 'EastOutside')

% Stop timer and return computer time
toc
fprintf('\n')

```

### OdeHold.m

```

% M.J. Appels (Student)
% Delft University of Technology
% Faculty of mechanical engineering
% Department of Biomechanical Engineering
% email: m.j.appels@gmail.com

```

```
function [dQ] = OdeHold(t, Q)

Friction_model_parameters

x = Q(1,1);
F_f = Q(2,1);
dx = Q(3,1);

F_ext = (dy*t-x)*K;

% Dahl model
[dF_f] = Dahl_model(Q, t);

ddx = (F_ext - F_f)/m;

dQ = [dx ; dF_f ; ddx ];
```

### Dahl model.m

```
% M.J. Appels (Student)
% Delft University of Technology
% Faculty of mechanical engineering
% Department of Biomechanical Engineering
% email: m.j.appels@gmail.com

function [dF_f] = Dahl_model(Q,t)

Friction_model_parameters

x = Q(1,1);
F_f = Q(2,1);
dx = Q(3,1);

%General Dahl model
dF_f = sigma_0*((1-F_f/F_C*sign(dx))^alpha_1)*dx;
```

### **LuGre model**

#### Friction\_model\_parameters.m

```
% M.J. Appels (Student)
% Delft University of Technology
% Faculty of mechanical engineering
% Department of Biomechanical Engineering
% email: m.j.appels@gmail.com

% Simulation parameters

% Mass (kg)
m = 0.690;
% Springs stiffness (N/m)
K = 116.04e3;
% Spring actuation velocity (m/s)
dy = 8.25e-8;

% Model parameters

% LuGre model parameters from: A New Model for Controls of Systems With
% Friction (C. Canudas de Wit)

sigma_0 = 2.2173e07; % Bristle stiffness (N/m)
sigma_1 = sqrt(2.2173e07); % Damping coefficient (Ns/m)
sigma_2 = 0.4; % Viscous friction (Ns/m)
v_s = 8.25e-8; % Stribeck velocity (m/s)
F_S = 0.3828; % Static friction (N)
```

```
F_C = F_S/1.5; % Coulomb friction (N)
```

### Spring mass example.m

```
% M.J. Appels (Student)
% Delft University of Technology
% Faculty of mechanical engineering
% Department of Biomechanical Engineering
% email: m.j.appels@gmail.com

% Start timer
tic
clc; clear all;

% Load model parameters
Friction_model_parameters

% Initial input ode23-solver
x_0 = 0;
z_0 = 0;
dx_0 = 0;
Q_0 = [x_0 ; z_0 ; dx_0 ];

% Timespan (s)
t_0 = 0;
t_end = 10;

% Numerical integration
[T Q] = ode23(@OdeHold, [t_0 t_end], Q_0);

%% Extract Data

% initialize output matrices
x = Q(:,1);
z = Q(:,2);
dx = Q(:,3);

% Actuator input position
y = dy.*T;
F_act = (dy.*T-Q(:,1)).*K;

dZ = zeros(length(Q),1);
F_f_Lugre = zeros(length(Q),1);

for n = 1:length(Q)
    % Lugre friction force
    [dz F_f] = Lugre_model(Q(n,:));
    dZ(n,1) = dz(1,1);
    F_f_Lugre(n,1) = F_f(1,1);
end

% Filter data
[B A] = butter(2, 0.0001, 'low');
F_f_Dahl = filtfilt(B ,A , F_f_Dahl);

% line color
Cl = [0 0.5 0];

% Linestyle for each mass
ls2 = '-';
ls1 = '--';
ls3 = '-.';
Ls = [ls1 ;ls2 ; ls3];

% plot simulation in figure containing experimental data. The plot is obtained
% from the m-file: Experiments_2_0_5mv
```

```

hold on
title('Simulation of force-displacement curves')
plot(x, F_f_Lugre, 'color', Cl, 'linestyle', Ls(3,:))
xlabel('Displacement mass [m]')
ylabel('Friction force [N]')
legend('Experimental data, m = 0.352 kg', 'Experimental data, m = 0.563 kg',
'Experimental data, m = 0.690 kg',...
'LuGre model, m = 0.352 kg', 'LuGre model, m = 0.563 kg', 'LuGre model, m =
0.690 kg',...
'end of pre-sliding regime', 'location', 'EastOutside')

% Stop timer and return computer time
toc
fprintf('\n')

```

### OdeHold.m

```

% M.J. Appels (Student)
% Delft University of Technology
% Faculty of mechanical engineering
% Department of Biomechanical Engineering
% email: m.j.appels@gmail.com

function [dQ] = OdeHold(t, Q)

% Load model parameters
Friction_model_parameters

x = Q(1,1);
z = Q(2,1);
dx = Q(3,1);

F_ext = (dy*t-x)*K;

% Lugre model
[dz F_f] = Lugre_model(Q, t);

ddx = (F_ext - F_f)/m;

dQ = [dx ; dz ; ddx ];

```

### Lugre\_model.m

```

% M.J. Appels (Student)
% Delft University of Technology
% Faculty of mechanical engineering
% Department of Biomechanical Engineering
% email: m.j.appels@gmail.com

function [dz F_f] = Lugre_model(Q,t)

Friction_model_parameters

x = Q(1,1);
z = Q(2,1);
dx = Q(3,1);

% Lugre model
g_v = F_C/sigma_0 + ((F_S - F_C)/sigma_0)*exp(-(dx/v_s)^2);
dz = dx - (abs(dx)/g_v)*z;
F_f = sigma_0*z + sigma_1*dz + sigma_2*dx;

```

## C.6 Calibration sensors

Calibration data analysis.m

```

%% Load data into workspace

% M.J. Appels (Student)
% Delft University of Technology
% Faculty of mechanical engineering
% Department of Biomechanical Engineering
% email: m.j.appels@gmail.com

clc; clear all; close all;

%% Load data into workspace
load Master_1.txt
load Master_2.txt
load Slave_1.txt
load Slave_2.txt

% Rename Data
RawData_Master_1 = Master_1;
RawData_Master_2 = Master_2;
RawData_Slave_1 = Slave_1;
RawData_Slave_2 = Slave_2;

%% Filter Data

% Filter
[B A] = butter(2, 0.0025, 'low');
Data_Filter_Master_1 = filtfilt(B ,A , RawData_Master_1);
Data_Filter_Master_2 = filtfilt(B ,A , RawData_Master_2);
Data_Filter_Slave_1 = filtfilt(B ,A , RawData_Slave_1);
Data_Filter_Slave_2 = filtfilt(B ,A , RawData_Slave_2);

% Rename data
MMaster_1 = Data_Filter_Master_1(:, 3);
MMaster_2 = Data_Filter_Master_2(:, 3);
SSlave_1 = Data_Filter_Slave_1(:, 2);
SSlave_2 = Data_Filter_Slave_2(:, 2);

%% Range

% Conversion factor digital output to mm
cf = 0.02;

% Measurement values
DM1 = [0 ; 0.00005 ; 0.0001 ; 0.00015 ; 0.0002 ; 0.00025 ; 0.0005 ; ...
       0.00075 ; 0.001 ; 0.00125];
DM2 = [0 ; 0.00005 ; 0.0001 ; 0.00015 ; 0.0002 ; 0.00025 ; 0.0005 ; ...
       0.00075 ; 0.001 ; 0.00125 ; 0.0015 ; 0.00175 ; 0.002 ; 0.00225];
DS1 = [0 ; 0.00005 ; 0.0001 ; 0.00015 ; 0.0002 ; 0.00025 ; 0.0005 ; ...
       0.00075 ; 0.001 ; 0.00125 ; 0.0015 ; 0.00175 ; 0.002 ; 0.00225 ; ...
       0.0025 ; 0.00275 ; 0.003 ; 0.00325 ; 0.0035 ; 0.00375 ; 0.004 ; ...
       0.00425 ; 0.0045 ; 0.00475];
DS2 = [0 ; 0.00005 ; 0.0001 ; 0.00015 ; 0.0002 ; 0.00025 ; 0.0005 ; ...
       0.00075 ; 0.001 ; 0.00125 ; 0.0015 ; 0.00175 ; 0.002 ; 0.00225 ; ...
       0.0023 ; 0.00235 ; 0.0024 ; 0.00245 ; 0.0025 ; 0.00255 ; 0.0026 ; ...
       0.00265 ; 0.0027 ; 0.00275 ; 0.003 ; 0.00325 ; 0.0035 ; 0.00375 ; ...
       0.004 ; 0.00425 ; 0.0045 ; 0.00475];

%% Data sets

% Master_1
M1_1 = Data_Filter_Master_1(10000:12000, 3);
M1_2 = Data_Filter_Master_1(14500:16500, 3);
M1_3 = Data_Filter_Master_1(18000:19000, 3);
M1_4 = Data_Filter_Master_1(20000:21000, 3);

```

```

M1_5 = Data_Filter_Master_1(22000:22500, 3);
M1_6 = Data_Filter_Master_1(24000:25000, 3);
M1_7 = Data_Filter_Master_1(27000:28000, 3);
M1_8 = Data_Filter_Master_1(30500:31000, 3);
M1_9 = Data_Filter_Master_1(33500:34500, 3);
M1_10 = Data_Filter_Master_1(37500:38500, 3);

Mean_M1 = [mean(M1_1) mean(M1_2) mean(M1_3) mean(M1_4) mean(M1_5)...
           mean(M1_6) mean(M1_7) mean(M1_8) mean(M1_9) mean(M1_10)];

% Master_2
M2_1 = Data_Filter_Master_2(2500:3500, 3);
M2_2 = Data_Filter_Master_2(5500:6500, 3);
M2_3 = Data_Filter_Master_2(8500:9500, 3);
M2_4 = Data_Filter_Master_2(11500:12500, 3);
M2_5 = Data_Filter_Master_2(14500:15500, 3);
M2_6 = Data_Filter_Master_2(17500:18000, 3);
M2_7 = Data_Filter_Master_2(20500:21000, 3);
M2_8 = Data_Filter_Master_2(23500:24000, 3);
M2_9 = Data_Filter_Master_2(26500:27500, 3);
M2_10 = Data_Filter_Master_2(30500:32500, 3);
M2_11 = Data_Filter_Master_2(35500:36000, 3);
M2_12 = Data_Filter_Master_2(38000:39000, 3);
M2_13 = Data_Filter_Master_2(41000:41500, 3);
M2_14 = Data_Filter_Master_2(43500:44000, 3);

Mean_M2 = [mean(M2_1) mean(M2_2) mean(M2_3) mean(M2_4) mean(M2_5)...
           mean(M2_6) mean(M2_7) mean(M2_8) mean(M2_9) mean(M2_10) mean(M2_11)...
           mean(M2_12) mean(M2_13) mean(M2_14)];

% Slave_1
S1_1 = Data_Filter_Slave_1(2500:4500, 2);
S1_2 = Data_Filter_Slave_1(8000:8500, 2);
S1_3 = Data_Filter_Slave_1(10500:11000, 2);
S1_4 = Data_Filter_Slave_1(13000:13500, 2);
S1_5 = Data_Filter_Slave_1(15500:16000, 2);
S1_6 = Data_Filter_Slave_1(17700:18200, 2);
S1_7 = Data_Filter_Slave_1(20000:20500, 2);
S1_8 = Data_Filter_Slave_1(22000:22500, 2);
S1_9 = Data_Filter_Slave_1(24500:25000, 2);
S1_10 = Data_Filter_Slave_1(27000:27500, 2);
S1_11 = Data_Filter_Slave_1(29500:30000, 2);
S1_12 = Data_Filter_Slave_1(32000:33000, 2);
S1_13 = Data_Filter_Slave_1(35000:35500, 2);
S1_14 = Data_Filter_Slave_1(37500:38500, 2);
S1_15 = Data_Filter_Slave_1(40500:41000, 2);
S1_16 = Data_Filter_Slave_1(43500:44500, 2);
S1_17 = Data_Filter_Slave_1(46500:47500, 2);
S1_18 = Data_Filter_Slave_1(49500:50000, 2);
S1_19 = Data_Filter_Slave_1(52500:53000, 2);
S1_20 = Data_Filter_Slave_1(55500:56000, 2);
S1_21 = Data_Filter_Slave_1(58500:59000, 2);
S1_22 = Data_Filter_Slave_1(61000:62000, 2);
S1_23 = Data_Filter_Slave_1(65000:67000, 2);
S1_24 = Data_Filter_Slave_1(70000:70500, 2);

Mean_S1 = [mean(S1_1) mean(S1_2) mean(S1_3) mean(S1_4) mean(S1_5)...
           mean(S1_6) mean(S1_7) mean(S1_8) mean(S1_9) mean(S1_10) mean(S1_11)...
           mean(S1_12) mean(S1_13) mean(S1_14) mean(S1_15) mean(S1_16)...
           mean(S1_17) mean(S1_18) mean(S1_19) mean(S1_20) mean(S1_21)...
           mean(S1_22) mean(S1_23) mean(S1_24)];

% Slave_2
S2_1 = Data_Filter_Slave_2(1000:1500, 2);
S2_2 = Data_Filter_Slave_2(3000:4000, 2);
S2_3 = Data_Filter_Slave_2(6500:7500, 2);
S2_4 = Data_Filter_Slave_2(9500:10500, 2);

```

```

S2_5 = Data_Filter_Slave_2(13000:14000, 2);
S2_6 = Data_Filter_Slave_2(15500:16500, 2);
S2_7 = Data_Filter_Slave_2(19000:20000, 2);
S2_8 = Data_Filter_Slave_2(22000:23000, 2);
S2_9 = Data_Filter_Slave_2(25500:26500, 2);
S2_10 = Data_Filter_Slave_2(28500:29500, 2);
S2_11 = Data_Filter_Slave_2(31000:32000, 2);
S2_12 = Data_Filter_Slave_2(34000:35000, 2);
S2_13 = Data_Filter_Slave_2(37000:38000, 2);
S2_14 = Data_Filter_Slave_2(40500:41500, 2);
S2_15 = Data_Filter_Slave_2(43500:44000, 2);
S2_16 = Data_Filter_Slave_2(45500:46500, 2);
S2_17 = Data_Filter_Slave_2(48500:49000, 2);
S2_18 = Data_Filter_Slave_2(51000:51500, 2);
S2_19 = Data_Filter_Slave_2(54000:54500, 2);
S2_20 = Data_Filter_Slave_2(57000:57500, 2);
S2_21 = Data_Filter_Slave_2(60000:61000, 2);
S2_22 = Data_Filter_Slave_2(63500:64000, 2);
S2_23 = Data_Filter_Slave_2(66500:67500, 2);
S2_24 = Data_Filter_Slave_2(69500:70000, 2);
S2_25 = Data_Filter_Slave_2(72500:73500, 2);
S2_26 = Data_Filter_Slave_2(75500:76000, 2);
S2_27 = Data_Filter_Slave_2(78500:79500, 2);
S2_28 = Data_Filter_Slave_2(82000:82500, 2);
S2_29 = Data_Filter_Slave_2(85000:85500, 2);
S2_30 = Data_Filter_Slave_2(88000:89000, 2);
S2_31 = Data_Filter_Slave_2(91500:92000, 2);
S2_32 = Data_Filter_Slave_2(94500:95500, 2);

Mean_S2 = [mean(S2_1) mean(S2_2) mean(S2_3) mean(S2_4) mean(S2_5)...
           mean(S2_6) mean(S2_7) mean(S2_8) mean(S2_9) mean(S2_10) mean(S2_11)...
           mean(S2_12) mean(S2_13) mean(S2_14) mean(S2_15) mean(S2_16)...
           mean(S2_17) mean(S2_18) mean(S2_19) mean(S2_20) mean(S2_21)...
           mean(S2_22) mean(S2_23) mean(S2_24) mean(S2_25) mean(S2_26)...
           mean(S2_27) mean(S2_28) mean(S2_29) mean(S2_30) mean(S2_31)...
           mean(S2_32)];

% Calculate mean value
figure
hold on
plot(cf*DM1, Mean_M1, 'r')
plot(cf*DM2, Mean_M2, 'b')
plot(cf*DS1, Mean_S1, 'k')
plot(cf*DS2, Mean_S2, 'm')
legend('Master_1', 'Master_2', 'Slave_1', 'Slave_2')
hold off

```

## **Appendix D - Contacts**

### **D.1 Manufacturers measurement equipment**

#### **Piezo stack actuator**

Physik Instrumente (PI) GmbH & Co.KG  
Auf der Römerstr. 1  
D-76228 Karlsruhe, Germany  
Tel: +49 721 4846-0  
Fax: +49 721 4846-100  
Email: info@pi.ws  
Internet: www.pi.ws

#### **Capacitive sensors**

Microsense, LLC  
70 Industrial Avenue East  
Lowell, Massachusetts 01852, USA  
Tel: +1 978 843 7673  
Internet: www.microsense.net

*The Netherlands, Belgium and Luxembourg*

Martek sprl  
Av. René Comhaire 82  
BE 1082 Bruxelles, Belgium  
Tel: +32 2 467 00 40  
Fax: +32 2 467 00 49  
Email: info@martek.be  
Internet: www.martek.be

### **D.2 Suppliers measurement equipment**

Ir. J.W. Spronck  
Faculty of Mechanical, Maritime and Materials Engineering  
Department of Precision and Microsystems Engineering  
Mekelweg 2  
2628CD Delft, The Netherlands  
Tel: +31 15 27 81824  
Email: J.W.Spronck@tudelft.nl

Ir. J.P. van Schieveen  
Faculty of Mechanical, Maritime and Materials Engineering  
Department of Precision and Microsystems Engineering  
Mekelweg 2  
2628CD Delft, The Netherlands  
Tel: +31 15 27 89503  
Email: J.P.vanSchieveen@tudelft.nl

### **D.3 Manufacturer and material supplier of measurement setup**

#### **Material supplier and manufacturer of sliding\_body and ground\_support\_1**

Heemskerk Fijnmechanica bv  
Coenecoop 645 - 2741 PV Waddinxveen  
Tel : +31 182-647010  
Fax : +31 182-647011  
Internet: [www.heemskerkfijnmechanica.nl](http://www.heemskerkfijnmechanica.nl)  
Email: [info@heemskerkfijnmechanica.nl](mailto:info@heemskerkfijnmechanica.nl)

#### **Material supplier for all parts except for sliding\_body, ground support\_1 and base**

Facultaire Werkplaats  
Ing. J. van Frankenhuyzen  
Faculty of Mechanical, Maritime and Materials Engineering  
Mekelweg 2  
2628CD Delft, The Netherlands  
Tel: +31 15 27 85614  
Email: [J.vanFrankenhuyzen@tudelft.nl](mailto:J.vanFrankenhuyzen@tudelft.nl)

#### **Manufacturer of all parts except for sliding\_body, ground support\_1 and base**

M.J. Appels (student member)  
Email: [m.j.appels@gmail.com](mailto:m.j.appels@gmail.com)

P.P. Pluimers (student member)  
Email: [pieter\\_pluimers@hotmail.com](mailto:pieter_pluimers@hotmail.com)

#### **Manufacturer of the actuation spring**

Verenfabriek Roveron BV  
Graafstroomstraat 15-17  
3044 AN Rotterdam, The Netherlands  
Tel: +31 10 41 52577  
Fax: +31 10 43 79801  
Email: [info@roveron.nl](mailto:info@roveron.nl)  
Internet: [www.roveron.nl](http://www.roveron.nl)